CHARACTERIZATION OF EBOLAVIRUS ENTRY

A Dissertation

Presented to the Faculty of the Graduate School

of Cornell University

In Partial Fulfillment of the Requirements for the Degree of

Doctor of Philosophy

by

Lakshmi Nathan

August 2019

CHARACTERIZATION OF EBOLAVIRUS ENTRY

Lakshmi Nathan, Ph.D.

Cornell University 2019

Ebola virus disease is a global concern given its periodic occurrence, high lethality, and rapid spread, coupled with a lack of approved therapeutics and vaccines. New tools are needed to gain fundamental insight into the virus life cycle, particularly entry and fusion of the viral envelope with the host membrane, and to combat the spread of the disease.

Some drugs that alter endo-lysosomal calcium can inhibit Ebola virus infection, hinting that calcium may play a role in Ebola virus entry. Calcium is known to mediate fusion of other enveloped viruses as well as synaptic vesicles (Chapter 1). Chapter 2 demonstrates that Zaire ebolavirus (EBOV) infection is increased in the presence of calcium and that increased infectivity is a result of calcium interacting with the EBOV fusion peptide. Calcium interacts with viral glycoprotein residues D522 and E540 to promote insertion of the fusion peptide into the host membrane. Notably, these residues are highly conserved across Filoviridae, suggesting that calcium-interfering drugs are important candidates in the search for antivirals against not only Ebola, but all filoviruses.

Although receptor binding, low pH, removal of the glycan cap, and calcium have all been implicated in Ebola virus fusion, the exact trigger remains unknown. Techniques that enable the visualization of individual virions undergoing fusion can

contribute substantially to clarifying the fusion trigger. Methods that track virions in live cells lend themselves to “top-down” experiments where individual cellular factors are knocked out either genetically or by drug treatment. Alternatively, biomimetic systems, such as those that monitor viral fusion with supported lipid bilayers, enable “bottom-up” approaches where factors are added in one by one. These approaches are discussed in detail in Chapter 3. Chapter 4 describes the construction of a biomimetic platform for investigating Ebolavirus fusion, including incorporation of the host receptor and control over exposure to potential fusion triggers.

The speed at which new outbreaks can emerge necessitates new methods for preventing viral spread. Mammalian cell plasma membrane blebs functionalized with viral proteins are novel vaccine candidates (Chapter 5). They require less optimization than inactivated viruses or virus-like particles, and are particularly well-suited to viruses with heavily glycosylated proteins, like Ebola virus.

BIOGRAPHICAL SKETCH

Lakshmi Nathan graduated *magna cum laude* from Texas A&M University in December 2013 with a B.S. in Chemical Engineering. Prior to joining Cornell, she conducted research with Professor Arul Jayaraman at Texas A&M University from 2011 to 2014 and Professor Cynthia Collins at Rensselaer Polytechnic Institute in 2013. She began her PhD in Chemical and Biomolecular Engineering in August 2014 at Cornell University in the labs of Professor Susan Daniel and Professor Gary Whittaker.

අද මා ඉන්නා මේ තැනට පැමිණීම වෙනුවෙන් තම සහයෝගය, ආදරය නොමසුරුව පුදකළ අම්මාට සහ වසර ගණනාවක් තිස්සේ මේ කාර්යයට මා පෙළඹ වූ කරුණාරත්න පවුලට ද සැමදා මා දිරිමත් කළ කීත් ඔඩ්වයර්ට ද මේ නිබන්ධය ආදරයෙන් පිළිගන්වමි.

This dissertation is dedicated to my mother whose love and support has made me who I am today, the Karunarthne family who have inspired me so much over the years, and Keith O'Dwyer, who never let me give up.

ACKNOWLEDGMENTS

I thank the members of my thesis committee Prof. Susan Daniel, Prof. Gary Whittaker, and Prof. Matthew DeLisa for their guidance. I would also like to thank Dr. Jean Millet for his invaluable advice on much of the work presented here. My graduate work has been supported by the NSF Graduate Fellowship Program (Grant No. DGE-1650441) and the Samuel C. Fleming Family Graduate Fellowship. Paper coauthors and additional funding sources are acknowledged in each chapter.

TABLE OF CONTENTS

CHAPTER 1
CALCIUM AS A MEDIATOR OF FUSION OF SYNAPTIC VESICLES AND VIRUSES WITH CELL MEMBRANES

1.1 Introduction

Fusion between membranes is a molecular process that has been described to occur in several physiological processes in eukaryotic cells. The fusion between two membranes is regulated by specific membrane proteins present in both of the fusing membranes; these proteins allow the contact and subsequent mixing of the membrane components to create the fusion pore. Perhaps the most studied example of this phenomenon is the fusion of intracellular vesicles in neural cells, where the cellular and secreting vesicle membranes fuse to allow the release of cellular signals necessary for neuronal function. In these cells, the process is modulated by a set of proteins anchored to both membranes. These soluble N-ethyl maleimide sensitive factor attachment protein receptors (SNAREs) also interact with accessory proteins including the calcium binding protein synaptotagmin in order to induce the fusion of the secretory vesicle membrane with the cellular membrane[1]. While the mechanism is mainly carried out by the SNARE proteins, fusion will only occur when the synaptotagmin is bound to the SNARE complex, and synaptotagmin function is regulated by calcium ions that bind to the specific C2 domain of the protein, making calcium a key element in the membrane fusion process[2,3].

Similar to physiological membrane fusion, enveloped viruses have to undergo to membrane fusion events to establish an infection in the host cell[4]. These viruses

need to induce the formation of a fusion pore between the viral and the cell membrane to release their genetic material into the host cell. The viral-cell membrane fusion can occur at different stages during viral entry, from the cellular membrane during virus-cell attachment, to the endosomal membrane during intracellular trafficking. While this process is common in enveloped viruses and most of its mechanism has been solved, there are still gaps in the understanding of the viral-cell membrane fusion. Similar to the neural cells, viral-cell fusion processes are regulated by specific viral membrane proteins, which are known as viral fusion proteins and have been grouped in three classes (I, II and III) according to specific structural and functional characteristics[5,6]. However, differences in the fusion mechanisms among viral fusion proteins from the same class can be observed. Recent publications have showed the role of calcium ions during viral-cell membrane fusion, suggesting a new addition to the previously known mechanisms for viral fusion protein function[7–9]. These pioneering studies have shown how viral fusion proteins interact with calcium ions to stabilize the fusion machinery (i.e. fusion peptide) to induce fusion between the viral and the cellular membrane during viral entry. This new evidence opens a new perspective for the study of the mechanisms used by enveloped viruses to entry into the cell. Here, we discuss the membrane fusion mechanisms used by both synaptic vesicles and viruses, and the role of calcium in these processes; we also summarize the available evidence of calcium interaction with viral fusion proteins and predict the structural organization of these interaction using protein structures and models.

1.2 Calcium-mediated membrane fusion in eukaryotic cells

Fusion between biological membranes is an event that occurs in many physiological processes. These events allow the exchange of molecules between cellular compartments as well as adjacent cells[10]. Perhaps the most well-studied eukaryotic membrane fusion mechanism is the one that occurs in secreted vesicles in synaptic cells, which characteristically is tightly regulated by intracellular calcium[11]. In this mechanism, known as regulated exocytosis, the secretory vesicles are stored in pools at specialized locations in the cytoplasm and then transported to the cellular membrane after activation or membrane depolarization occurs. Once both the vesicle and cell membranes are in contact, fusion is triggered by calcium moieties that act as second messengers or regulators of the fusion event. In contrast to this mechanism, constitutive exocytosis occurs in absence of these regulators. In constitutive exocytosis, vesicles are not stored but excreted as they are generated and transported to the cellular membrane[1].

The membrane fusion processes in eukaryotic cells mainly relies on the function of a set of membrane molecules, the SNARE proteins[10,11]. These proteins are receptor-type molecules that are suggested to participate principally in neural exocytosis processes, but have been also described to have a role in intracellular membrane fusion between organelles[12,13]. In the synaptic cell, SNARE proteins interact with the soluble proteins N- ethylmaleimide-sensitive factor (NSF), and α- and γ-soluble NSF attachment proteins (SNAPs) which are also membrane proteins and are also known to participate in membrane fusion[14]. This interaction occurs once

the secreting vesicle is transported to the cellular membrane; then the SNAP and NSF proteins form a complex with the SNAREs and other accessory proteins, which will facilitate the fusion between the membranes in the presence of high concentrations of calcium[1]. An example of this mechanism was described more than two decades ago by Söllner et al.[14]. In their work, they concluded that SNARE proteins at both the vesicle and the target membrane in nerve terminals (v-SNARE: synaptobrevin, and t-SNARE: syntaxin, respectively), complexed with NSF and SNAP-25 proteins to bring the membranes together and induce a conformational change in the complex, resulting in membrane fusion. Interestingly, after the formation of the complex and before the induction of fusion, the SNARE proteins also interact with another protein called synaptotagmin, which happens to be a calcium sensor protein and plays a major role in the induction of the membrane fusion[1].

Calcium sensor proteins are ubiquitous and mainly participate in the second messenger systems. These proteins react to external or internal signaling and bind to calcium moieties to carry out their biological function[15]. In the neurons, calcium sensors react to changes in the calcium concentrations in the intracellular environment that result from activation or depolarization in the cell. The calcium sensor synaptotagmin binds to the SNARE protein complexes and induces function only in presence of free calcium ions, which trigger the fusion event upon getting captured by the sensor protein[2]. The mechanism through which synaptotagmins interact with SNARE complexes and calcium ions is well known. The synaptotagmins are anchored to the vesicle membrane, exposing its two C2 domains (C2A and C2B) to the cytoplasm side; these C2 domains capture free calcium ions in the cytoplasm and upon

binding to the SNARE complex, they trigger the fusion event[2,16]. The C2 domains of synaptotagmin are part of a larger family of calcium sensor proteins that bind to membranes in response to changes in environmental calcium concertation. The structure of the C2A and C2B domains of synaptotagmin is composed of eight β-strands connected by small loops, and together forming β-sandwiches (Figure 1.1a). The connecting loops can vary, producing two different topologies (i.e. type I and II) that do not affect the overall structure and function of the protein[17]. The "top" loops of the two domains of synaptotagmin are known to have specific negatively charged residues organized in acidic chains that bind up to five calcium residues (three in the C2A domain and two in the C2B domain). In these domains, the calcium ions act as stabilizers of the flexible loops at the top of each domain (Figure 1.1f)[18]. Oligomerization of the C2 domains of synaptotagmin appears to be highly dependent on calcium and some functional interactions of the C2A and C2B domains are also dependent of calcium concentrations in the cell. This demonstrates the key regulatory role of calcium for synaptotagmins and how cellular concentrations of this ion can dramatically affect their function.

Calcium ions have different roles in cellular physiology. The major concentration of calcium in the body can be found in the bones, where it is trapped and stored and in some cases provides a reservoir to maintain the calcium homeostasis in the extracellular compartments[3,19]. Concentration of calcium in the extracellular and intracellular compartments is much lower compared with bones and just a small portion is available free for biological functions. In fact, concentrations of extracellular calcium are usually around 1-3 mM, while intracellular calcium

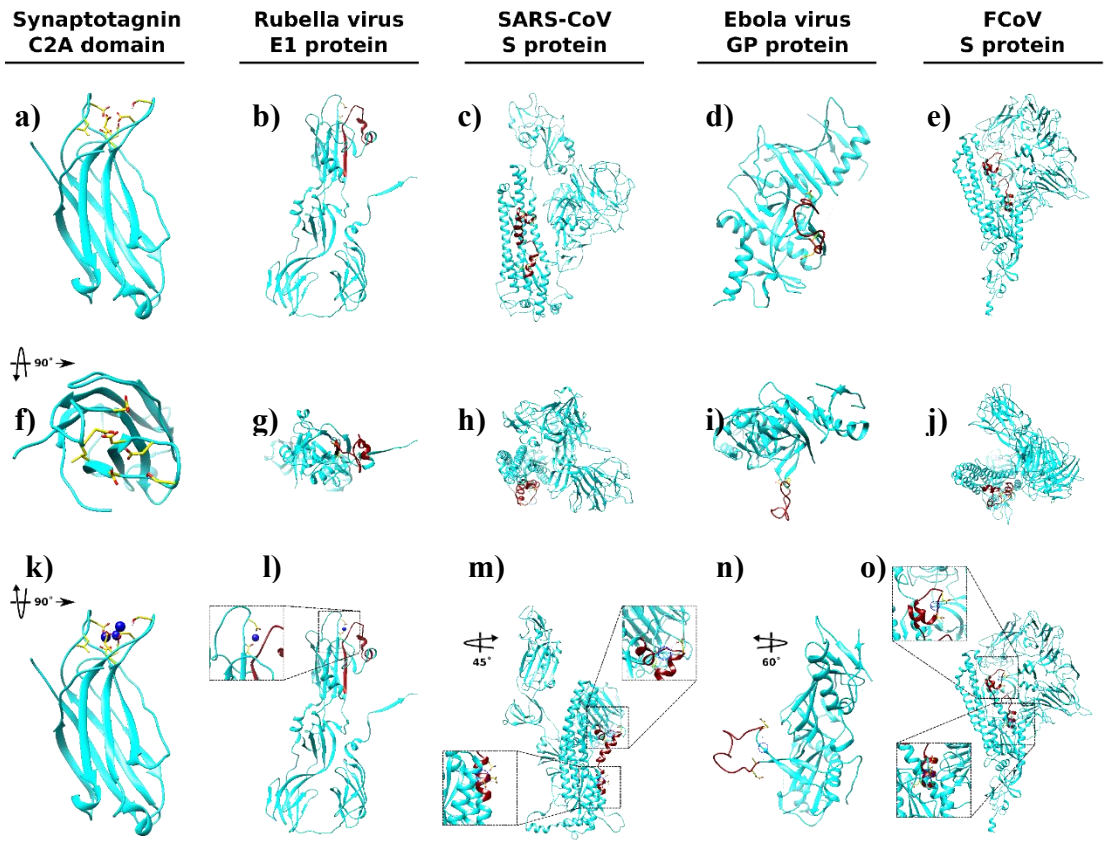

Figure 1.1 Fusion proteins that interact with calcium. Fusion peptides (red ribbons) and key negatively charged amino acid side chains (yellow sticks) are indicated as regions of interest. a-e) side view of monomer, f-j) top view indicating exposure/burial of fusion peptide k-o) Ca^{2+} binding pockets. Blue spheres indicate known Ca^{2+} binding sites, circles outlined in blue indicate hypothesized binding sites.

concentrations reach a maximum of 500 µM in some organelles e.g. the endoplasmic reticulum (ER). Interestingly, concentrations of calcium at the endosomal level can reach 100 µM, making this organelle the second most calcium-rich in the cell[3]. In the cell, calcium principally participates in molecule transport (e.g. ion channels), but also has functional properties for calcium binding proteins (e.g. protein kinase C, phospholipase-A, SNARE proteins)[3].

1.3 Calcium-mediated viral fusion

Calcium mediates many cellular process and viruses often hijack cellular process during infection. Therefore, it is unsurprising that calcium plays a role in many viral infection processes. Viruses interact with calcium 1) by disturbing calcium homeostasis 2) by directly binding calcium 3) via host-pathogen interactions that depend on proteins or pathways regulated by calcium[20]. Within the context of enveloped virions, calcium has been demonstrated to play a role in replication of human immunodeficiency virus (HIV)[21], human T-cell lymphotropic virus type 1[22], hepatitis B virus[23], hepatitis C virus[24,25], Kaposi sarcoma-associated herpesvirus[26], and human cytomegalovirus[27]. Viral envelope or spike proteins may also bind calcium; these include HIV gp 160[28,29], influenza neuraminidase[30], rubella virus E1[31], severe acute respiratory syndrome coronavirus (SARS-CoV) S[8], Ebola virus GP[9], and feline coronavirus (F-CoV)[32]. Such spike proteins typically mediate fusion of the viral envelope with the host membrane and indeed calcium has been demonstrated to be critical in the fusion of HIV[29], rubella virus[7], SARS-CoV[8], Ebola virus[9], and F-CoV[32], and murine leukemia virus[33].

The fusion machinery of HIV, gp41, contains a calcium binding domain that is similar to an EF hand[28] and binds calcium with an affinity of $K_a = 2.5 \times 10^4$ [34]. This binding pocket is selective for calcium; magnesium and manganese do not compete for binding with calcium[28]. The formation of syncytia between cells either expressing HIV gp120-gp41 or infected by HIV and target cells expressing the receptor CD4 requires calcium. Binding of gp120-gp41 to soluble CD4 is calcium-independent whereas cargo and lipid transfer between cells during syncytia formation requires calcium; this indicates that calcium is important for the fusion process itself[29].

Calcium is able to trigger fusion of the virus with liposomes, depending on the lipid composition of the vesicles[35]. Part of calcium's role in HIV fusion may be altering the secondary structure of the HIV fusion peptide[34,36]. In solution, the peptide containing the calcium binding pocket is alpha α-helical and the binding of calcium further increases this helicity[34]. In the presence of POPG the peptide is α-helical in nature and becomes more β-stranded when calcium is added[36].

The fusion protein of rubella virus, E1, contains two fusion loops; calcium coordinates between residue N88 of fusion loop 1 and D136 of fusion loop 2[31] (Figure 1.1l). Calcium is required for fusion and consequently overall infection[7]. Other cations, including sodium, magnesium, manganese, and zinc, did not enable fusion[7]. Although calcium binding enables synaptotagmin to interact with anionic lipids and thereby promote fusion[16,37], fusion of rubella does not require anionic lipids[38]. Instead, the binding of calcium changes the conformation of rubella's fusion loops, which may orient them properly for insertion into the target membrane. Within the fusion process, calcium is necessary for insertion of E1 into the target membrane; subsequent lipid mixing requires low pH[38]. There is strong selective pressure for the virus to maintain its calcium dependence, and the binding pocket does not tolerate substitution or switching of residues N88 and D136[7,38].

Calcium directly binds to the fusion peptide of SARS-CoV[8]. The fusion peptide contains two calcium binding sites[8]. The binding constant of calcium is K_b = 3.76×10^4 M^{-1} for the pocket nearest to the S2' cleavage site and $K_b = 2.34 \times 10^4$ M^{-1} for the pocket further downstream of S2' [8]. Calcium increases the ability of the SARS-CoV fusion peptide to induce lipid ordering upon insertion into the target membrane[8].

The impact of calcium on the fusion process results in calcium-dependent infection. In live cells, removal of extracellular calcium reduces infection of particles pseudotyped with the SARS-CoV spike protein nearly 3-fold and chelation of intracellular calcium reduces infection ~60-fold[8].

Calcium interacts with D522 and E540 of the Ebola virus glycoprotein[9] (Figure 1.1n). These residues flank the fusion peptide, which is part of a larger disulfide-bonded loop. Calcium increases lipid ordering induced by insertion of the fusion peptide into the target membrane, both for the fusion loop in solution as well viral particles pseudotyped with the Ebola glycoprotein[9]. Lipid mixing is similarly calcium-dependent[9,39]. Consistent with these observations, removal of extracellular calcium reduces infection with pseudotyped viral particles by roughly 60% and chelation of intracellular calcium reduces infection by 97%[9]. Substitution of these amino acids with neutral residues greatly reduces the effect of calcium on peptide-mediated membrane ordering, removes the calcium-dependence for lipid mixing, and alters the impact of calcium on infection[9]. Calcium does not significantly alter the secondary structure of the fusion loop in aqueous solution[9]; instead, it may act to stabilize the conformation that is favorable for fusion. The smaller fusion peptide is disordered in solution, α-helical in the presence of vesicles containing anionic lipids, and β-structured in the presence of both liposomes and calcium[40]; reminiscent of the calcium-induced conformations changes of the HIV fusion peptide.

In contrast to the preceding examples, calcium depletion increases fusion and infectivity of MLV[33]. When calcium is present it inhibits isomerization of the MLV envelope protein env, possibly by stabilizing the inactive form of the protein[33].

Depletion of calcium from the environment releases calcium from binding env and incuses isomerization[33]. The calcium binding pocket is not in the receptor binding fragment of env, but its exact location has not been identified[33].

1.4 Calcium pockets in viral fusion proteins

Several reports have demonstrated the role of calcium in the membrane fusion mechanisms of enveloped viruses. In those studies, the scientific evidence suggest that calcium ions interact with specific negatively charged amino acids located in selected loops of the protein[7,8]. This characteristic appears to be similar to what have been described for C2 domains of synaptotagmin[17,18]. It is also suggested that this interaction aims to stabilize specific a structural conformation needed by the calcium-binding protein[2]. While the interactions between calcium and the C2 domains of synaptotagmin have been well described in protein structures, structural evidence of these interactions in viral fusion proteins is limited. We used available viral fusion structures for rubella virus (PDB 5KHC and 4ADJ), Ebola virus (PDV 3CSY), and the modeled spike protein of SARS-CoV[8] and F-CoV[41] and compared them with the structure of the C2A domain of synaptotagmin (PDB 1BYN) to identify similarities in the structure organization of these proteins (Figure 1.2). We also drew the predicted localization and interaction of calcium ions with the viral fusion proteins, based on the available evidence for the C2A domain of synaptotagmin and the E1 glycoprotein of rubella virus[31,42]. All the structures and models were modified for this manuscript using Chimera software (UCSF Chimera v. 1.11.2, University of California) and PyMOL 2.0 (PyMOL Molecular Graphics System v.2.0.3, Schrodinger LLC).

1.5 Future research directions in calcium-mediated viral fusion

In identifying the fusion mechanism of enveloped viruses, commonly considered factors are pH, receptor biding, and protease cleavage of the spike protein. As described here, calcium can have a substantial effect on the fusion process, and is a factor that should be taken into account as well. It is likely that other viruses undergo calcium-dependent fusion beyond the five that have already been identified. The spike proteins of murine hepatitis virus, rat coronavirus, human parainfluenza virus are predicted to contain EF-hand like motifs[20], so calcium may influence the fusion of these viruses. Calcium dependence for fusion is a distinguishing feature of certain viruses; a handful of viruses are known to be calcium-independent for fusion, including Sendai virus[43] and Semliki Forest virus[7]. Further study could indicate whether calcium dependence for fusion is a defining characteristic across an entire family of viruses, or whether it is a species-specific trait.

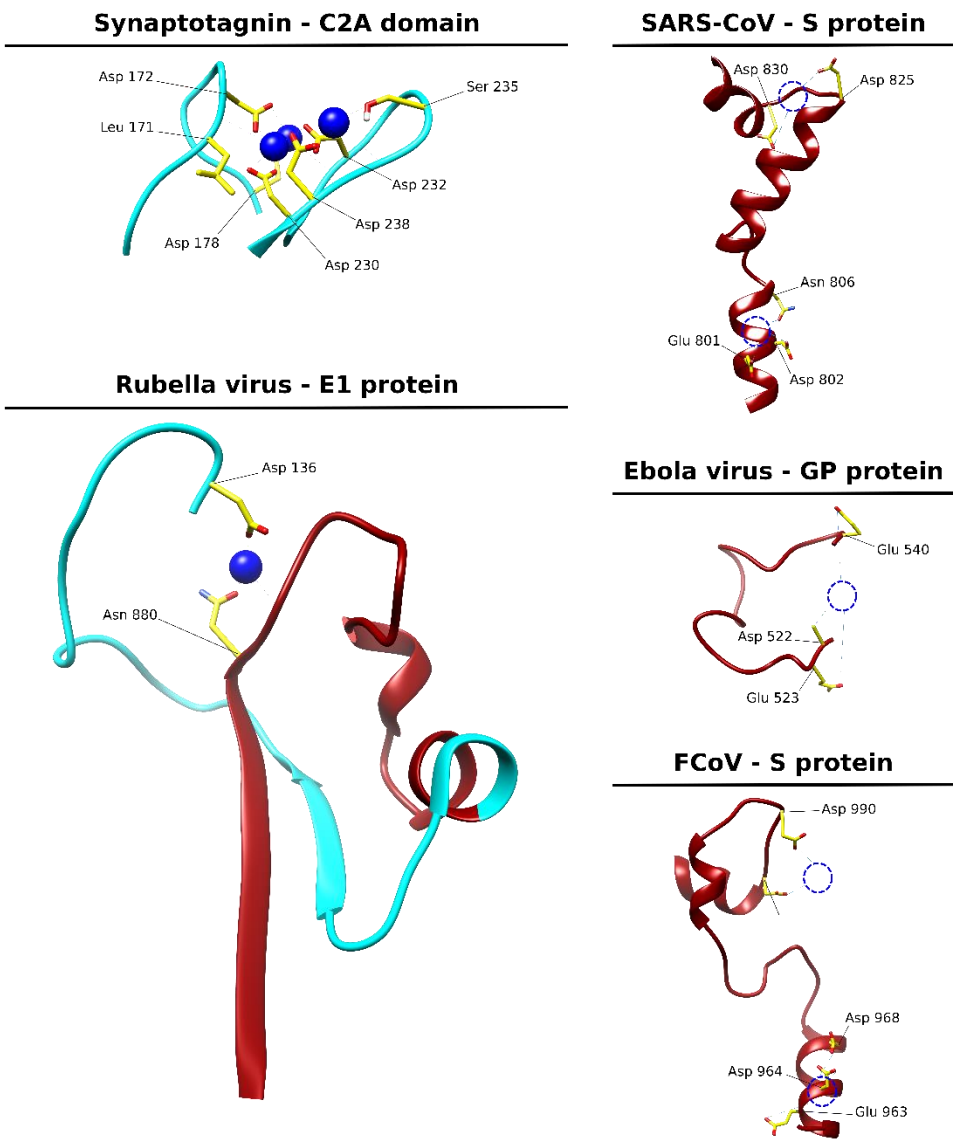

Figure 1.2 Calcium binding pockets in fusion protiens. Fusion peptides (red ribbons) and key negatively charged amino acid side chains (yellow sticks) are indicated as regions of interest. Blue spheres indicate known Ca^{2+} binding sites, circles outlined in blue indicate hypothesized binding sites.

Additional fundamental investigation of both calcium levels and the dynamics of its interaction with viral fusion proteins is required. Measurements of calcium levels within cellular compartments remains difficult and therefore the calcium concentration of all the sub-populations of endosomes has not been measured. Furthermore, the measurements that have been obtained reflect the concentration of

the overall compartment, but for viral fusion the local concentration in the proximity of the membrane is more relevant. Detailed temporal dynamics of calcium interaction with viral proteins remain masked; is it necessary for only hemifusion or for pore formation as well? Does calcium remain associated with the viral proteins after the onset of fusion? Is calcium needed before, after, or simultaneously with receptor binding?

The dependence of certain viruses on calcium for fusion and therefore successful entry into host cells could be exploited for therapeutic development. Inhibition of endosomal calcium channels is effective at preventing Ebola virus infection[44] and this approach may successfully inhibit infection of other calcium-dependent viruses. Although not known to need calcium for fusion, inhibition of calcium flux through endosomes inhibits entry of Middle East respiratory syndrome coronavirus[45]. Several calcium channel blockers are approved by the FDA[46], which makes this an attractive antiviral therapeutic approach.

1.6 Acknowledgements

The authors of this work are Lakshmi Nathan, Javier Jaimes Olaya, Susan Daniel and Gary Whittaker. LN summarized the literature on calcium-dependent viral fusion and proposed future directions, JJO summarized the synapotagmin literature and performed modeling of fusion proteins with input from LN, and SD and GW will review the work. LN is supported by the NSF Graduate Fellowship Program (Grant No. DGE-1650441) and the Samuel C. Fleming Family Graduate Fellowship. The

authors also acknowledge support from National Institutes of Health R01 AI135270 (to GRW and SD).

CHAPTER 2

CALCIUM IONS ENHANCE ENTRY OF EBOLA VIRUS BY DIRECTLY TARGETING THE FUSION PEPTIDE

2.1 Abstract

Ebola virus disease is a serious global health concern given its periodic occurrence, high lethality, and the lack of approved therapeutics. Certain drugs that alter intracellular calcium, particularly in endo-lysosomes, have been shown to inhibit Ebola virus infection; however, the mechanism responsible for this observation is unknown. Here, we provide evidence that *Zaire ebolavirus* (EBOV) infection is promoted in the presence of calcium as a result of the direct interaction of calcium with the EBOV fusion peptide. We identify the glycoprotein residues D522 and E540 in the FP as functionally critical to EBOV's interaction with calcium. Notably, these residues are highly conserved across *Filoviridae,* suggesting that calcium-modulating drugs are important antiviral candidates against not only Ebola, but all filoviruses. We show that interactions of the fusion peptide with Ca^{2+} ions lead to specific changes in lipid ordering in the host membrane during membrane fusion, and these changes are promoted at low pH and can be correlated with infectivity. We further demonstrate that calcium interaction with the fusion peptide promotes α helical structure of the fusion peptide—a conformational change that enhances membrane fusion, which we validate using functional assays of membrane fusion. This study shows that calcium directly targets the Ebola virus fusion peptide and influences its conformation.

Calcium's impact on fusion and subsequently infectivity is a key interaction that can be leveraged for developing strategies to defend against infection. This mechanistic insight provides a rationale for the use of calcium-interfering drugs already approved by the FDA as therapeutics against Ebola and enables further development of novel drugs to combat the virus.

2.2 Introduction

Ebola virus disease, a hemorrhagic fever in humans and non-human primates, has an average lethality of ~ 50%[47]. The most widespread epidemic to-date occurred in West Africa in 2014, with nearly 30,000 cases reported and over 11,000 deaths[48]. Outbreaks happen periodically; in the current outbreak in the Democratic Republic of Congo approximately 2,000 individuals have contracted the disease[49]. There are currently no therapies approved by the Food and Drug Administration specifically to treat the disease, though there are vaccines in clinical trials[50–53] and the development of antivirals against Ebola is ongoing[53–58]. Given its importance in global health, and the few countermeasures available, understanding the Ebola virus lifecycle to identify targets for therapeutic intervention is critical.

Ebola virus disease is caused by Ebola virus, a single-stranded negative-sense RNA virus belonging to the *Filoviridae* family. The Ebola virus genome is enclosed in a lipid envelope derived from the host cell membrane. The Ebola virus spike glycoprotein (GP) is embedded in this envelope and mediates viral entry, particularly receptor binding and fusion. GP is a class I fusion protein and undergoes proteolytic priming by furin, likely during virus assembly, to cleave pre-GP into its mature form

containing subunits GP_1 and GP_2. GP is not a prototypical class I fusion protein as it contains an "internal" fusion peptide (FP) incorporated within a larger disulfide-bonded loop (Figure 2.1 c,d). After initial binding to a cell-surface receptor, the virus enters cells via macropinocytosis or endocytosis[59]. Within the endosome, cathepsins cleave off a heavily glycosylated region of GP, known as the glycan cap[60,61]. The virus is then able to bind its endosomal receptor, NPC1[62–65]. After binding to NPC1, a subsequent trigger induces a conformational change in GP that allows the virus to fuse its envelope with the endosomal membrane[66], thereby releasing the viral genome. The exact nature of this fusion trigger remains unknown.

During membrane fusion, the hydrophobic FP buries into the endosomal membrane, which facilitates mixing of lipids between the viral and endosomal membranes. Further conformational changes in GP then allow a pore to form between the two membranes for genome escape. The Ebola virus FP is located within an unstructured loop and is flanked by negatively charged residues[67]. NMR studies of *Zaire ebolavirus* (EBOV) FP indicate that it has a flexible conformation at both neutral and acidic pH, but the structures at pH 7 and 5.5 are different[68], which points to a possible role for pH in fusion.

It is well-appreciated that lumenal pH changes during endosome maturation, however it is less appreciated that levels of other ions, including calcium (Ca^{2+}), change as well[69,70]. Initially the Ca^{2+} concentration in endosomes drops rapidly[71], but it increases later in the endocytic pathway to 2.5 μM in late endosomes[72] and 400 μM in the lysosome[73]. The current model of Ebola virus entry is that the virus undergoes fusion in endolysosomes that contain both NPC1 and two-pore Ca^{2+} channels

(TPC2)[62], but the role of TPC2 or calcium ions in the infection process is unknown. Here we elucidate this role, describing a mechanism for Ebola virus entry specifically in the membrane fusion process, which points to calcium ions directly targeting the fusion peptide. As the search for antivirals against Ebola continues, our findings indicate Ca^{2+} disruption is a powerful therapeutic tool and our uncovering of the mechanism responsible enables the rational design of drugs to exploit this Ca^{2+} dependence.

2.3 Results

2.3.1 Depletion of Ca^{2+} inhibits Ebola virus infection

To investigate the impact of Ca^{2+} on EBOV infection of cultured cells, we measured infectivity of EBOV pseudotyped virus containing a luciferase gene reporter while modulating Ca^{2+} in the extracellular and intracellular environment. First, cells were infected with Ebola GP-pseudotyped virus with or without extracellular Ca^{2+} present during the entry step. In the presence of external Ca^{2+}, Ebola GP-pseudotyped virus was nearly 3 times more infectious than when in Ca^{2+}-free media (Figure 2.1a).

To measure the impact of Ca^{2+} in the intracellular environment, we utilized 1,2-bis(2-aminophenoxy)ethane-*N*,*N*,*N*′,*N*′-tetraacetic acid tetrakis (BAPTA-AM), a chelator which is only active intracellularly[74]. Vero E6 cells were pre-treated with 50 μM BAPTA-AM, a concentration which does not significantly impact their viability[8]. EBOV infection was about 12 times higher with unaltered intracellular Ca^{2+} levels than when Ca^{2+} was chelated. (Figure 2.1b). For comparison of raw RLU values to noninfectious control see Supplementary Fig. S1.

2.3.2 Residues D522 and E540 are involved in Ca^{2+}-dependent infection

Ca^{2+} is known to play a role in the fusion of a few other enveloped viruses. Rubella virus depends on Ca^{2+} for proper orientation of its fusion loops[7]. Specifically, Ca^{2+} coordinates with the residues N88 and D136 located on adjacent fusion loops within E1. Previously we showed that viral entry of severe acute respiratory syndrome coronavirus (SARS CoV) is Ca^{2+} dependent, and the FP cannot induce membrane ordering when chelator is present[8]. The Ebola virus FP is flanked by negatively charged residues that may coordinate with Ca^{2+} ions (Figure 2.1d). Combined with evidence that drugs that interfere with cellular Ca^{2+} inhibit EBOV infection[57,75,76] and the implication of TPC2 in EBOV entry, the presence of these negatively charged amino acids motivated us to explore whether Ca^{2+} plays a role in Ebola virus fusion via direct interaction with the FP, similarly to that demonstrated for rubella virus and SARS CoV.

We hypothesized that Ca^{2+} might be interacting with negatively charged amino acids in the viral FP region and thus influencing the conformational changes necessary for fusion. The presence of negatively charged residues flanking the FP is highly conserved among the three genera of *Filoviridae*: *Cuevavirus*, *Marburgvirus*, and *Ebolavirus* (Figure 2.1e). The presence of negatively charged residues at positions 522 and 540 is conserved, though the exact identity of the residue at position 522 varies between aspartate and glutamate from one genus to another. Within the *Ebolavirus* genus, the species Zaire, Reston, Bundibugyo, and Taï Forest contain an aspartate at position 522, whereas for the Sudan species, that position is occupied by glutamate.

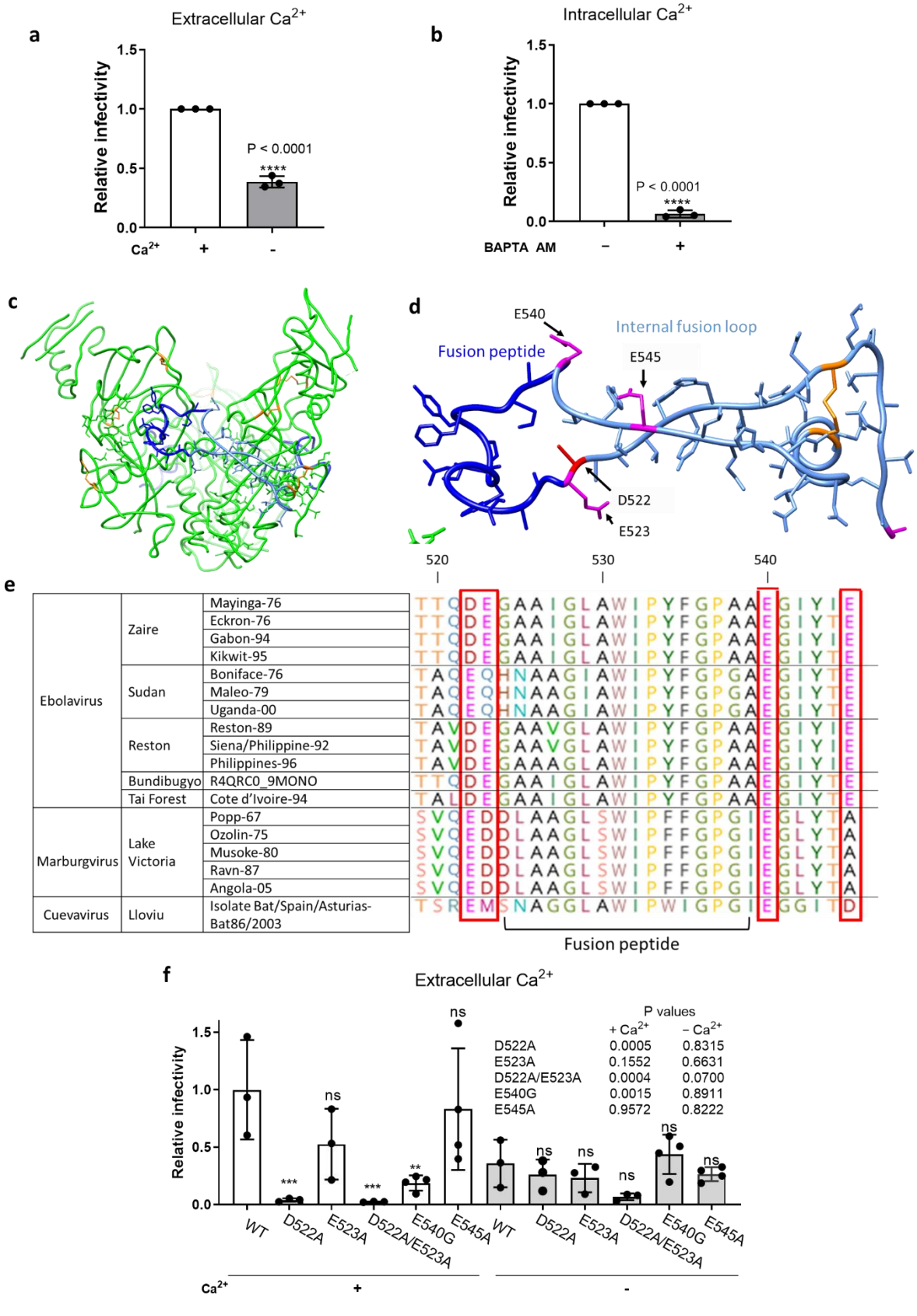
a
Extracellular Ca2+
Relative infectivity
1.5
1.0
0.5
0.0
P < 0.0001
****
Ca2+ + -
b
Intracellular Ca2+
Relative infectivity
1.5
1.0
0.5
0.0
P < 0.0001
****
BAPTA AM – +
c
d
E540
Internal fusion loop
Fusion peptide
E545
D522
E523
e
520
530
540
Ebolavirus
Zaire
Mayinga-76
Eckron-76
Gabon-94
Kikwit-95
Sudan
Boniface-76
Maleo-79
Uganda-00
Reston
Reston-89
Siena/Philippine-92
Philippines-96
Bundibugyo
R4QRC0_9MONO
Tai Forest
Cote d'Ivoire-94
Marburgvirus
Lake Victoria
Popp-67
Ozolin-75
Musoke-80
Ravn-87
Angola-05
Cuevavirus
Lloviu
Isolate Bat/Spain/Asturias-Bat86/2003
Fusion peptide
f
Extracellular Ca2+
Relative infectivity
1.5
1.0
0.5
0.0
P values
+ Ca2+ – Ca2+
D522A 0.0005 0.8315
E523A 0.1552 0.6631
D522A/E523A 0.0004 0.0700
E540G 0.0015 0.8911
E545A 0.9572 0.8222
ns
***
**
WT
D522A
E523A
D522A/E523A
E540G
E545A
Ca2+ + -

Figure 2.1. Ebolavirus entry is enhanced in the presence of extracellular and intracellular calcium. Viral particles pseudotyped with Zaire Ebolavirus GP were added to a) Vero E6 cells and allowed to internalize in calcium-free DMEM (- Ca^{2+}) or DMEM with 1.8 mM calcium (+ Ca^{2+}) for 2 h to assess the impact of extracellular calcium and b) Vero E6 cells pretreated with 50 μM of the chelator BAPTA AM or DMSO for 1 h. Pseudovirus particles were then added to cells with 50 μM BAPTA AM or DMSO and allowed to internalize for 2 h. Data normalized so that infection + Ca^{2+} is equal to 1. Error bars represent standard deviation for 3 independent experiments. c) Trimer of Zaire EBOV GP with fusion peptide (dark blue) fusion loop (pale blue) and disulfide bonds (orange). d) Zaire EBOV fusion loop and nearby negatively charged residues that may be involved in binding calcium. e.) Glycoprotein sequences of different filovirus strains were retrieved from UNIPROT and aligned using CLUSTAL. Horizontal lines demarcate different species. f.) Infectivity of pseudotyped viral particles with WT or mutated EBOV GP. Data normalized such that infectivity of WT EBOV in the presence of Ca^{2+} is 1. Error bars represent s.d. from 3 independent experiments, each with 3 technical replicates, with the exception of E545A and E54G , for which 4 independent experiments were conducted. Dots represent the mean of the technical replicates. P values determined by one-way ANOVA comparison to WT.

The FP is embedded in a loop, which brings residues D522, E523, E540 and E545 in close proximity to each other (Figure 2.1c,d).

In investigating the activity of these conserved negatively charged residues, we used site-directed mutagenesis to generate pseudotyped virus with neutral residues in these positions. We generated the amino acid substitutions D522A, E523A, and E545A. Attempts to produce the mutation E540A were unsuccessful due to recombination within the bacteria used for plasmid amplification; because alanine and glycine have similar affinities for Ca^{2+}[77], the mutant E450G was characterized instead. The presence of two negatively charged residues on each side of the FP implies possible redundancy, where a single mutation might still allow Ca^{2+} to coordinate with the remaining neighboring negatively charged residue. To test this possibility, we also generated the double mutant D522A/E523A. These mutations did not prevent the incorporation of GP into pseudotyped virus particles (Figure A2). In cell infectivity assays, pseudotyped virus containing D522A exhibited behavior drastically different than pseudotyped virus with wild type (WT) GP, and yielded higher infectivity in the

absence of extracellular Ca^{2+} (Figure 2.1f). E523 showed lower overall infectivity than WT but matched the WT Ca^{2+}-dependent behavior, displaying higher infectivity in the presence of extracellular Ca^{2+}. The double mutant D522A/E523A was infectious albeit at a very low level, as determined by comparison to a non-infectious negative control (Figure A3). D522A/E523A behaved similarly to D522A, with higher infectivity in the absence of extracellular Ca^{2+}. This suggests that D522 plays a central role in Ebola's response to Ca^{2+} and E523 likely does not serve a redundant function to D522. E540G had low infectivity and was relatively unaffected by extracellular Ca^{2+}. E545A had similar overall infection and Ca^{2+}-dependent behavior to the WT, indicating that it may not be critical in interacting with Ca^{2+}. Of the mutations tested, D522A, D522A/E523A, and E540G exhibited altered or no Ca^{2+} dependence compared to the WT. Given the location of these residues adjacent to the FP, we reasoned that the altered entry behavior of the particles bearing mutated GPs might be related to fusion. Extracellular and intracellular Ca^{2+} may alter cellular processes beyond directly impacting viral entry, so it is hard to decouple these effects in interpreting the results of solely cell-based experiments. Therefore we next employed biophysical approaches to isolate and further investigate the role of Ca^{2+} by examining the structure and fusion activity without the additional complications of concurrently occurring cellular pathways.

2.3.3 Ca^{2+} increases EBOV fusion in vitro

To further define the role of Ca^{2+} and isolate its impact on membrane fusion, we employed vesicle fusion assays that report lipid mixing. We used an *E.coli*-expressed EBOV FP construct containing residues 501-560 of GP^{68} (Figure 2.2a).

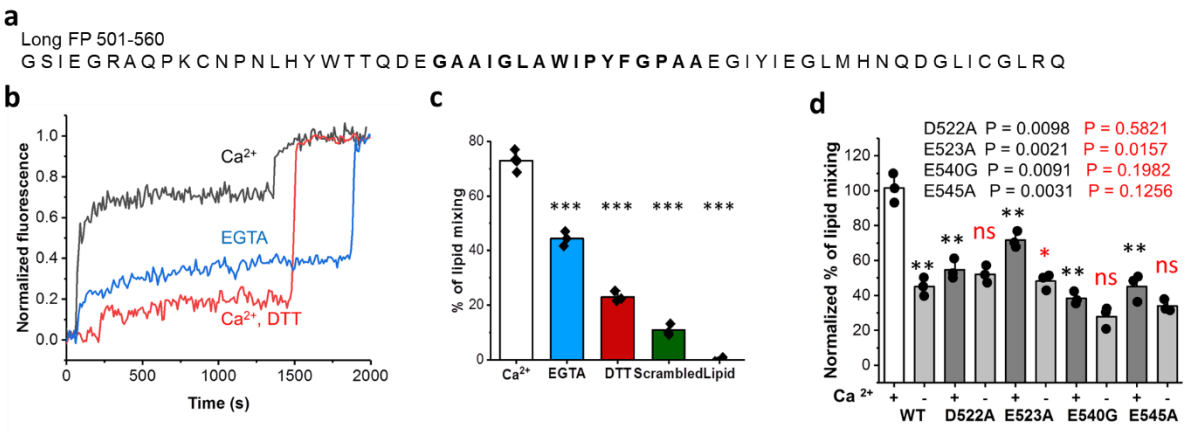

Figure 2.2. Mutants have reduced entry and fusion Ca2+ dependence. a) Sequence of the FP used in lipid mixing, ESR, and CD experiments with the core hydrophobic FP in bold. b) Raw data from a representative lipid mixing experiment using the expressed long FP... c) Normalized % lipid mixing induced by the fusion peptide from three independent experiments except for WT in the presence of Ca^{2+} where four independent experiments were conducted. Error bars indicate s.d. d) Normalized lipid mixing where 0 is the basal lipid mixing level of the WT with 5 mM DTT (c, red), and 100% is the level of WT with 2 mM Ca2+ (c, black). Error bars represent s.d. from three independent experiments except for WT where four independent experiments were conducted. Dots represent the mean of the replicates. ns = $p > 0.05$, * = $p < 0.05$, ** = $p < 0.01$, *** = $p < 0.001$ compared to WT (for 3d, red indicates comparison between $+Ca^{2+}$ and $- Ca^{2+}$ for each mutant), as calculated by Student's T test or ANOVA.

Compared to the "short version" FP containing residues 524-539, this "long" FP includes the disulfide-bonded loop that is critical to the structure and function of the FP[68]. In the lipid mixing experiment, the FP construct was mixed with large unilamellar vesicles (LUVs), 10% of which were fluorescently-labeled with a FRET pair. Upon fusion of these labeled vesicles with unlabeled vesicles, FRET is relieved, resulting in a large increase in fluorescence intensity (Figure 2.2c). After adding the FP to the mixture, detergent was added to rupture the LUVs and fully release the dye. The resulting fluorescence intensity was set to 100% to normalize data from one trial to the next.

In 2 mM Ca^{2+}, roughly 70% lipid mixing is observed (Figure 2.2b,c). In the presence of 1 mM EGTA to chelate Ca^{2+}, the lipid mixing ratio is greatly reduced

(39%). As a negative control, in the presence of 5 mM DTT, which removes the disulfide bond of the FP, lipid mixing is greatly reduced (21%). Taken together, these data indicate that Ca^{2+} interacts with the FP to promote fusion. Execution of these same lipid mixing studies with pseudovirus yielded lipid mixing levels comparable to the DTT control, even in the presence of both low pH and calcium, indicating that the receptor NPC1 or some other fusion trigger is needed for lipid mixing (Figure A8) mediated by the full viral particle.

We produced modified FP constructs matching the mutations used in our cell-based assays. WT FP consistently yielded high levels of lipid mixing in the presence of Ca^{2+} and only half as much mixing when Ca^{2+} was removed (Figure 2.2c). FP with the D522A mutation yielded roughly 50% lipid mixing regardless of whether Ca^{2+} was present or absent (Figure 2.2d). In infectivity studies (Figure 2.1f), this mutant did show behavior different from the WT, but yielded less infection in the presence of extracellular Ca^{2+}. The mutation E523A resulted in a modest decrease in lipid mixing compared to the WT, but still induced more fusion when Ca^{2+} was present rather than absent (Figure 2.2d), agreeing with our cell infectivity observations. E540G was the least fusion-competent, agreeing with our infectivity studies where it was also the least infectious mutant tested, and was relatively unaffected by Ca^{2+}. E545A yielded similarly low levels of lipid mixing, and was also unaffected by the addition of Ca^{2+}. This differs from our infectivity experiments, where Ca^{2+} did enhance infection of pseudotyped virus with the mutation E545A. Given that these modified FPs no longer exhibit strong Ca^{2+} dependence, our data suggest that having negatively charged

residues at positions 522, 540, and 545 is important for coordinating with Ca^{2+} and that removal of these negatively charged amino acids is detrimental to fusion.

2.3.4 Ca^{2+} increases EBOV FP membrane insertion and lipid ordering

Our fusion assay experiments indicate that calcium is targeting the fusion peptide and in turn, influencing the membrane fusion process. Because the fusion peptide inserts into the host membrane during the fusion process, we next focused on examining the impact of calcium on this insertion using electron spin resonance (ESR). In this technique, spin labels are incorporated into lipids at various positions, acting as depth probes. Liposomes containing dipalmitoylphosphatidyl-tempo-choline (DPPTC) are spin labeled in the head region whereas those with phosphocholine are labeled in either the upper tail region (5PC) or lower tail region (14PC) (Figure A4). The ordering parameter, S_0, of each spin-labeled lipid was extracted from the ESR spectra using NSSL program with the microscopic order-macroscopic disorder (MOMD) model[78]. S_0 is an indication of the amount of membrane ordering at a given depth and serves as a readout for FP membrane penetration depth[79]. More importantly, FP-induced changes in S_0 are thought to be functionally significant because changes in lipid ordering can lower the energy barrier between closely approaching membranes by dehydration, enabling fusion to occur[80]. Previous ESR studies with other viral FPs, indicate that membrane ordering by the viral FP is a critical step for viral membrane fusion[8,80–82].

The S-shaped curves of S_0 as a function of increasing WT peptide to lipid (P/L) ratio (Figure 2.3a-c) suggest cooperativity in membrane ordering, consistent with the requirement for class I and class II fusion proteins to oligomerize for efficient

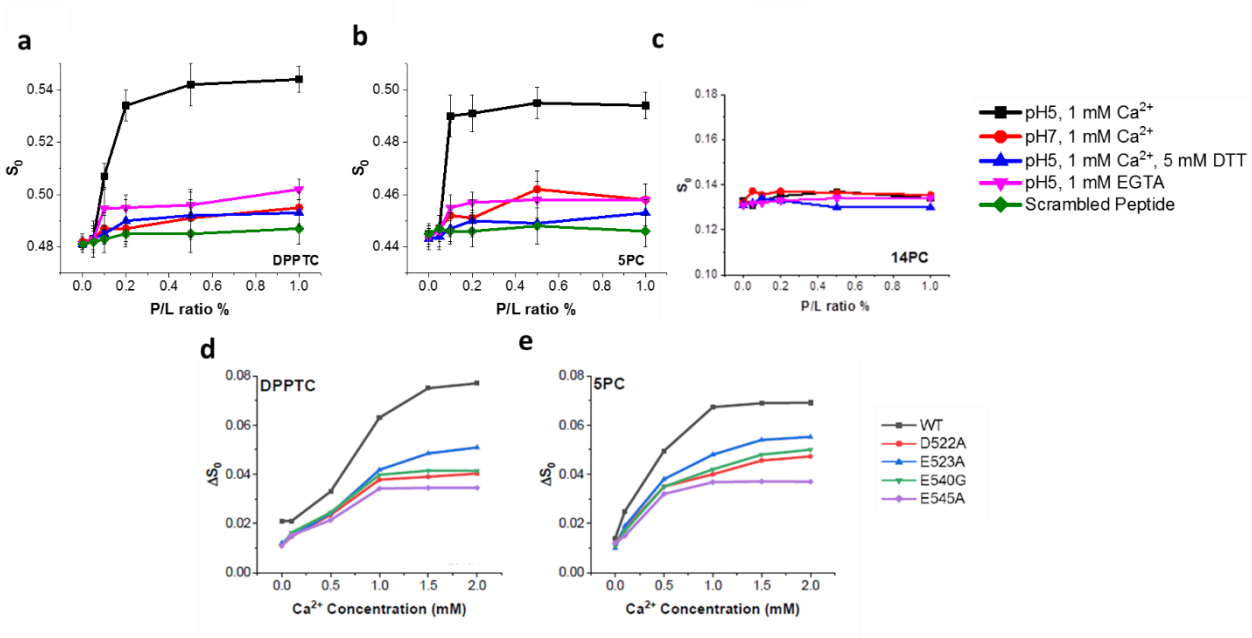

Figure 2.3. ESR spectroscopy shows FP induces membrane ordering in a Ca^{2+} dependent fashion. A-C) Plots of order parameters (S_0) of **a)** DPPTC, **b)** 5PC, **c)** 14PC versus peptide:lipid ratio (P/L ratio) of FP in POPC:POPG:Chol = 3:1:1 MLVs. D-E) the plot of ΔS_0 of **d)** DPPTC and **e)** 5PC versus Ca^{2+} concentration of the WT and mutant FPs at 1% P/L ratio. Each experiment was repeated two to three times. Typical uncertainties found for S_0 are 6×10^{-3} [80].

fusion to occur. The WT peptide was able to induce the most ordering of the head and upper-tail regions at acidic pH with 2 mM Ca^{2+} (Figure 2.3a, b), but the deep hydrophobic region (14PC) was virtually unaffected (Figure 2.3c). The scrambled peptide which has the same residues as the FP but in a shuffled order has no ordering effect on the membrane, indicating the ordering effect is sequence specific. When Ca^{2+} was chelated with EGTA, the WT FP induced little lipid ordering and was similar to our negative control, the FP with the disulfide bond removed by DTT, which had virtually no lipid ordering effect (Figure 2.3a-c).

If Ca^{2+}'s effect on the WT peptide was strictly due to mediating the electrostatic repulsion between the negative lipids and negative charges in the FP, we would expect that when mixed with DTT, the FP would still be able to induce ordering

because the charges of the amino acids have not been altered. The observation that DTT is detrimental to peptide-induced lipid ordering indicates that Ca^{2+} is not simply promoting peptide insertion by screening charge, as has been suggested in other work[40]. To further test the effect of Ca^{2+} on S_0, we increased the Ca^{2+} concentration while fixing the P/L ratio at 1% (Figure 2.3d, e). The direct impact of Ca^{2+} on the FP-induced lipid ordering was accounted for by subtracting S_0 measured when only liposomes and Ca^{2+} were present from S_0 measured when all three components (liposomes, peptides, and Ca^{2+}) were present, yielding ΔS_0. As Ca^{2+} increased, so did ΔS_0, indicating that there is more FP-induced membrane ordering at higher Ca^{2+} concentrations in the lipid head (Figure 2.3d) and mid-tail (Figure 2.3e) regions. Our prior observations of influenza HA, which does not show increased membrane interaction in the presence of Ca^{2+} [8], indicate that Ca^{2+} does not act as a blanket promoter of viral FP insertion into target membranes. ESR measurements of mutant peptides all showed the induction of lipid ordering with increasing P/L ratio, but less than the WT peptide (Figure A6). Chelating Ca^{2+} with EGTA removed the ordering effect for all peptides. Increasing Ca^{2+} increased the FP-induced membrane ordering in head (Figure 2.3d) and mid-tail (Figure 2.3e) regions, but also had less of an effect on the mutated peptides than the WT. Of the mutants tested, D522A and E545A had the least membrane ordering at all Ca^{2+} concentrations tested. These results imply that the ability of the mutated peptides to induce membrane ordering is impaired due to their reduced ability to bind Ca^{2+}.

2.3.5 Ca^{2+} promotes insertion of viral GP into the target membrane

The N-terminal FPs for viruses such as influenza and HIV have only one end anchored to the remainder of the entire fusion protein, so they are easily able to form the functional domain by itself. However, as the GP FP is internal, i.e. both ends connected to the remainder of GP, it is questionable whether the isolated FP functions the same way as that for the entire GP. To address this question, we used the technique of time-resolved ESR to monitor the change of S_0 during fusion of small unilamellar vesicles (SUV) and pseudovirus particles (PP).The PP are pre-treated with thermolysin to remove the glycan cap from GP and when the PP is mixed with the SUV containing DPPTC, the GP FP will insert into the SUV membrane during the docking of the PP on the SUV. If the function of the FP in the entire GP is similar to that of the isolated one, then the membrane ordering effect should be observed. In the time-resolved ESR experiments, we reduced the conversion time and scanning times, which shortened the collection time and allowed collection of the spectra every 30 sec. The noisier signals were denoised using the Wavelet Denoising Package[83] before NLSL analysis if necessary. As shown in Fig. S7a, the shape of the ESR signal changes during the time course, indicating a change of membrane structure. After denoising (Figure A7b), the details of the difference are more obvious. As shown in Fig 4a, the S_0 increases in the presence of Ca^{2+} and at pH5, and the IC_{50} occurs at about 3.5 min. However, when either the Ca^{2+} or the GP is removed, no increase of S_0 is observed. This time dependent S_0 change is also observed at a lower PP:SUV ratio, though the IC_{50} time is longer (Figure A7c). This can be explained as the more GP is available, the more docking events happen. Fig 4b shows the S_0 at 10.5 min versus different ratio of

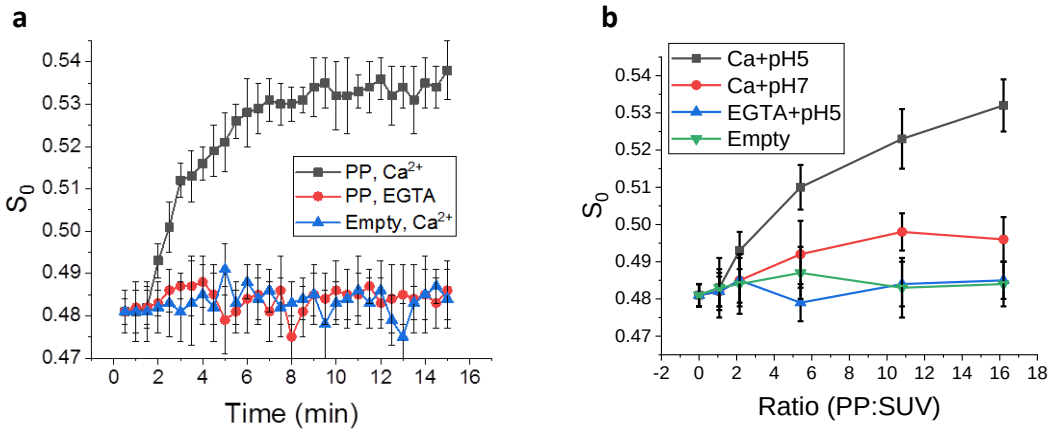

Figure 2. 4 Time-dependent ESR experiments on DPPTC in the pseudoviral particle - SUV interaction. a) The plot of order parameters of DPPTC changes during the time course of measurement. The ratio of PP:SUV is about 15. Black, with 1 mM Ca2+; red, with 1 mM EGTA; blue, using the empty particles instead of the pseudoviral particles. b) the plot of order parameter of DPPTC in different PP:SUV ratios. The order parameters are extracted from the curves collected at 10.5 min after activation.

PP:SUV. The S-shaped pattern similar to the isolated FP cases (Figure 2.3a) is observed also only in the presence of Ca^{2+} and at pH 5. The SUV-PP lipid mixing experiments show very low mixing ratios (Figure A9), indicating no fusion in this condition. Thus, the membrane ordering is due to the docking, not fusion. Put together, the FP-induced membrane ordering is reported in the time-resolved method and in the "biological" system for the first time, which fully supports the hypothesis that the isolated FP functions in the same way as the FP in the entire GP.

2.3.6 Ca^{2+} increases FP helical content

To better understand the structural importance of the negatively charged amino acids on FP conformation, we used circular dichroism (CD) spectroscopy to examine the secondary structures of mutant and WT FPs in membranes with and without Ca^{2+} present (Figure 2.5). In our control condition, where the disulfide bond of the fusion loop is removed by the addition of DTT, the peptide adopts a random coil structure. The WT FP exhibits a well-formed alpha helical structure in the presence of SUV at

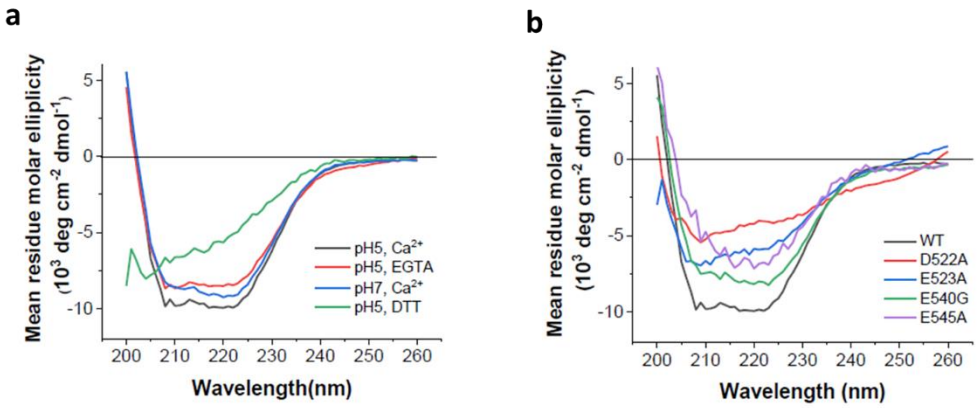

Figure 2.5 CD spectra of EBOV FPs show that Ca^{2+} and mutation of negatively charged residues alters FP structure. a) WT FPs at acidic or neutral pH and +/- Ca^{2+}. **b)** Mutated FPs at pH 5, 1 mM Ca^{2+} and WT (black) for reference. Two to three spectra were collected independently for each sample; representative spectra are shown.

pH 5 in 1 mM Ca^{2+}(22.7 ± 1.8 %). At higher pH with Ca^{2+}, there is a decrease in helical content (12.1 ± 2.2 %). When Ca^{2+} is chelated by EGTA at pH 5, the helical content is even lower (10.8 ± 1.7 %). All mutants exhibit less helical structure than the WT, indicating that these negatively charged amino acids are important for maintaining the structure of the FP. The mutant E545A exhibits the least helical structure, indicating E545 is important for maintaining the FP structure. When interacting with lipid bilayers, the mutants have a less well- formed secondary structure. Combined with our functional studies, these results indicate that Ca^{2+} influences FP structure, which impacts its interaction with membranes, and thereby its membrane fusion function.

2.4 Discussion

The direct role of Ca^{2+} in Ebola virus fusion has not previously been identified, although there have been previous links between potential therapeutics and intracellular Ca^{2+} levels. Screens of potential filovirus therapeutics indicated that ion

channel inhibitors, such as amiodarone, dronedarone, bepridil, lomerizine, verapamil, and tetrandrine[57,75,84], and drugs that induce Ca^{2+} efflux from endosomes, such as U18666A, tamoxifen, and clomiphene[76], are able to inhibit EBOV infection. Expression of the endosomal EBOV receptor, NPC1, is also linked to Ca^{2+} levels in the endosomal lumen. Removal of NPC1 results in Ca^{2+} depletion in late endosomes and lysosomes[85], in addition to blocking EBOV entry[63,65]. Sakurai et al. demonstrated that blocking or knocking out the calcium transport channel TPC2 can also inhibit infection of Ebola virus[75]. The anti-EBOV nature of these Ca^{2+} inhibiting drugs agrees with our results and indicates that further development of similar therapeutics may be fruitful. Our studies indicate that from a therapeutic standpoint, modulation of both extracellular and intracellular Ca^{2+} are attractive targets.

We identified residues D522 and E540 as key players in the dependence of Ebola virus infection on Ca^{2+}. Mutation of other nearby negatively charged residues did not alter calcium dependence, indicating that D522 and E540 play specific roles in interaction with the ion, rather than calcium dependence being driven by the overall charge of GP. Previous studies of E523 and E540 found these residues to be detrimental to fusion in the context of the hydrophobic core fusion peptide alone[86]. In ESR, the "long" FP, which extends beyond the core and includes the disulfide bond, is more efficient in inducing membrane ordering than the short hydrophobic core alone (Figure A5), indicating that the larger context of these residues within the peptide is functionally important. Our work with a longer peptide clarifies the roles of these residues in mediating FP conformation and interaction with Ca^{2+} as well as their effect on virion infectivity. Others have observed reduced binding of the mutant D522A to

the membrane proximal external region of GP.[87] Our work links this mutation to reduced interaction with Ca^{2+} and thereby reduced fusion competence due to alteration in the direct interaction of the FP with the membrane, adding new insight into the role of D522 in fusion. Given that D522 and E540 are implicated in Ca^{2+}-dependent entry of EBOV and that negative residues at those sites are conserved across *Filoviridae*, Ca^{2+}-targeting drugs might be effective against all viruses within the family. Indeed, the drugs toremifene and clomiphene increase Ca^{2+} release from endosomes[76] and are able to inhibit multiple strains of both EBOV and MARV[56].

As the endosome matures, the endosomal membrane becomes enriched with anionic lipids[88]. Others have observed that negatively charged lipids are necessary for partitioning of the Ebola FP into the target membrane[86] and suggested that calcium alters the hydrogen-bonding network at the surface of the membrane rather than targeting the fusion peptide itself.[40,86] Our spectroscopic data combined with our mutant studies suggest a wholly orthogonal mechanism. Our work shows that the conformational changes in FP are due to its interaction with the ion, which we further show leads to specific changes in lipid ordering in the host membrane and an increase in fusion activity. Our work thus sheds further insight into how these conformational changes are functionally important within the context of viral fusion and entry and links these biophysical observations to the mechanism that enables Ca^{2+}- perturbing drugs to inhibit filovirus infection. As pH decreases, the FP forms an alpha-helical fist-like structure[68]. Our studies indicate Ca^{2+} may act to stabilize or promote that alpha-helical structure. This results in higher extents of fusion as Ca^{2+} concentration

increases, aligned with higher levels infection of the virus in the presence of both extracellular and intracellular Ca^{2+}.

Our previous ESR work with the FPs of influenza virus, HIV (both are N-terminal FP of class I glycoproteins), and dengue virus (an internal FP of a class II glycoprotein) suggested that FP- induced membrane ordering is a result of dehydration due to FP insertion, which is a prerequisite step for reducing repulsive forces between two opposing membranes to initiate membrane fusion[80,89]. Our current study extends these concepts to the Ebola FP, an internal FP within a class I glycoprotein. We show that Ebola FP also induces membrane ordering, while the functionally impaired mutated peptides have significantly lower membrane ordering capacity. This result upholds the theory that membrane ordering induced by the FP is a common prerequisite for viral entry. Taken together, the Ca^{2+} dependent EBOV FP conformational changes, membrane ordering effect, and subsequent modifications in fusion activity found here point to the FP being at least one of the direct targets of Ca^{2+} in entry of EBOV.

Blocking two-pore channels (TPC2), which are involved in calcium efflux from the endosome[90], inhibits Ebola infection[44]. Perhaps when the channels are functional, they create a locally high concentration of calcium near the membrane, encouraging fusion and thereby infection. However, the exact role of TPC2 in Ebola infection remains unclear.

In our studies, low pH and calcium seem to act synergistically to promote insertion of GP into the target membrane. During endosomal maturation, the concentration of calcium within the endosome initially drops from 2 mM

extracellularly to 3 μM[91] within the early endosome. However, the calcium concentration then goes back up to 400-600 μM[92] as lysosomes merge with late endosomes. Simultaneously, the pH drops from 6.8 in the early endosome to 4.8 in the late endosome[93]. Given that Ebola virus fuses in late endosomes[62,66], after binding NPC1 the virus may undergo fusion in response to these dual environmental cues of low pH and high calcium. Our ESR studies with both fusion peptide and pseudovirus indicate that low pH and calcium together promote insertion of the fusion peptide. We saw little lipid mixing between pseudovirus and liposomes, indicating that even with the glycan cap removed from GP an additional factor beyond low pH and Ca^{2+}, such as NPC1 binding, is needed for insertion of the fusion peptide into the host membrane to progress to full fusion.

Ca^{2+} has been implicated in the fusion of a few other enveloped viruses. Rubella virus, which utilizes the class II fusion protein E1, depends on Ca^{2+} for proper orientation of its fusion loops[7]. Specifically, Ca^{2+} coordinates with the residues N88 and D136 located on adjacent fusion loops within E1. Previously we showed that viral entry of severe acute respiratory syndrome coronavirus (SARS) is Ca^{2+} dependent, and the FP cannot induce membrane ordering when chelator is present[8]. Our work adds to this nascent understanding of the role of Ca^{2+} in viral fusion, and points to Ca^{2+} as an attractive host factor for antiviral therapeutic intervention.

2.5 Methods

2.5.1 Peptides

The EBOV FP was expressed using a vector developed by the Tamm Lab[68]. The mutant FPs were generated using a USB Change-IT site directed mutagenesis kit (Affymetrix). The protocol of expression and purification also follows published procedures[68]. Briefly, the relevant plasmids were transformed in BL21(DE3) *Escherichia coli* competent cells and grown at 37 ˚C to an optical density ~0.8. Protein expression was induced for 3 hours at 30˚C by 0.5 mM IPTG. The harvested cells were lysed by sonication and clarified by centrifugation at 40,000 rpm for 45 minutes. The supernatant containing the His-tagged fusion protein was transferred to a pre-equilibrated Ni-NTA agarose resin column, and the supernatant and resin were incubated for 2 hours at 4 ˚C on a rotator in wash buffer (containing 25 mM Tris, 500 mM NaCl, 20 mM Imidazole, 5% glycerol, 5 mM β-ME, and 10 mM CHAPS, pH 8). The resin was then rinsed with digestion buffer (containing 25 mM Tris, 50 mM NaCl, 5 mM $CaCl_2$, and 5% glycerol, pH 7.5). 125 µL of Factor Xa (1 mg/mL) in 15 mL digestion buffer was added to the resin and incubated overnight at room temperature. The proteins were eluted using 50 mL wash buffer, dialyzed against dialysis buffer (25 mM Tris, 50 mM NaCl, 5% Glycerol, pH 8.5), and purified using a Superdex Peptide 10/300 GL gel-filtration column (GE Healthcare).

2.5.2 Cell lines and plasmids.

HEK 293T (accession no: CRL-11268, ATCC) cells and Vero E6 cells (accession no: CRL-1586, ATCC) were grown in complete DMEM [DMEM with 10% fetal bovine serum (FBS) , 100 U/mL penicillin, 10 µg/mL streptomycin , and 1

% HEPES]. Cells were maintained at 37°C, 5% CO_2. pcDNA3.1-EBOV-GP (BEI Resources) encodes Zaire ebolavirus GP. The mutations D522A, E523A, E540G, E545A, and D522A/E523A were produced by site directed mutagenesis of pcDNA3.1-EBOV-GP using the QuickChange XL site-directed mutagenesis kit (Agilent) with primers designed using the Agilent online tool.

2.5.3 Lipid and vesicle preparation

The lipids POPC, POPG, and the chain spin labels 5PC and 14PC and a head group spin label dipalmitoylphosphatidyl-tempo-choline (DPPTC) (Fig. S4) were purchased or synthesized by our laboratory. The composition of membranes used in this study is consistent with our previous study[89]. The desired amount of POPC, POPG, cholesterol and 0.5% (mol:mol) spin-labeled lipids in chloroform were mixed well and dried by N_2 flow. The mixture was evacuated in a vacuum drier overnight to remove any trace of chloroform. To prepare MLVs, the lipids were resuspended and fully hydrated using 1 mL of pH 7 or pH 5 buffer (5 mM HEPES, 10 mM MES, 150 mM NaCl, pH 7 or pH 5) at room temperature for 2 hours. To prepare SUVs for CD measurements, the lipids were resuspended in pH 5 buffer and sonicated in an ice bath for 20 minutes or when the suspension became clear. The SUVs solution was then further clarified by ultracentrifugation at 13,000 rpm for 10 min.

2.5.4 Sequence analysis

Sequences of *Filoviridae* spike proteins were aligned using CLUSTAL with Geneious software and the following UniProt accession numbers: Zaire ebolavirus: Mayinga-76 (Q05320), Gabon-94 (O11457), Eckron-76 (P87671), Kikwit-95 (P87666), Reston ebolavirus: Reston-89 (Q66799), Philippines-96 (Q91DD8),

Siena/Philippine-92 (Q89853), Uganda-00 (Q7T9D9), Sudan ebolavirus: Boniface-76 (Q66814), Maleo-79 (Q66798), Taï Forest ebolavirus: Cote d'Ivoire-94 (Q66810), Lake Victoria marburgvirus: Musoke-80 (P35253), Ozolin-75 (Q6UY66), Popp-67 (P35254), Ravn-87 (Q1PDC7), Angola/2005 (Q1PD50), Lloviu cuevavirus isolate Bat/Spain/Asturias-Bat86/2003 (G8EFI5), and Bundibugyo ebolavirus (R4QRC0).

2.5.5 Pseudotyped virus production

Pseudotyped viruses were produced following published protocols [94,95]. Briefly, particles were produced by transfecting HEK 293T cells with plasmids encoding for luciferase, Murine Leukemia Virus gag and polymerase, and the viral spike protein of interest using Lipofectamine 2000 following the manufacturer's instructions. Supernatant was harvested 48 h post-transfection, filtered through a 0.45 μm membrane, and stored at -80 °C. To remove the glycan cap, pseudovirus particles were pelleted by ultracentrifugation at 42000 rpm, 4°C, for 2h in a TLA 55 rotor (Beckman Coulter), the resuspended in a buffer (50 mM Tris, 10 mM $CaCl_2$, 150 mM NaCl, 0.05% Brij, pH 7.3) containing 0.167 mg/mL thermolysin. The particles were then placed at 37°C overnight. Removal of the glycan cap was confirmed by Western Blot (Fig. S8), and is consistent with published literature[60].

2.5.6 Infection

Vero E6 cells were seeded at 5×10^5 cells/mL in a 24-well plate. Twenty-four h after seeding, cells were rinsed three times with Ca^{2+}-free PBS then incubated with 200 μL of pseudotyped virus and 300 μL RPMI supplemented with 0.2% BSA and 10 mM Hepes, at pH 7 on ice at 4 ˚C with rocking for 1.5 h. Cells were washed with Ca^{2+}-free PBS to remove unbound viral particles, and incubated at 37˚C for 2 h in 200

μL of DMEM with the specified concentration of Ca^{2+} for internalization. Complete DMEM with 20 mM NH_4Cl was added to the cells to block further infection and 48 h later luciferase activity was measured using the Luciferase Assay System (Promega) and Glomax 20/20 luminometer.

2.5.7 BATPA-AM treatment

Vero E6 cells were seeded at 5×10^5 cells/mL in a 24-well plate. Twenty-four h after seeding, cells were pre-treated with 50 μM of BATPA-AM or an equivalent volume of DMSO diluted in DMEM with 2% FBS for 1 h at 37 ˚C. Cells were then infected with 200 μL of pseudotyped virus at 37 ˚C in the presence of 50 μM of BATPA-AM or an equivalent volume of DMSO. After 2 h, complete DMEM was added and the cells were incubated for 72 h. Luciferase activity was measured as described above.

2.5.8 Lipid mixing assays

Fluorescently labeled LUVs (2.5 μM, final concentration) containing 1% 7-nitrobenz-2-oxa-1,3- diazole (NBD)-egg-POPE and 1% Rhodamine-egg-POPE) and unlabeled LUV (22.5 μM, final concentration) were mixed in 1 mL of pH 5 buffer. Fusion peptides were then added from concentrated stock solutions to give a 1 μM final concentration of each peptide. 10% Triton X-100 was added to achieve a 1% final concentration after fusion reactions were completed. The fluorescence spectra were collected on a Varian Cary Eclipse Fluorescence Spectrometer. Fluorescence intensities of the samples before addition of fusion peptides and after the addition of Triton X-100 were used to set the baseline (0%) and 100% fusion levels, respectively. The fluorescence yields of the experimental samples were normalized to these levels

to determine % lipid mixing. Fluorescence intensity variations due to volume changes were corrected in each case. All experiments were performed at least 3 times and representative curves are shown.

2.5.9 Electron spin resonance (ESR) spectroscopy and nonlinear least-squares fit of ESR spectra

To prepare the samples for lipid ESR study, a stock solution of the Fusion Peptide (FP) (1 mg/mL) was added to the lipid POPC:POPG:Chol=3:1:1 MLV dispersion (above) at the experimentally indicated ratios. After 20 min of incubation, the dispersion was centrifuged at 13,000 rpm for 10 min. The pellet was transferred to a quartz capillary tube for ESR measurement. For the SUV-PP interaction, SUV was prepared by sonication, and the concentration of the SUVs and PP are determined using a Nanosight. Desired ratio of vesicles were mixed then acidified immediately before the acquisition. ESR spectra were collected on an ELEXSYS ESR spectrometer at X-band (9.5 GHz) at 25 ˚C using a N2 Temperature Controller). The ESR spectra from the labeled lipids were analyzed using the NLLS fitting program based on the stochastic Liouville equation[78] using the MOMD (Microscopic Order Macroscopic Disorder) model as in previous studies[8,78,96]. The fitting strategy is the same as previously reported[80]. S_0 is defined as follows: $S_0=<D_{2,00}>=<1/2(3\cos2\theta-1)>$, where $D_{2,00}$ is the Wigner rotation matrix elements and θ is the polar angle for the orientation of the rotating axes of the nitroxide bonded to the lipid relative to the director of the bilayer, i.e. the preferential orientation of lipid molecules and the angular brackets imply ensemble averaging. S_0 indicates how well the chain segment to which the nitroxide is attached, is aligned along the normal to the lipid bilayer.

2.5.10 Circular dichroism spectroscopy (CD)

Fusion peptides (0.2 mg/mL in pH 5 solution) were mixed with SUVs composed of POPC:POPG:Chol=3:1:1 at a ratio of 1:100 peptide:lipid at room temperature for 10 min before measurement. The CD spectra were collected at 25 ˚C on an AVIV Model 202-01 Circular Dichroism Spectrometer. The signals from pure SUVs or pure solution were subtracted from the sample spectra as blanks. The CD spectra were analyzed using K2D3[97].

2.5.11 Statistical analysis

Exact numbers of replicates are defined in each figure legend. All p-values were determined using a two-tailed Student's t-test unless otherwise noted in the figure legend. All error bars indicate standard deviation among independent experiments.

2.6 Acknowledgements

The authors of this work are Lakshmi Nathan, Alex L. Lai, Jean Kaoru Millet, Marco R. Straus, Jack H. Freed, Gary R. Whittaker, and Susan Daniel. L.N, S.D, and G.R.W conceived the project, L.N., A.L.L., J.K.M, S.D., and G.R.W. designed research; L.N., A.L.L., and M.R.S. performed research; L.N., A.L.L., J.H.F., S.D., and G.R.W. analyzed data; and L.N., A.L.L, S.D, and G.R.W wrote the paper.

L.N. would like to thank Tiffany Tang and Dr. Judith White for helpful discussion. The plasmid pcDNA3.1 containing the sequence for Ebolavirus, Zaire Glycoprotein, NR-19814 was obtained through the Biodefense and Emerging Infections Research Resources Repository, National Institute of Allergy and Infectious

Diseases, National Institutes of Health. Molecular graphics were generated with the Chimera package developed by the Resource for Biocomputing, Visualization, and Informatics at the University of California, San Francisco (supported by the National Institute of General Medical Sciences P41-GM103311). L.N. acknowledges support from a Samuel C. Fleming Family Graduate Fellowship and National Science Foundation Graduate Research Fellowship Program under Grant No. DGE-1650441. A.L.L. acknowledges Dr. Lukas Tamm and Dr. Sonia Gregory for the Ebola FP construct plasmid and advice. A.L.L. also acknowledges Dr. Brian Crane and Dr. Richard Cerione for access to instrumentation. This work is supported by National Science Foundation 1504846 (to S.D. and G.R.W.) and National Institutes of Health P41GM103521 and R01GM123779 (to J.H.F.). Any opinions, findings, and conclusions or recommendations expressed in this material are those of the author(s) and do not necessarily reflect the views of the National Science Foundation.

CHAPTER 3

SINGLE VIRION TRACKING MICROSCOPY FOR THE STUDY OF VIRUS ENTRY PROCESSES IN LIVE CELLS AND BIOMIMETIC PLATFORMS

3.1 Abstract

The most widely-used assays for studying viral entry, including infectivity, cofloatation, and cell-cell fusion assays, yield functional information but provide low resolution of individual entry steps. Structural characterization provides high-resolution conformational information, but on its own is unable to address the functional significance of these conformations. Single virion tracking microscopy techniques provide more detail on the intermediate entry steps than infection assays and more functional information than structural methods, bridging the gap between these methods. In addition, single virion approaches also provide dynamic information about the kinetics of entry processes. This chapter reviews single virion tracking techniques and describes how they can be applied to study specific virus entry steps. These techniques provide information complementary to traditional ensemble approaches. Single virion techniques may either probe virion behavior in live cells or in biomimetic platforms. Synthesizing information from ensemble, structural, and single virion techniques ultimately yields a more complete understanding of the viral entry process than can be achieved by any single method alone.

3.2 Overview of virus entry

Viruses can be broadly classified as non-enveloped or enveloped. Non-enveloped viruses are encapsulated by a protein coat, called a capsid, while enveloped viruses are encapsulated in a host-derived lipid membrane implanted with viral proteins called spikes. The coat protein of non-enveloped viruses and spike proteins of enveloped viruses facilitate the virus's entry into the cell. These viral proteins engage receptors on host cells to promote attachment to the host cell surface, but after that initial binding event, non-enveloped and enveloped viruses breach host cell membranes through different pathways[98]. Non-enveloped viruses typically enter cells by endocytosis and then either lyse the intracellular compartment, or release genetic material through a pore created in the membrane of the intracellular compartment[99,100]. Enveloped viruses, on the other hand, must undergo membrane fusion with a cellular membrane to release their genetic material into the host cell (Figure 3.1.). Some enveloped viruses, like coronaviruses or human immunodeficiency virus (HIV), can undergo fusion at the plasma membrane (A), while others, like influenza, fuse within endosomes (B)[6].

Binding and uncoating of nonenveloped viruses is mediated by the capsid surface or capsid proteins projecting from it. For enveloped viruses, the fusion or spike proteins embedded in the envelope are responsible for both receptor binding and membrane fusion. Membrane fusion proteins can be subdivided into three categories based on their structure [5]. Class I fusion proteins are primarily α-helical, Class II fusion proteins contain mainly β-sheets and β-strands, and Class III fusion proteins

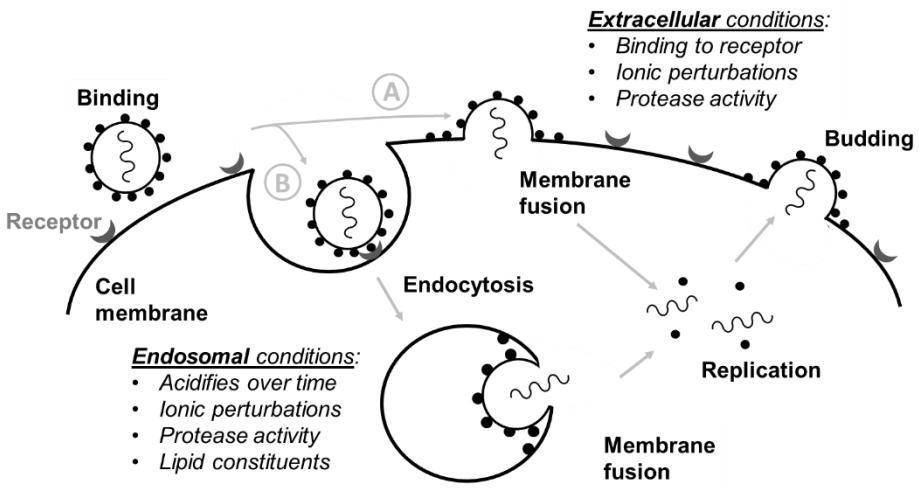

Figure 3.1. Overview of the life cycle of an enveloped virus. The entry process begins with the virus binding to a receptor on the surface of the cell. This binding may result in A) release of the viral genome via fusion at the plasma membrane or B) uptake by endocytosis or macropinocytosis (not shown) followed by fusion within the endosome. The location and mechanism of fusion can be impacted by environmental conditions, including pH, ions, protease activity, and lipid composition. Once the genome has been released into the cytosol, it can access cellular machinery, leading to replication of the viral genome and synthesis of new viral proteins. Newly synthesized virions can then exit the cell by budding.

contain a mix of both α-helices and β-sheets. Class I and II fusion proteins require a proteolytic priming event to convert them from a fusion-incompetent state to a fusion-competent one. Once the fusion protein is in a fusion-competent state, the structural rearrangement necessary for exposure of the fusion peptide and its burial into the target membrane is often triggered by some change in environmental conditions. Fusion may be triggered by receptor binding itself, lowering of pH, protease action [101], or a combination of these [6,102]. Viruses that fuse at the plasma membrane may be triggered by receptor binding or protease activation, while those that fuse within the endosome generally require low pH and may require other additional cues, such as changes in other ions than protons, or endosome-specific protease exposure.

Despite the diversity in structure and triggering mechanisms, fusion proteins typically follow a common pathway for merging the viral envelope with the host

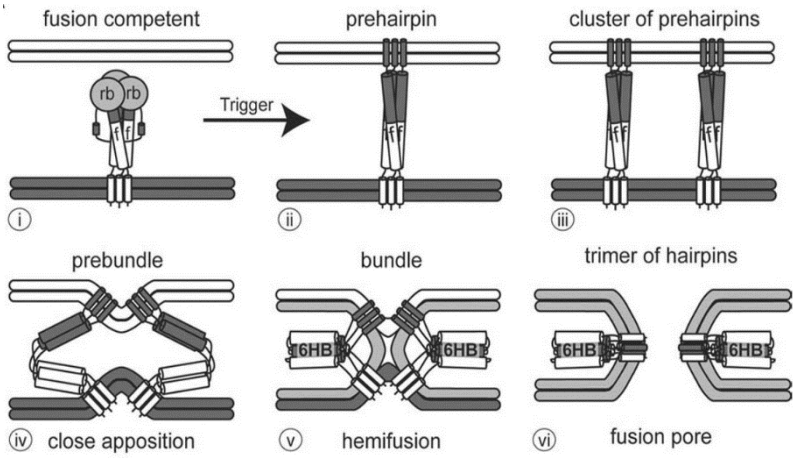

Figure 3.2 Steps in viral fusion. i) The viral envelope (bottom) approaches the target membrane (top). The viral fusion protein consists of a receptor binding domain (rb) and a fusion domain (f). ii) The prehairpin structure embeds into the target membrane. iii) Several prehairpin trimers cluster together. iv) The prehairpins begin to fold back to form the prebundle state and bring the membranes close together. v) Fusion proteins further fold into a six helix bundle (6HB). Lipids in the outer leaflets of the viral and target bilayers mix during hemifusion. vi) A pore opens between the target membrane and the viral envelope as the fusion proteins become a trimer of hairpins. Source: White et al. 2008, Taylor & Francis Ltd, www.tandfonline.com

membrane (Figure 3.2), as described in White et al. 2008 and Harrison 2015. After fusion is triggered, the protein rearranges into a prehairpin intermediate (ii) with the fusion peptide inserted into the host membrane. While the fusion protein may be found as dimers or trimers on the surface of the virus (iii), the prehairpin intermediate consists of a trimer. It is thought that several prehairpin intermediates cluster together then fold back on themselves to bring the membranes close to each other (iv). As the prehairpins fold into a six-helix bundle, the membranes are brought close enough that lipids from their outer leaflets are able to mix, creating a structure often referred to as a “stalk” (v). This step is known as hemifusion. Lastly, a pore forms (vi) enabling the viral genome to pass through this opening as the fusion proteins form into a stable trimer of hairpins.

Although all viral fusion proteins studied to date follow this common pathway, much remains unknown about viral entry itself. For example, the dynamics of these fusion steps are not fully understood, the fusion trigger of some viruses remains ambiguous, and developing antivirals to halt virus entry requires further characterization of all of the steps between initial viral contact with the host cell and viral genome release.

Techniques for studying virus entry can be broadly classified as those that examine the entry of a collective group or ensemble of virions and those that track individual virion entry. Ensemble methods provide information on the broader context of entry steps, while single virion imaging provides detailed information on the dynamics of those steps. Ensemble methods include many of the most well-established techniques for studying viral entry and may probe overall infection, receptor binding, fusion, or cargo transfer. Single virion imaging techniques can provide mechanistic detail and kinetics for steps that are masked in ensemble methods. In addition, for HIV [104], influenza [105], and Ebola virus [66], most virions that encounter a cell are not involved in productive entry so the ability of single virion techniques to distinguish entry-competent particles from non-competent ones and characterize their individual behavior provides valuable data on heterogeneity in viral populations and its ultimate impact on infection.

The remaining part of the chapter will focus on single particle tracking microscopy techniques compatible with dynamic/temporal data acquisition, their salient features, and how the data generated complement ensemble methods for studying viral entry processes and their intermediate steps and mechanisms.

3.3. Single Virion Tracking Techniques

3.3.1 Enabling technologies

Over the past 30 years, microscopy optics, fluorescent labeling strategies, computing power and image processing have enabled the dynamic tracking of individual virions throughout the entry process and the decomposition of their intermediate steps. For some examples see the following references: [106–112]. In particular, charge coupled device (CCD) cameras combined with advanced microscopy enable single particle resolution [113]. The frame rates of today's cameras dictate temporal resolution of dynamic studies, which can range from a few to hundreds of milliseconds [114,115]. In the following sections, the main advances enabling single virion tracking techniques are summarized.

3.3.1.1 Microscope configurations

Three microscopy configurations are commonly employed in virology research: epifluorescence, total internal reflection fluorescence (TIRF), and confocal microscopy [116,117]as illustrated in Figure 3.3.

The epifluorescence configuration (Figure 3.3 A, D) illuminates everything within the field of view. So, unbound virions in the bulk phase or cells with high background autofluorescence result in high noise that obscures signals from individual virions. As a result, epifluorescence is not typically used for single virion tracking. In the TIRF configuration (Figure 3.3 B, E), only particles within a shallow field are illuminated, eliminating noise from the bulk solution and thereby enhancing the signal-to-noise. This configuration is achieved by setting the incidence angle of the laser to be higher than the critical angle for total internal reflection of the laser light at

the glass/water or glass/cell interface, resulting in an exponentially decaying evanescent field that penetrates roughly 100 nm into the sample [118,119]. The advantage with this configuration is that a two-dimensional plane can be monitored precisely, enabling the distinction between binding and fusion events of the virions, with appropriate virion labeling (described next). However, no three dimensional tracking information can be obtained; data collection is confined to the interfacial region of interest. This configuration is most suitable for examination of virus behavior at biomimetic surfaces like supported lipid bilayers or live cell plasma membranes close to the glass surface.

In the confocal microscopy configuration (Figure 3.3 C), a pinhole optic assists in filtering out background noise while scanning across a sample one Z-plane at a time. Cross sections may be stacked to yield a three-dimensional image, making this configuration suitable for imaging live or fixed cells and observing trafficking of viruses in the cytosol. The disadvantage of this configuration is the difficulty in temporally tracking phenomena in real-time, while simultaneously scanning across slices of the sample and reconstructing the image. Furthermore, exposure to strong light can be toxic to living cells [120]. As technology advances, these drawbacks should subside.

3.3.1.2 Virion labeling

In all of these microscopy techniques, virions must be labeled to visualize them. Virions are commonly labeled by attaching fluorescent proteins to viral proteins, by incorporating chemical dyes into the virion, or by incorporating quantum dots[121–123]. Here, we focus on fluorescent and chemical labels; for a review of quantum dot

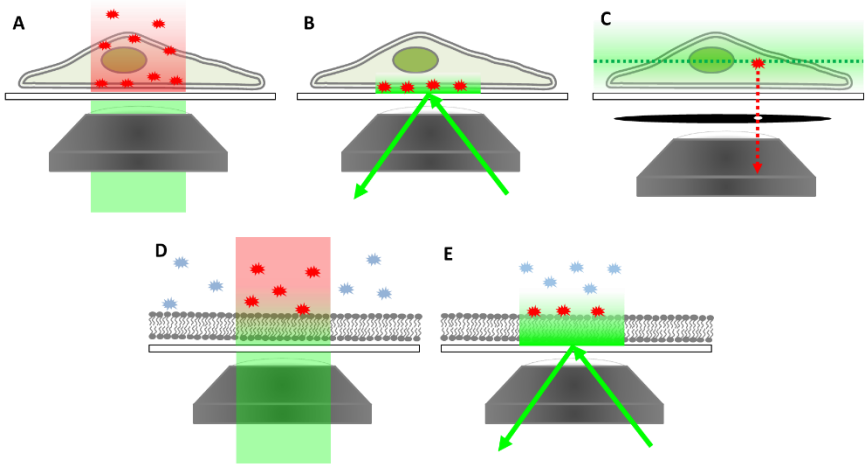

Figure 3.3. Microscope configurations for viewing virus interactions with cells and biomimetic membrane surfaces. Green color denotes excitation light and red denotes emission light. (A) The epifluorescence configuration illuminates an entire light path through the cell and excites any fluorophores within it, making it impossible to track virions in live cells this way due to the overall background signal. (B) TIRF microscopy illuminates a thin layer near the interface between the glass microscope slide and buffer solution. Cell membranes residing in this zone with fluorescently labeled virions can be visualized as individuals, provided they are far enough apart from each other. (C) Confocal microscopy with a pinhole arrangement can examine specific Z-planes within the cell and block out nearly all background signals from the surrounding media excited by out-of-plane light. Here, the green dashed line denotes the focal plane of excitation, the green gradient denotes out-of-plane light, and the red star and its dashed line arrow indicate only the emission from this fluorophore travel to the camera. (D) Epifluorescence illumination in the biomimetic platform suffers the same poor background issue as whole cells when fluorescently labeled virions are in the bulk. (E) TIRF microscopy enables individual virion visualization bound to the membrane surface without exciting those in the bulk above it.

techniques we refer the reader to Liu et al. 2016. Both fluorescent proteins and chemical labels have been used to label viral coatings as well as contents. Fluorescent viral protein constructs can be prepared for enveloped [124] or non-enveloped viruses [125,126] and virions are labeled as they are synthesized. Chemical labels, including Alexa dyes, octadecylrhodamine B (R18), and carbocyanine perchlorates (DiD, DiI, or DiO) may be added during virion synthesis or post-production. Some chemical labels, like lipophilic dyes, are only suitable for labeling enveloped viruses while others, like amino-reactive dyes, may be employed with either enveloped or non-enveloped virions[117].

Membrane hemifusion is typically monitored with lipophilic dyes that undergo dequenching when the virion fuses with the target membrane, while pore formation is typically tracked with a dye that can partition into the capsid and then dissipate upon release from the virion[127,128]. It is also possible to incorporate pH sensors into the envelope of virions to measure the pH of the fusion environment[129]. In all cases, care must be taken to ensure that labeling does not adversely impact viral infectivity. This can be easily assessed by conducting cell infectivity assays with labeled virions. In general, these labeling approaches can be optimized to mitigate any significant negative impact.

3.3.1.3 Image processing

Once the microscopy configuration and virion labeling method have been chosen, image processing assists in extracting information from the images. Today's fast computers and image processing algorithms assist in noise filtering, virion tracking, and trajectory mapping, as described in the references that follow. In single virion imaging, noise is always a primary concern, regardless of the microscope configuration. To combat this, several particle detection and image restoration techniques have been developed specifically for single virion tracking[130,131]. Coordinates of the particles are obtained by scanning filtered images for areas of fluorescence intensity that exceed a certain threshold or fit a particular intensity profile [132,133]. The next challenge is obtaining accurate virion tracking from one frame to the next (temporal trajectories). Particle trajectories can be calculated from nearest-neighbor associations [114,134]. Measurements of virion movement and mean squared displacements are then used to determine whether the virions exhibit directed, normal,

or anomalous diffusion [135]. The diffusion type can indicate the type of interactions the virion is having with the surface of the cell or extracellular environment. Tracking frame-to-frame is important in measuring binding residence times as well, and by extension, binding strength characteristics [130]. Once bound, the progression of membrane fusion can be tracked from frame-to-frame using strategies like fluorescence dequenching, where the evolution of the fluorescence signal reports on the merging of membranes, the rate of membrane mixing, and the release of viral genome. Finally, obtaining good statistical data from virion tracking experiments requires collecting data on hundreds of individual virions.

3.3.2 Experimental approach

Single virion tracking may follow virions through the infection process in live cells using confocal microscopy or within an in vitro biomimetic platform using TIRF microscopy. Cell-based virion imaging techniques enable direct visualization of the viral entry pathway and interactions between virions and host cell machinery within the native complexity of the cellular environment. On the other hand, biomimetic platforms utilizing the TIRF configuration enable observation of membrane surface phenomena and can be integrated with tools like microfluidics that allow the user to define and test a tightly controlled environment. This control enables decoupling of factors that may be hard to detangle in vivo. Sections 2.2.1 and 2.2.2 provide overviews of these two approaches while Section 3 provides examples of specific implementations of single virion tracking to the investigation of viral entry and contrasts them with ensemble approaches.

3.3.2.1 Live cell imaging

In current cell-based fluorescence assays, both virions and cellular components are fluorescently labeled so their interactions can be tracked with multicolor real-time microscopy. Live cell virion tracking can be used to observe cell-cell spread, receptor binding, intracellular trafficking and membrane fusion. Virions may be labeled with fluorescent proteins, chemical dyes, or quantum dots while intracellular components are typically labeled using fluorescent proteins. Epifluorescence, TIRF, and confocal microscopy have all been used in live cell single virion tracking. Virions may be tracked in two or three dimensions depending on the microscope configuration, as described above. Certain cell types may be easier to image due to autofluorescence of cellular components [66].

As early as the 1980s, fusion of individual virions at the plasma membrane surface was observed. Virions were labeled with R18, which self-quenches at high concentrations, and dequenching of the R18 upon fusion of the virion with a membrane was detected by a simple fluorescence microscope. Early assays monitored fusion at the plasma membrane of erythrocytes, where fusion of influenza could be triggered by lowering the pH [136,137].

An important aspect of live cell approaches is that it is possible to inhibit cellular machinery by drug treatment or gene knock-out. Such cells can be used in combination with live cell imaging to identify key cellular components that are necessary for virus entry. A review of implementations and insights gained from live cell single virion imaging will be provided in Section 3. We also recommend the reviews in references [109,115–117,121].

3.3.2.2 Biomimetic platforms

In early work, perhaps the first, observations of membrane fusion of individual virions to biomimetic membranes was monitored with video fluorescence microscopy [138,139]. In this work, planar bilayers were suspended over a small hole in a Teflon sheet, a so-called black lipid membrane (BLM), to serve as the host cell membrane mimic. However, BLMs are fragile and prone to rupture and continued progress using this approach was slow. In recent years, supported lipid bilayers, which are more robust than BLMs, have become more widely used in in vitro single virion tracking experiments. Because these SLB platforms are becoming the backbone of many types of single virion tracking experiments, it is worth describing them in some detail here. A supported lipid bilayer is a planar, single bilayer, typically self-assembled by rupturing liposomes at the surface of hydrophilic silica surfaces like glass microscope slides. For reviews of supported lipid bilayer technologies, we encourage the reader to consult Sackmann 1996, Tanaka and Sackmann 2005, and Castellana and Cremer 2006. These supported lipid bilayers act as mimics for cellular membranes and the

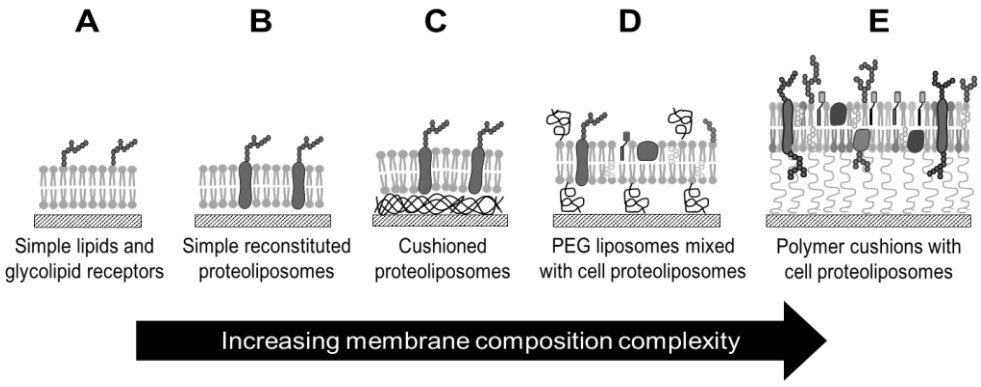

Figure 3.4. Supported lipid bilayers (SLBs) and their increasing complexity and features. (A) A simple SLB with glycolipid receptors. (B) A SLB made from reconstituted lipids and protein receptors. (C) Cushioned SLB to enhance protein receptor mobility. (D) Mixed liposome and cell-derived SLB containing polyethylene glycol cushions. (E) Plasma membrane-derived SLB on polymer cushion.

compatibility of these bilayers with flat glass surfaces makes them ideal for coupling to microscopy techniques. Additionally, supported bilayers may be assembled within a flow cell or microfluidic device, which enables the exchange of buffers and, consequently, the precise control over the binding and fusion environment during single virion tracking microscopy. The composition of these bilayers is highly tunable, ranging from the simplest lipid components, to recapitulating the complexity of the plasma cell membrane of specific cell types (Figure 3.4).

Initial studies employed purely lipid bilayers with glycolipid viral receptors[107,127,128,143]. More recent work has used reconstituted proteoliposomes that contain protein receptors [144]. There has also been progress in using composite membranes made from cell-derived membrane components mixed with PEGylated liposomes to engender the SLB with both biologically relevant material (receptors, etc.) and a built-in cushion to maintain constituent mobility [145,146]. Other work has demonstrated the ability to form bilayers from cell plasma membrane blebs as a way to incorporate transmembrane proteinaceous receptors and complete native cell materials into planar geometries [112,147,148]. The incorporation of transmembrane proteins greatly expands the range of viruses that can be studied with single virions tracking techniques [112].

Notably, the simplest lipid-only bilayer on glass is roughly 4 nm thick and sits above a thin layer of water on the order of a nanometer thick [149,150]. This feature enables the two-dimensional mobility of lipids within the bilayer necessary for membrane fusion, but mobility is also a key property for allowing receptors to rearrange to permit multivalent binding interactions, as they do in live cell

membranes. Mobility of protein receptors, particularly those with transmembrane domains, can be a challenge in these platforms if the water gap is insufficient for limiting interaction between the protein and the glass support. To overcome this challenge, various cushions, such as polyethylene glycol (PEG) [146], bovine serum albumin, dextran [127,151], or polyelectrolyte brushes[148], have been placed between the bilayer and the supporting surface to improve protein mobility[152].

It is also possible to form supported lipid bilayers that mimic the *viral membrane* instead of the host membrane and conduct experiments in the opposite configuration. Here, binding and fusion is studied by monitoring liposomes decorated with host cell receptors interacting with the planar virus-like bilayer containing embedded viral proteins [153–155]. Such an arrangement could be used for screening applications of antivirals that target entry processes, without the need for live virus or pseudotyped particles.

In summary, biomimetic platforms enable a level of environmental control that cannot be attained in live cell particle tracking techniques. First, there is a degree of control over the host cell membrane mimic's composition that is difficult to alter in live cells. Second, in these platforms, the buffers in contact with the virus can have a defined composition and the experimenter controls the timing and order of exposure to proteases, pH, or any other component of interest to the virus. But perhaps the most salient feature of this experimental approach is that these platforms allow detailed examination of the binding and membrane fusion process and gathering of dynamic data from these processes. However, the two-dimensional, in vitro nature of these platforms make them unsuitable for measuring cytoskeletal involvement in entry.

Thus, to obtain the most complete information about the infection process, combining data from complementary approaches using live cells and biomimetic platforms is an excellent strategy.

3.4 Applications of Single Virion Tracking and Complementary Ensemble Approaches

In the following sections we describe how single virion tracking has been applied to investigate different steps in virus entry. We also include overviews of a selection of ensemble methods to appreciate the synergy between the data collected by the different techniques in providing a complete description of virus entry. Table 1 provides a quick reference of techniques and the data that can be obtained in each approach for each entry stage.

3.4.1 Tracking extracellular movement of virions

There are two scales of transport to be observed during virus spread and infection. On the larger scale is the transport and spread of virions between neighboring cells. Also of interest is the smaller-scale tracking of an individual virion on a cell plasma surface before it is internalized by that particular cell. In the following sections, experiments at each scale will be described with selected examples and references.

Table 3.1. Comparison of single virion and ensemble methods for studying particular viral entry steps, including key features of each method.

Virus Entry Step	Single Virion Tracking		Ensemble methods
	Live cell	Biomimetic	
Extracellular transport	• Direct cell-cell spread • Extracellular diffusion	• Movement through mucosa	
Cell-surface trafficking	• Cytoskeletal interaction • Movement toward entry site	• Diffusion, rolling, and rocking along surface • Bilayer composition • Bilayer fluidity	
Binding	• Colocalization with receptor	• Attachment/detachment rates • Bilayer composition • Bilayer fluidity • Receptor mobility • Adhesion-strengthening	QCMD Coflotation ELISA SPR TEM
Internalization	• Clathrin dependence/independence • Internalization timescale • Cytoskeletal interaction	n/a	IFA TEM
Fusion	• Differentiate plasma membrane fusion from endosomal fusion • Escape from early vs. late endosomes	• Bilayer composition • Bilayer fluidity • Viral fusion environment • Timing/sequence of fusion triggers • Hemifusion and pore formation rate constants • Number of rate-limiting fusion steps • Acid stability	TEM Syncytia formation Bulk solution fluorescence Infectivity BlaM release
Intracellular trafficking	• Cytoskeletal interaction • Extra- and intra-nuclear movement	n/a	IFA

Acronyms:
QCMD- Quartz crystal microbalance with dissipation
ELISA- Enzyme-linked immunosorbent assay
SPR- Surface plasmon resonance
TEM- transmission electron microscopy
BlaM- beta lactamase

3.4.1.1 Tracking virion movement between cells

Tracking virion movement in the in vivo environment has revealed various avenues of virus spread to surrounding cells. The predominant transport mechanisms of virus spreading between cells are: 1) virions freely diffusing through the extracellular environment to neighboring cell surfaces, or 2) spreading to neighboring cells through direct transmission across adjoining membranes. For the first mechanism, the mean-squared displacement of virions over time is used to classify their motion as diffusive or sub-diffusive through the extracellular environment. For example, live cell single virion tracking of adeno-associated viruses [111] and simian virus 40 virus-like particles [156] indicates that particles undergo normal diffusion in the extracellular environment. Adeno-associated viruses slow down when in the vicinity of a cell, and touch the cell membrane multiple times before penetrating the cell [111]. In contrast, HIV follows the second mechanism and preferentially transmits directly from one neighboring cell to another through virological synapses rather than transmission by extracellular diffusion [157–159] Some viruses exploit cytoskeletal components to facilitate transport from one cell to another. Vaccinia virus, for example, induces the formation of actin protrusions from the cell surface and is transported along these to spread from cell to cell [160]. Looking at viral transport over a longer distance scale, single virion imaging has shown that pseudorabies virus is able to spread from the site of infection to the peripheral nervous system ganglia for replication then back along axons to reseed the initial infection site [161]. In vitro experiments have been used to study how respiratory mucosa hinders the ability of pseudorabies virus to cross into the epithelium, revealing that both size and charge interactions are important[162].

3.4.1.2 Tracking virion movement on live cell plasma membranes

There are multiple strategies for observing lateral viral movement along the plasma membrane of a live cell. One method is labeling the core of virions and cellular actin (to delineate the border of cells) and track virion movement along the periphery of the cell [163]. Another method is to label the viral membrane and look at diffusion on top of membrane until the virion overlaps with an endocytosis site [164]. Some examples of virion movement are as follows. Simian virus 40 undergoes actin independent diffusive movement on the cell membrane until it reaches caveolae [165]. Dengue virus similarly freely diffuses on the membrane until it reaches an existing clathrin-coated pit [164]. Murine polyomavirus-like particles also freely diffuse at first, then become confined and follow actin-directed trajectories afterwards [166]. Vaccinia bound to microtubules have been observed to move towards the cell body along the plasma membrane [167].

Some viruses employ a mix of two mechanisms, free diffusion and directed motion. Some examples of this type of movement is as follows. After binding to microtubules, murine leukemia virus, avian leucosis virus, vesicular stomatitis virus, and rabies virus appear to "surf" on top of the membrane via actin and myosin II driven transport towards entry sites [163,168]. Similarly, adenovirus binds its receptor then drifts along the cell surface with the assistance of actin and myosin II [169,170]. Coxsackievirus has been shown to bind on the apical surface of epithelia, which then triggers cytoskeletal rearrangement that transports the virus to the site of viral entry, the tight junctions [171]. Finally, influenza virus appears to undergo actin-directed motion in the area near its initial binding site on the cell surface [105,172]

3.4.1.3 Tracking virion movement on biomimetic cell surfaces

In the in vitro environment of supported lipid bilayer platforms, virions diffusing along the bilayer follow a continuous trajectory, whereas those that bind, detach, and rebind elsewhere on the surface "appear" and "disappear" under TIRF microscopy. These modes of transport are easily distinguished from each other using this microscopy approach [173]. Supported lipid bilayers have an advantage over live cells for certain types of studies because of the ability to tightly control composition, receptor density and mobility, and surface geometry and heterogeneity. For example, supported lipid bilayers have been used to observe sliding and tumbling of quantum dot–labeled simian virus 40 virus-like particles on bilayers containing low concentrations of GM1 and back-and-forth rocking at high receptor concentrations [131]. However, because lipid bilayers do not contain the full cytoskeletal network of cells, it is possible that virion motion in these platforms could be different from their motion in vivo.

3.4.2 Binding

Studies of virus binding kinetics and determination of binding strength are often carried out in in vitro assays, either by monitoring many single virion events or following ensemble behavior of a population. In this section, we describe these approaches and highlight some selected studies that illustrate their utility.

3.4.2.1 Single virion tracking of binding

Direct observation of many individual virion interactions with supported lipid bilayers can be used to measure receptor binding and detachment rates, multivalent avidity characteristics, and equilibrium binding constants. TIRF microscopy is the

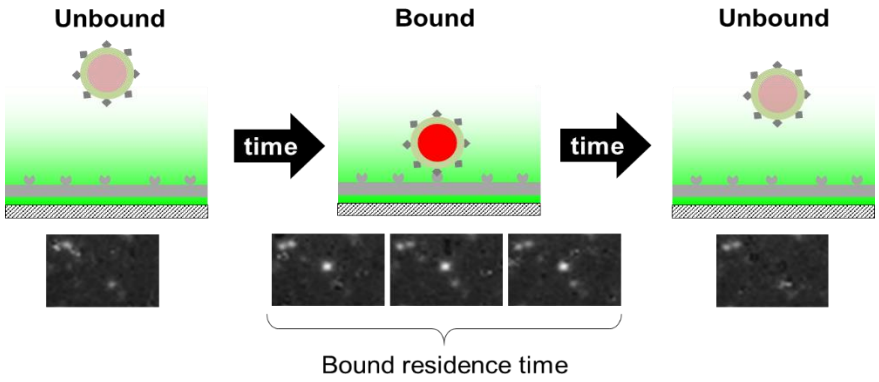

Figure 3.5. TIRF microscopy visualization of virions. Virions bound on the membrane surface (gray) within a 100 nm deep evanescent wave (green) are visible. Fluorophores in unbound virions are not excited by the evanescent wave, while virions bound to the bilayer are illuminated, denoted here by the bright red color in the center cartoon. Residence times can be determined by the number of frames the virion remains observable, as shown in the images below the cartoons, before the virion unbinds.

most common method used in monitoring individual virions binding to biomimetic membranes because it clearly distinguishes labeled virions that are bound to the lipid bilayer from unbound virions in the bulk solution (Figure 3.5). In this experimental approach, the residence time of bound virions can be collected for each individual virion. As experimental conditions change, shifts in residence times can be monitored. From this data, binding characteristics can be quantified.

Initial work monitoring nanoparticle binding to supported bilayers and surface-tethered vesicles demonstrated the advantage of using TIRF microscopy in this application. Here, a useful approach, equilibrium-fluctuation-analysis, was developed to quantify apparent kinetic rate constants of carbohydrate-bearing particles with carbohydrate presenting SLBs [174]. This analysis was then extended to studies of virus-like particles [143,175] and live virions [175] interacting with glycosylated bilayers to provide new insight into virus attachment to cell surfaces and applications in biosensing [176]. The kinetics of particle detachment [177] can also be studied in these

platforms, as can multivalent binding behavior [156,178]. Such studies can revel changes in binding behavior that promote viral attachment. For example, both influenza and canine parvovirus undergo "adhesion-strengthening" where the longer a virion is bound, the more strongly it adheres to the bilayer [130,179]. Overall, these platforms are convenient for gathering insight on this critical virus entry step and how it depends on the host cell surface.

One advantage of this platform is the control of the bilayer compositions and heterogeneity. For example, single particle binding studies have revealed the importance of microdomains in binding of norovirus-like particles, which preferentially bind the edges of glycosphingolipid-enriched domains [143]. Later it was also shown that HIV particles prefer to bind at the edges of cholesterol-rich lipid domains that were reconstituted in supported bilayers [180,181]; however, observing this preference in live cells due to the small scale and dynamism of lipid rafts is difficult, illustrating the power of using an in vitro system for such studies. Focusing further on the receptors themselves, TIRF microscopy has also been used to measure the affinity of HIV gp120 for the glycosphingolipids galactosyl ceramide, glucosylceramide, lactosylceramide and α-hydroxy glucosylceramide in SLBs [182,183]. The affinity of gp120 for these lipids is roughly 5 times lower than its affinity for CD4 [184].

The importance of studying the binding step is that the tropism of a virus is strongly tied to its ability to bind various receptors. A nice example illustrating the power of combining single virion binding measurements with cell infectivity studies, clearly showed that a single mutation in the canine parvovirus capsid is able to alter

binding to dog and raccoon transferrin receptors and completely change the tropism of the virus [179].

3.4.2.2 Ensemble-based approaches for studying virion binding

Binding can be monitored using ensemble approaches that monitor the overall change in an aggregate signal from many virions interacting with a target surface. The simplest manner to measure virion binding to a particular host cell receptor is the cofloatation assay. In these assays, viral particles or purified fusion proteins are labeled with a probe and mixed with liposomes containing the receptor for the virus. After the virus has bound, the mixture can then be added to a sucrose gradient and fractionated. The fractions are analyzed with PAGE or Western Blot to determine under which conditions the virus and liposomes comigrate or cofloat [185,186]. Altering the composition of the liposomes can be used to determine what lipids and proteins the virus binds to. This assay is able to probe virus-receptor interactions but does not provide information on binding kinetics. An additional limitation is that it may be difficult to purify or prepare liposomes containing the receptor, particularly if it is a transmembrane protein.

Some ensemble viral binding assays, like enzyme-linked immunosorbent assay (ELISA) or glycan arrays, immobilize proteins, carbohydrates, or glycans on a rigid surface. These arrays do not preserve the structure, complexity, or two-dimensional fluidity of cellular membranes, which may limit accurate assessment of binding avidity. However, they can be useful for rapidly identifying binding partners in screening, for example, potential tropism changes [187].

Measurements of real-time binding and desorption can be assessed using techniques like surface plasmon resonance (SPR) [188] and quartz crystal microbalance with dissipation (QCM-D) [143,189]. SPR uses changes in refractive index to report the binding behavior, while QCM-D uses a shift in resonance frequency to report virus interaction. In both approaches, biomimetic membranes can be used to preserve many properties of the host cell surface, including integration of the receptor. Kinetic analysis of binding with these techniques requires two experimental phases to decouple binding and unbinding of virions. In the first phase, virions are added to a biomimetic surface and bind to the receptors. In this way, an "on" rate can be obtained. In the second phase, a virus-free buffer is added and the dissociation of the virus from the receptor is monitored. In this arrangement, an "off" rate can be obtained.

It should be noted that averaged data from many single virion tracking binding/unbinding events should match the ensemble results generated with SPR or QCM-D. However, direct imaging with single virion tracking allows collection of a richer set of data for on and off rates simultaneously because each particle trajectory is captured [130]. Furthermore, by having the signature of each individual virion's binding behavior, heterogeneities in the virus population or membrane surface can be identified, which can then be compared to infection trends to understand how population dispersity impacts infection [190].

3.4.3 Internalization

Internalization, or the uptake of the virus particle into the cytosol, can be assessed either with live cell imaging or in fixed cells through immunofluorescence imaging.

3.4.3.1 Live cell imaging

In live cell virion tracking, cellular components, like clathrin and caveolin, can be fluorescently labeled and colocalization of these components with virions enables determination of whether the primary means of viral entry is through clathrin-dependent endocytosis, caveolin-dependent endocytosis, or a clathrin/caveolin independent uptake mechanism. When tracking labeled virions on live cells, rapid unidirectional motion indicates that particles have been internalized [164,172,191]. Live-cell tracking has revealed myriad information about virus internalization, including identifying viral dependence on clathrin or caveolin for uptake as well as the ability of viruses to promote their own uptake. For example, reovirus induces the formation of clathrin-coated pits for uptake [191]. However, simian virus 40 has the ability to induce actin rearrangement to further promote its own internalization whereas echovirus 1 does not [165,192]. Clathrin-mediated endocytosis is utilized for the uptake of many viruses including Australian bat lyssavirus [193], HIV [194], infectious hematopoietic necrosis virus [195], and rabies virus [168]. Other viruses are caveolin-independent or use macropinocytosis. For example, mouse polyomavirus is also delivered to early endosomes by a caveolin independent pathway [196]. Adenovirus 2 enters the cell via both clathrin dependent and independent endocytosis and triggers macropinocytosis[197–200]. Still other viruses have been shown to be agile in their

internalization route, for example, in the absence of caveolin, simian virus 40 can exploit a clathrin/caveolin independent pathway [201]. Studies have shown that bound influenza virions have the ability to induce the formation of clathrin-coated pits, but can also enter in a clathrin/caveolin independent manner [172]. Influenza is then preferentially sorted into a population of early endosomes that quickly matures [202].

3.4.3.2 Immunofluorescence imaging

To monitor virus entry without live-cell particle tracking, infected cells can be fixed and imaged with an immunofluorescence assay. Permeablized cells can be probed with antibodies against viral proteins, and cytoskeletal elements, or endocytosis markers. Colocalization of viral particles and cellular components can then reveal the general entry pathway of the virus [203–205]. Cells can be fixed at various time points after infection to determine the general time course of entry [206,207]. This method provides snapshots of the viral entry process because the cells are fixed before imaging, but it requires less specialized microscopes and cameras than live-cell imaging.

3.4.3 Intracellular trafficking

For viruses that are internalized, live-cell fluorescent imaging can provide insight into how viruses use cellular machinery, such as the cytoskeleton or microtubules, to propel their movement within the cell. One common approach to determining if cytoskeletal elements are involved is to compare the speed and shape of virion trajectories in the presence and absence of cytoskeletal inhibitors such as nocodazole, and cytochalasin D [208]. This strategy has been employed to determine that movement after endocytosis is microtubule-directed [208]. Microtubules are involved in

the cytosolic movement of adeno-associated virus type 2 [209], HIV [124,210] infectious hematopoietic necrosis virus [195], rabies virus [168], In contrast, polio movement inside cells is actin dependent, but microtubule independent [211]. Adenovirus interacts with minus-end dynein and a plus-end directed factor to traffic along cytoplasmic microtubules [212]. Influenza in endosomes undergoes unidirectional dynein-directed translocation to the perinuclear region followed by intermittent back-and-forth microtubule-dependent motion within the perinuclear region prior to virion fusion with endosomes [105].

In addition to investigating movement towards the nucleus, live-cell single virion tracking has been used to monitor movement within the nuclear region. Adenovirus utilizes microtubules for movement within the cell, but detaches from them when the virions reach close proximity to the nucleus [213]. HIV cores move toward the nucleus with a microtubule- and actin-dependent motion; within the nucleus, the motion is slow and diffuse [194,210,214]. HIV RNA alone moves through the cytoplasm by diffusion [215]. After reaching the nucleus, HIV pre-integration complexes target areas of decondensed chromatin [216]. For influenza, genes are transported to and within the nucleus by diffusion [217].

Intracellular movement of virions is not necessarily mediated by spike or capsid proteins alone; for herpes simplex virus, the inner tegument proteins promote movement along microtubules and are necessary for movement away from the cell body along axons [218–220].

An alternative method is to use immunofluorescence assays of fixed cells to obtain snapshots of intracellular virion trafficking, including what cytoskeletal

components are involved [221,222]. These do not allow for the tracking of individual virion trajectories and are more limited in temporal resolution than live cell virion tracking, but require less specialized equipment.

3.4.5 Fusion

Membrane enveloped viruses must fuse their membrane with the host membrane to deliver their genome to the cytosol for replication. Fusion can occur either at the plasma membrane surface or in endosomes after the virion is internalized. Fusion can be monitored in both live cells and in in vitro platforms. Each approach has advantages and disadvantages, and some examples of how these experiments are conducted follow next.

3.4.5.1 Tracking fusion in live cells

Viral fusion at the plasma membrane can be differentiated from fusion within endosomes in live cells. To do so, the viral contents can be labeled with a diffusible content marker while the envelope is labeled with an acid-stable lipophilic dye. If fusion occurs at the plasma membrane, both fluorescent markers will seem to disappear because they will be diluted into the plasma membrane and cytosol. If fusion occurs within an endosome, the viral content marker will disappear as it is released into the cytosol and diluted, but the lipid marker will continue to appear bright as the dye mixes into the relatively small endosomal membrane [223]. This approach has been used to show that HIV can undergo full fusion inside endosomes while fusion at plasma membrane is halted at the lipid mixing step. However, this may be cell-type dependent; HIV content release from plasma membrane fusion was observed for U87 cells but not JC5.3 or HOS cells [224].

The ability to detect viral fusion in live cells within the endocytic pathway often relies on labeling virions with quenched amounts of dye. Colocalization of dequenching virions with labeled cellular components, such as clathrin or Rab proteins, can reveal whether fusion occurs in early or late stage endosomes. This approach has been employed in the study of influenza virus, which fuses in early endosomes, revealing that the virus is able to enter a clathrin-dependent manner as well as a clathrin and caveolin independent fashion, and viral fusion can occur in both pathways [172]. In macrophages, HIV undergoes fusion in Rab5A positive endosomes [194]. Fusion of dengue virus [164] and Ebola virus [66] colocalizes with Rab7, a marker of late stage endosomes. Alternatively, endosomal fusion may be mimicked by binding virions to the plasma membrane then lowering the extracellular pH. This method of acid-induced endosomal bypass has been employed to characterize avian sarcoma and leukosis virus fusion behavior [225].

Viral fusion can also be monitored by observing the release of fluorescent viral cargo. Avian sarcoma and leukosis virions labeled with fluorescent cargo and an envelope pH sensor showed little correlation between endosomal pH and fusion lag time [226]. However fusion lag time and pore size did vary with surface receptor and endosome type, indicating that endosomal composition may modulate fusion [129,226,227]. In the case of vesicular stomatitis virus, cytoplasmic nucleocapsid release does not necessarily immediately follow fusion. VSV has been shown to undergo fusion between the early and late endosome stage [228].

3.4.5.2 Tracking fusion in biomimetic platforms

With the lipid bilayer platform, hemifusion and pore formation can be observed within the same particle by dual-labeling the viral envelope and contents with different colors (Figure 3.6). By using a flow cell or microfluidic device, this platform also enables control over the timing of fusion trigger(s) or other environmental changes within the viral environment.

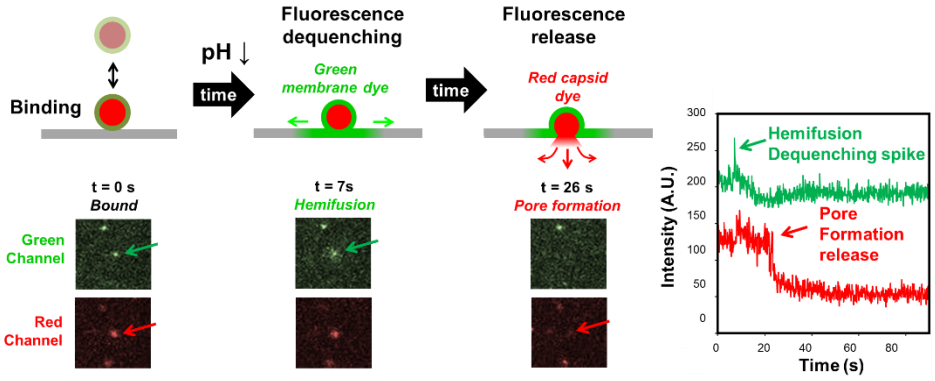

Figure 3.6. Fusion and intermediate steps can be tracked by a dual-labeling approach. Virions first bind their receptor within the supported lipid bilayer (gray) in the evanescent wave (not shown here) of TIRF. After a trigger (such as a pH drop shown here at t = 0) membrane fusion occurs between the virion membrane, labeled with a green fluorophore, and the unlabeled supported bilayer. Fluorescence dequenching during fusion indicates hemifusion. Finally, a fusion pore is formed and the internal capsid fluorophores (red) are expelled across the supported bilayer. The plot to the far right shows the intensity change for the virion highlighted by the arrows in the images to the left.

A common fusion trigger is a drop in pH. To trigger fusion, acidic buffer can be passed over the bilayer inside a microfluidic device. Incorporation of pH sensitive dye into the bilayer enables detection of the time at which bound virions encounter the acid [127]. Alternatively, ultraviolet light can be used to "uncage" protons from o-nitrobenzaldehyde in solution to rapidly acidify the bilayer and virions [107]. Both of these methods enable measurement of the lag time between exposure to a fusion trigger and the onset of hemifusion. By analyzing this lag time for hundreds of individual fusion events, the rate constants of hemifusion can be calculated. Pore

formation can be monitored by particles also containing internal capsid dyes. Monitoring the drop in signal of this co-localized fluorophore reports the opening of the fusion pore.

If there is a single rate liming step, the distribution of lag times will follow a simple exponential decay, with the decay constant corresponding to the rate constant of that limiting step. If there are multiple rate liming steps, the lag time distribution will rise and decay [229]. A simple approach to quantifying the kinetics of hemifusion and pore formation is fitting the cumulative distribution of fusion events to a convolution of Poisson processes with the equation:

$$P = \int_0^t \frac{k^N t^{N-1}}{\Gamma(t)} e^{-kt} dt$$

where P is the probability of a virion being in that state (hemifused or pore forming) at time t after the fusion trigger has been added and Γ (t) is the gamma distribution function. This fit yields k, the rate constant of that step, and N, the number of stochastic rate limiting events governing the kinetics of that step [127]. If there is only one rate-limiting step (N=1), the above equation simplifies to a single exponential decay. As the number of rate-limiting steps increases, more events must be observed to accurately calculate N. For processes with three steps or fewer, 50 events is sufficient to calculate N with a standard deviation of 1 [106]. There are other more complex methods for fitting lag time distributions that may capture more of the details of hemifusion [230].

Viruses with class I, class II and class III fusion proteins have been studied at the single virion level with SLBs. The kinetic analysis described here has indicated

that influenza virus hemifusion is controlled by three rate-limiting steps while the kinetics of pore formation is governed by a single step [127]. Chikungunya virus also has three-rate limiting steps governing hemifusion [231]. For West Nile virus, hemifusion has one or two rate-limiting steps, depending on the pH [232]. Vesicular stomatitis virus hemifusion also has multiple rate-limiting steps at higher pH and a single rate-limiting step at low pH [233].

While it cannot be assumed that the kinetics obtained from this method reflect the actual reaction rates within a cell, comparison of these rates under different conditions, such as different bilayer compositions, pH, or viral strains, can yield valuable insight. The ability to manipulate the composition of supported lipid bilayers has been used to determine that anionic lipids are essential for vesicular stomatitis virus fusion and that the lag between hemifusion and pore formation is shortened in the presence of bis(monoacylglycero)phosphate, a lipid found in late endosomes [151]. Precisely controlling the triggering pH has revealed that influenza virus requires a lower pH to trigger fusion than Sindbis virus [128], suggesting that it fuses later in the endocytic pathway. While the rate of influenza X-31 virus hemifusion increases at lower pH [127], the rate of Brisbane is much less pH dependent [234]. The rate of pore formation for influenza virus is pH independent. Multiple influenza hemagglutinin trimers are involved in fusion [235], although not all are active participants [236,237]. This platform is able to detect differences in the acid stability and fusion behavior of different strains and reassortants of influenza, which is tied to their tropism [234,238]. This platform can also be used to measure the number of antibodies required to neutralize fusion of a single virion [239]. Figure 3.7 provides a summary of the flexibility of the

biomimetic fusion assay and the kinds of insight that has been gained from these tunable assays.

With the advances in supported bilayer complexity and fabrication, these platforms can also be used to study viruses that bind proteinaceous receptors, such as feline coronavirus [112].

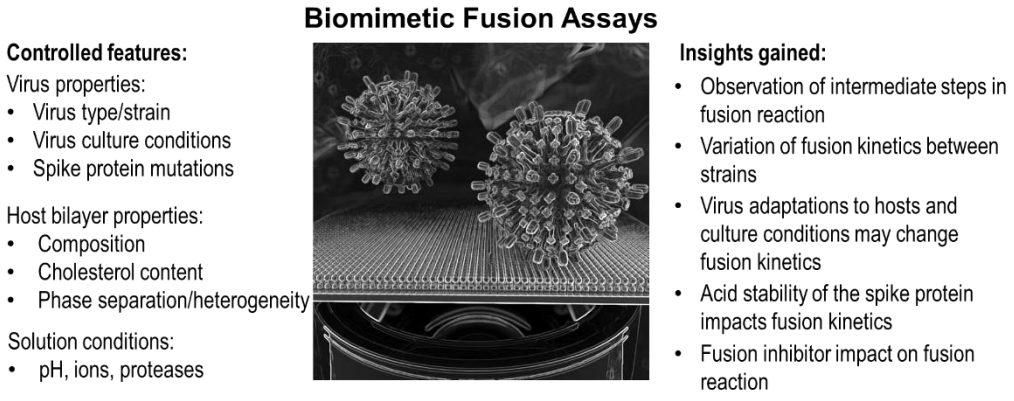

Figure 3.7. Characteristics of biomimetic fusion assays. (Left) Features that can be easily controlled in biomimetic fusion assays. By combining with a high throughput approach, these conditions can be evaluated to provide new insight into virus fusion. (Right) Examples of the kinds of insight that can be gained with a biomimetic assay that isolates the fusion reaction from other virus entry steps.

Finally, given the highly-defined nature of these platforms, viruses that do not have a known fusion trigger or receptor might be difficult to study, because each component must be intentionally added to the platform. However, because SLBs can be formed in a microfluidic device, it should be possible to formulate a high-throughput screen for possible fusion triggers or binding partners with this configuration.

3.4.5.3 Ensemble approaches for studies of fusion

A common method to study fusion behavior is cell-cell fusion assays, where fusion between target cells expressing the receptor for the virus and effector cells expressing the viral fusion protein is monitored. When the viral fusion protein is

triggered, for example by lowering the pH, the cells fuse to each other, leading to clusters of multiple nuclei surrounded by a single cell membrane [240]. These clusters are known as syncytia. Lipophilic and aqueous dyes can be used to label the membrane and contents of the effector cell, providing readouts for lipid mixing or pore formation. To isolate the hemifusion step, fusion can be triggered then arrested by quickly cooling the cells to 4°C [241,242]. This rapid-cooling approach has been used to determine that hemifusion of avian sarcoma and leukosis virus requires low pH, but expansion of the fusion pore does not [242]. As an alternative to monitoring pore formation by observing the transfer of intracellular fluorescent cargo from effector cells to target cells [243], whole cell patch-clamp electrical measurements can be used [244]. In this configuration, a pipette connected to an electrode and amplifier pierces the membrane of the effector cell. The voltage across the membrane can be manipulated and the resulting current measured. During cell-cell fusion, the cell surface area increases as the membranes merge, resulting in an increase in membrane capacitance. Such measurements can also allow for estimation of fusion pore size [245].

While syncytia assays do not require viral particles or specialized equipment, making them easy to carry out, there are some limitations. Syncytia form over the course of hours, so this technique is not suitable for obtaining kinetic data [246]. Furthermore, the extracellular environment can differ substantially from the endosomal environment, which may create artifacts when using this technique to study viruses that typically fuse within the endocytic pathway. In this approach, any impact of the virion size or shape on fusion is not captured.

In bulk fusion assays, viral particles are fluorescently labeled, then they are mixed with liposomes in a cuvette and the fluorescent signal of the solution is measured by fluorimetry as fusion triggers are added. In one labeling approach, particles and/or liposome membranes can be labeled with fluorescence energy resonance transfer (FRET) pairs. If fusion occurs, FRET will stop as the pairs become separated, and the fluorescence signal will change accordingly [247]. In the second labeling approach, particle membranes are labeled with a single quenched fluorescent marker [248]. Upon fusion with a liposome, the quenched fluorophores will become diluted and dequench, causing a marked increase in fluorescence.

In a third approach, the release of viral cargo can be detected by measuring β-lactamase (BlaM) activity. In this type of assay, target cells are loaded with a dye containing a β-lactam ring and a FRET pair. Chimeras of viral core proteins and BlaM are incorporated into virions. If virions are able to release their cargo during infection, BlaM will cleave the lactam ring, interrupting FRET and causing the cells to fluoresce a different color [249]. Infected and uninfected cells can then be sorted by flow cytometry for further analysis. This technique requires the ability to make chimeric proteins but otherwise does not require specialized equipment. BlaM activity assays have been combined with single virion imaging to indicate that HIV releases cargo by fusion inside endosomes and not fusion at the plasma membrane surface [250].
Bulk fusion provides information on the kinetics of the fusion of the overall population in the solution, including the lag time between when the viruses are exposed to a fusion trigger and when dequenching begins, with a resolution of less than a second [251]. Varying the composition of the liposomes can reveal how lipids

impact viral fusion [252]. However, liposomes containing the viral receptor may be hard to prepare if the receptor is a transmembrane protein. These assays cannot resolve intermediate steps like hemifusion, or resolve fusion of individual virions, but can be used to determine conditions interesting for further investigation with single virion tracking with SLBs [231].

It is worth noting that single virion fusion tracking experiments agree with data obtained from bulk fusion experiments. In a study directly comparing the two methods a combination of bulk fusion and single virion tracking showed that cholesterol enhances the extent of Sindbis virus fusion, but increases the lag between binding and fusion at pH less than 5, revealing a complicated relationship between lipids and viral fusion proteins in binding and fusion [128].

3.5 Conclusion

Methods for studying viral entry vary widely in functional characterization, and structural and temporal resolution. No single technique is sufficient to determine all the steps or details of viral entry. Single virion tracking techniques can bridge the gap between detailed structural information and overall infection measurements to inform our understanding of the structure-function relationship of viral fusion proteins. The development of single virion tracking techniques has been dependent on advances in viral labeling, microscopy, and image analysis. These single virion techniques can be applied to study the progression of infection in live cells as well as used in a tightly-controlled biomimetic platform. Top-down cell culture approaches where inhibition or knockout of cellular components reveals their role in viral entry complement bottom-

up biomimetic methods where components of interest are methodically added to the experimental platform. Combining information from these different techniques illuminates the framework of steps involved in viral entry and clarifies the mechanisms underlying each step.

3.6 Acknowledgements

The authors of this book chapter are Lakshmi Nathan and Susan Daniel. L.N. wrote the summaries of virus entry, live cell imaging, and applications of single virion tracking, S.D. contributed the review of biomimetic platforms, and both described the underlying enabling technologies. LN is supported by the NSF Graduate Fellowship Program (Grant No. DGE-1650441) and the Samuel C. Fleming Family Graduate Fellowship.

CHAPTER 4

DEVELOPMENT OF A SINGLE VIRION TRACKING PLATFORM TO STUDY EBOLA VIRUS FUSION

4.1 Introduction

The 2014 epidemic of Ebola virus resulted in more than 11,000 deaths[253] and outbreaks of the virus have been increasing in frequency since the early 1990s.[254] Despite its emergence as a global health threat, there are no approved treatments or vaccines against Ebola virus. Factors in the host environment, like calcium concentration, are potential targets for antiviral intervention.[44] Antivirals that aim to block viral replication require the ability to deliver drugs into specific parts of the cell, which remains challenging. Strategies aimed at blocking viral entry are less likely to be limited by intracellular delivery constraints.

Ebola virus enters cells through endocytosis or macropinocytosis after binding to a receptor on the surface of the host cell (Figure 4.1).[59] The identity of this extracellular receptor is currently unknown, but the wide range of cells susceptible to infection suggests the virus is able to recognize multiple receptors.[255] The virus is then trafficked through the cell within an endosome. Some cue in the endosomal environment causes viral fusion proteins to undergo a conformational change and facilitate merging of the viral and endosomal membranes to form a pore. Once the viral genome is released through this pore, viral replication can begin.

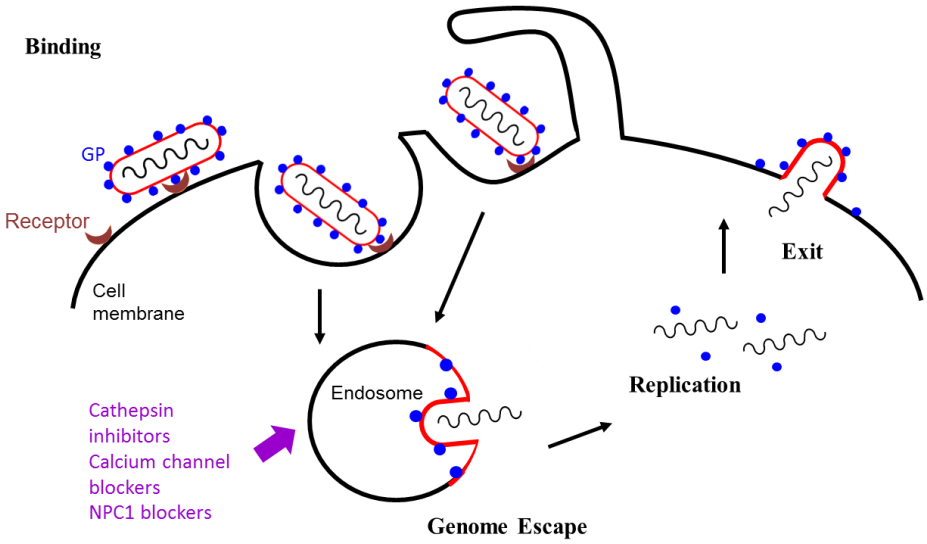

Figure 4.1. Ebola virus infection cycle. Infection begins with binding to a host cell followed by internalization via endocytosis or macropinocytosis. The virus escapes the endosome via fusion, which exposes its genome to host cell machinery. The genome then directs replication and synthesis of new virions, which exit the cell and acquire their envelope by budding. Several potential therapeutics that act on endosomal processes (purple) are known to inhibit Ebola virus infection.

Entry of Ebola virus is controlled by its spike protein, GP, a class I fusion protein. Class I fusion proteins are primarily α-helical in structure and form trimers oriented perpendicularly to the viral envelope.[5] These fusion proteins require proteolytic processing to become fusion-competent or mature. GP consists of two subunits: GP1 mediates receptor binding and GP2 controls fusion. When virions bud from a cell, pre-GP is cleaved into GP1 and GP2 by furin to create mature virions.[256] Within the endosome, GP1 is cleaved by cathepsins to remove a heavily glycosylated region of the protein known as the mucin domain/glycan cap (Figure 4.2).[61] This cleavage event is thought to allow the virus to bind to Niemann- Pick C1 (NPC1),[257–259] a cholesterol transporter found in late endosomes and lysosomes. Functional NPC1 contains three loops: A, C, and I, that project into the endosomal lumen but only the C-loop is necessary for Ebola virus infection.[257] Live-cell single virion-tracking

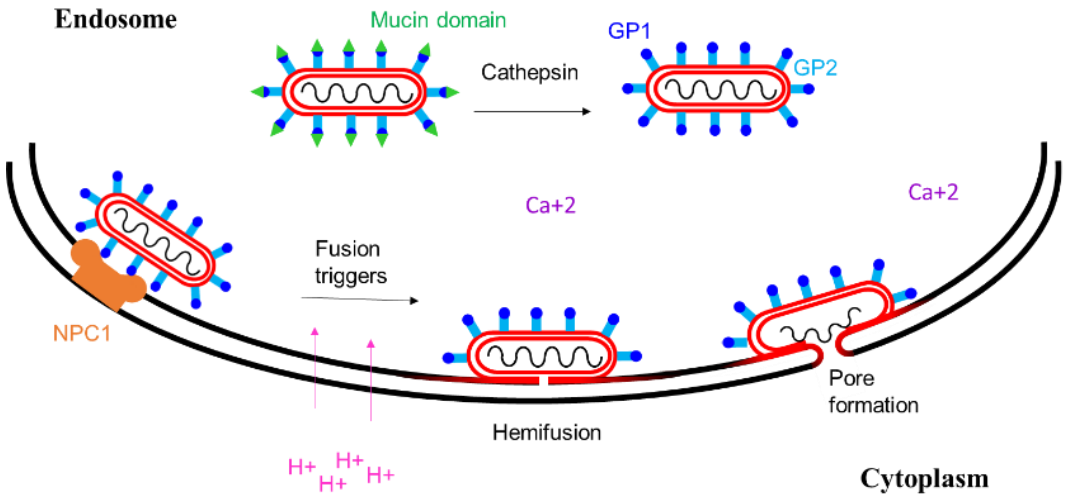

Figure 4.2. Endosomal escape of Ebola virus. Cathepsins cleave the mucin domain off of GP. This enables GP1 to bind to NPC1. After binding, a fusion tigger enables GP2 to insert into the endosomal membrane and induce fusion. First the lipids in the viral envelope mix with those in the endosomal membrane (hemifusion) and eventually the viral genome is released into the cytoplasm (pore formation).

experiments conducted with a GP construct lacking the mucin domain showed that the onset of fusion occurs several minutes after the virus has colocalized with NPC1, indicating that receptor binding is not sufficient to trigger fusion[66].

4.2 Characterization of NPC1 blebs and bilayers

Many enveloped viruses use acidification of maturing endosomes to trigger fusion, but for Ebola virus the exact fusion trigger remains unknown. Both cathepsin activity and pH have been implicated. Cathepsin requires low pH for proteolytic activity and it is thought that Ebola virus's dependence on cathepsin is the reason endosomal acidification is required for infection; cell-cell fusion assays suggest that pH does not directly trigger fusion.[260] Virion tracking in live cells indicates that lipid mixing between the viral envelope and endosomal membrane cannot occur if endosomal acidification is blocked, even if the mucin domain has already been

removed from GP.[66] This suggests that cathepsin may play a role in infection beyond removal of the mucin domain, or that the fusion trigger is another pH-dependent factor. Fusion of virions lacking the mucin domain does not occur until several minutes after reaching an NPC1 containing compartment,[66] indicating that the receptor binding is also not the fusion trigger. Cathepsin inhibition blocks infection by mucin-lacking virions but lipid mixing is not impaired under such conditions.[66] This suggests that cathepsin activity is needed for pore formation after fusion has been triggered. In vitro single particle techniques enable a precise level of control over exposure to fusion triggers that is unattainable in vivo. Using single particle tracking, it should be possible to decouple the effects of cathepsin and pH on Ebola virus binding and fusion. This tool provides an opportunity to gain insight into the fundamentals of Ebola virus entry, with the potential to be adapted for characterization of antivirals.

4.3 Principles of single-virion tracking

Cell based assays lend themselves to a deconstructionist approach where inhibitors to specifc processes can be used to determine whether or not they are involved in infection. However the complexity of the cellular environment makes it hard to decouple the roles of factors that may be present simultaneously or be co-dependent. *In vitro* techniques like single particle tracking (SPT) enable bottom-up investigation of fusion, where elements can be added selectively to isolate the minimum requirements for fusion, and factors like pH, proteolytic activity, and calcium can be decoupled.

The SPT platform consists of a membrane-derived supported lipid bilayer (SLB) within a microfluidic device. The bilayer is formed by rupturing cell membrane blebs (Figure 4.3). Using total internal reflection fluorescence (TIRF) microscopy,

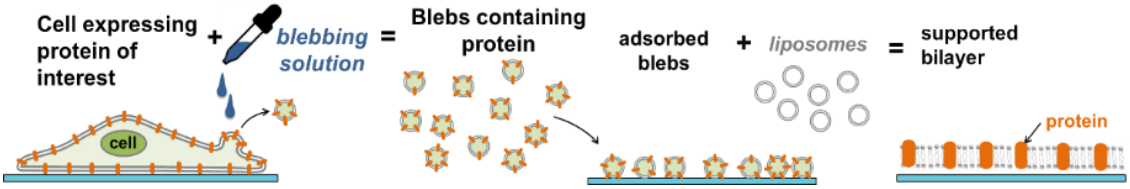

Figure 4.3. Blebbing enables formation of proteinaceous supported lipid bilayers. A protein of interest is overexpressed on the surface of a cell. Incubation of cells with a solution containing DTT and formaldehyde for 2 h induces blebbing. Blebs can be collected, adsorbed to a glass slide and ruptured with liposomes containing PEG to form a supported lipid bilayer.

fluorescently labled virions can be observed when they have bound to the bilayer. If the envelopes of virions are labeled with a high concentration of a lipophilic self-quenching fluorophore, hemifusion results in a measurable dequenching signal as lipids from the viral envelope mix with those in the bilayer and dilute the fluorophore (Figure 4.4). The release of viral cargo is monitored by adding an aqueous internal

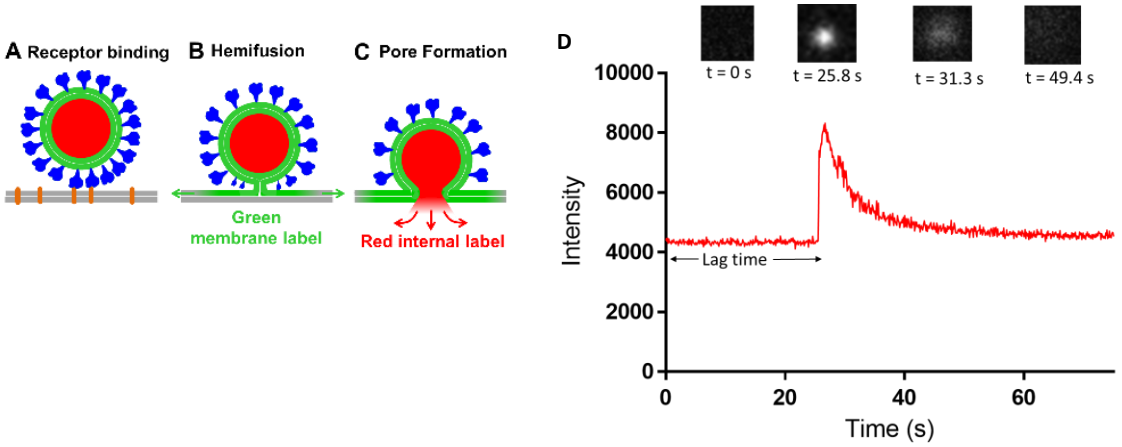

Figure 4.4. SPT enables observation of individual virion fusion events. A-C) Labeling scheme that enables differentiation between hemifusion and pore formation. D) Images of a virion dequenching and the trace of its fluorescent signal over time. The fusion trigger is added at t = 0.

label to the virions. The use of microfluidics allows for control over the timing and sequence of viral exposure to potential fusion triggers. SPT can differentiate between binding, hemifusion, and pore formation, which few other methods can achieve.

Data on the timing of hemifusion are collected for at least 100 individual virion fusion events and fit to a gamma distribution to obtain kinetic parameters (Equation 1.). In this model, *N* stochastic steps are required to reach the hemifused

$$P_H = \int_0^t \frac{k_H^N t^{N-1}}{\Gamma(t)} e^{-k_H t} dt$$

Equation 1. Gamma Distribution Function for calculation of viral fusion kinetics. k_H = hemifusion rate constant, N = number of stochastic steps, t = time at which hemifusion occurs.

state, each step has a rate constant of k_H, and t is the time at which hemifusion occurs.[127] Similarly, this distribution can be used to fit lag time data and describe the kinetics of pore formation. This approach has been used to describe the kinetics of other viruses with class I fusion proteins, including influenza[127] and feline coronavirus.[112]

4.4 Characterization of NPC1 blebs and bilayers

To enable investigation of fusion of Ebola virus with SPT, blebs containing NPC1 C-loop were prepared and used to form supported lipid bilayers. Western blot analysis confirms that NPC1 C-loop is incorporated into the blebs (Figure 4.5A). The

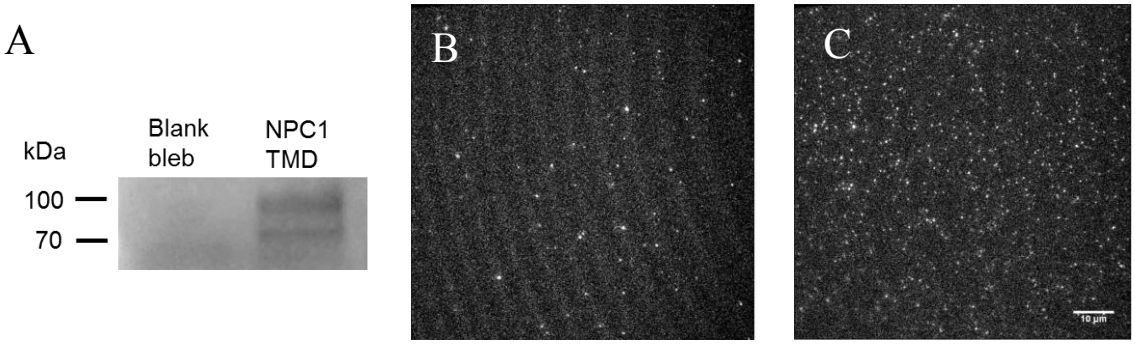

Figure 4.5. Blebs and bilayers contain NPC1 C-loop. A) Western blot of HEK 293T cell blebs from cells not overexpressing NPC1 C-loop (blank bleb) or expressing NPC1 C-loop (NPC1 TMD). Bilayers were blocked with streptavidin to fill in any bilayer defects that might enable non-specific binding. B) Fluorescent anti-HA tag antibodies bound to bilayer made from blank blebs or C) NPC1 TMD blebs. Scale bar = 10 μm.

NPC1 C-loop construct contains an HA tag; binding of anti-HA antibodies to a SLB made from NPC1 C-loop blebs indicates that the protein is present in the bilayers and oriented with the C-loop projecting out of the top of the bilayer (Figure 4.5C).

4.5 Thermolysin treatment enhances viral binding

SPT binding studies show that the virus binds cellular material other than NPC1, as indicated by binding to a blank bleb bilayer (Figure 4.6). The virus also

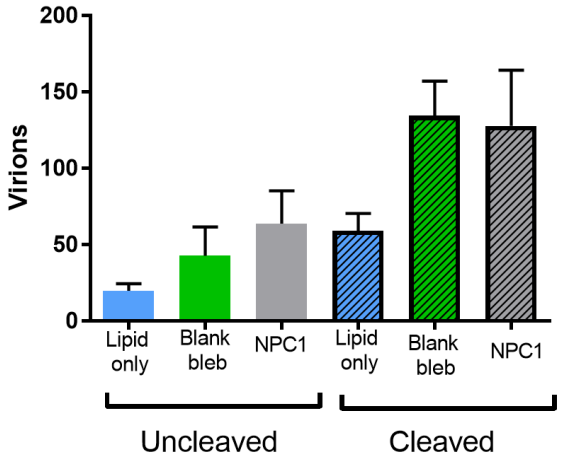

Figure 4.6. Thermolysin treatment increases virion binding to bilayers. Virions treated with thermolysin (cleaved) or untreated (uncleaved) were bound to bilayers made from POPC (lipid only), blank blebs, or NPC1 blebs for 20 min. Error bars represent deviation among 3 fields of view within the same sample.

appears to have the ability to bind to lipids, particularly once cleaved by thermolysin, which has not been described in the literature. Cleavage of the mucin domain by thermolysin, which is functionally analogous to cathepsin but does not require low pH,[61,261] significantly increases viral binding and agrees with behavior reported in the literature.[60] However, this enhancement in binding is not specific to binding of NPC1; binding to bilayers made from blank blebs or lipids also increases. For both cleaved and uncleaved particles there is no significant difference between the number of

particles bound to the blank bleb bilayer or the NPC1 bilayer. The antibody binding experiment in Figure 4.5 indicates this cannot be attributed to poor incorporation of NPC1. According to the current model of Ebola virus entry, only the cleaved particles bound to NPC1 should be able to fuse.

4.6 Acidification induces lipid mixing of virions and blebs

To determine whether or not acidification leads to hemifusion, fluorescently quenched thermolysin-treated virions were mixed with NPC1 blebs in a cuvette and the fluorescence intensity of the solution was measured. The extent of hemifusion shows a pH dependence, with more hemifusion occurring at more acidic pH (Figure 4.7A). The low amount of dequenching observed at pH 7 indicates that mucin

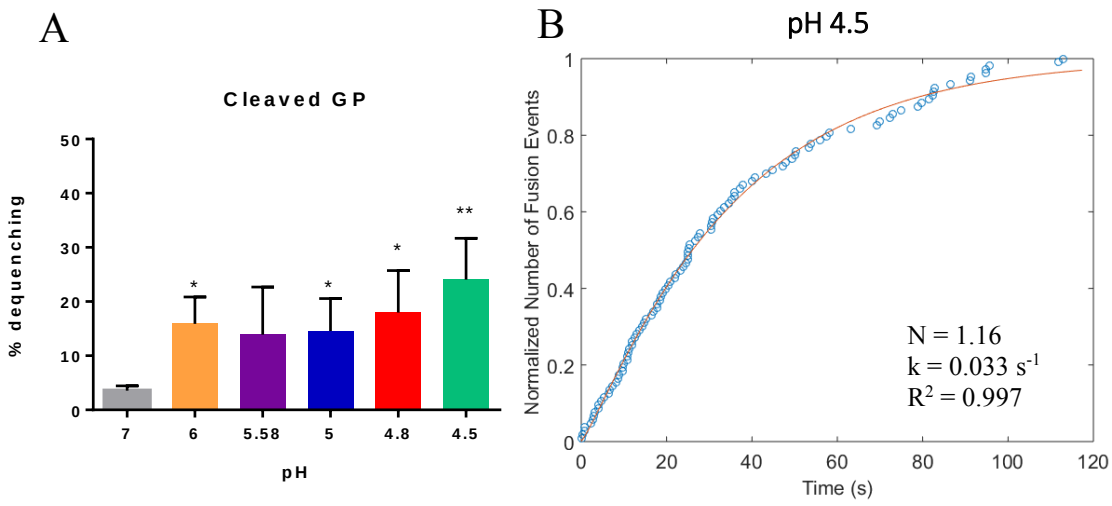

Figure 4.7 Acidification leads to hemifusion. A) pH dependence of hemifusion of thermolysin-treated virions with NPC1 blebs. Virions were bound for 3h then acidified to the specified pH.* = $p<0.05$, ** = $p<0.01$ compared to pH 7. Error bars represent deviation among three trials. B) Hemifusion of thermolysin-treated virions with NPC1 bleb bilayer as measured by SPT. Virions were bound to bilayers for 30 min before acidification to pH 4.5 at t = 0. Lag times of 103 individual virions are represented by open circles (103 virions) and the gamma distribution function is represented with a red line.

cleavage followed by receptor binding is not sufficient for fusion. The fusion kinetics of thermolysin treated virions with NPC1 SLBs at pH 4.5 was measured with SPT (Figure 4.7B). Hemifusion appears to have one rate-limiting step with a rate constant of $0.033s^{-1}$, which is one order of magnitude slower than the hemifusion rate of influenza upon acidification,[234,238] but is comparable to the rate of Ebola virus lipid mixing from cell-based particle tracking experiments.[66]

These experiments were all conducted in the absence of calcium. In light of the results presented in Chapter 2, it is possible that the presence of calcium would alter the trends observed here. Preliminary studies indicate that in the presence of calcium, mucin removal and receptor binding may be sufficient for hemifusion. It is also possible that in the presence of calcium, the hemifusion rate would be faster.

My results are in agreement with the work of Markosyan et al. who observed pH-dependent cell-cell fusion of thermolysin-treated GP in the absence of cathepsin inhibitors.[260] However, they concluded that pH is not the fusion trigger based on the observation that in the presence of cathepsin inhibitors, a lower amount of fusion occurs but the pH dependence disappears. They attributed the initially observed pH dependence to cathepsin in the plasma membrane becoming activated. If cathepsins are present in the plasma membrane, they are likely present in the NPC1 blebs as well. This could also explain the relatively slow fusion rate; acidification would activate the cathepsins which then act on the bound virus to trigger a conformational change.

4.7 Outlook

Single virion tracking with biomimetic membranes has the potential to unravel the factors involved in fusion. However, developing biomimetic single virion tracking techniques has many challenges. Over-labeling of virions can yield false "fusion events", which are actually excess dye partitioning into the supported lipid bilayer. Under-labeling of virions can make it impossible to observe fusion events, even when they occur. Improper rupture of blebs can leave portions of glass exposed to the bulk solution, causing virions to bind to the glass rather than their receptor. Transfection and blebbing efficiency may vary from one bleb batch to another, presenting reproducibility challenges. Many of these technological difficulties have now been addressed, laying the groundwork for applying bilayer-based single virion tracking to the study of Ebolavirus. This technology is now poised for additional study to fully characterize the Ebola fusion trigger.

The role of cathepsins in initiating fusion, particularly those that may be present in the plasma membrane, is one avenue of future research. Removal of the mucin domain appears to enhance binding to all cell membrane surfaces, not just those with NPC1. This indicates that one of the functions of the glycan cap may be to prevent non-specific binding of the virus. By utilizing cathepsins which require low pH for activity to cleave off the glycan cap, the virus is able to ensure it only binds to cellular membranes one it has been internalized because low pH is primarily found in the endosome. Careful control over exposure to calcium, which is achievable with microfluidic handling, is needed to conclusively determine whether or not it acts in conjunction with NPC1 binding to trigger fusion. Calcium may also act in

conjunction with low pH to promote GP conformations that are conducive to fusion, which could result in a faster fusion rate.

Even after the fusion trigger has been established, there are many exciting research questions that could be answered using this platform. Filoviruses are filamentous in nature, and the effect of particle shape on binding and fusion of the virions could be studied. Filamentous virus-like particles can be produced by expressing Ebolavirus GP and VP40[262] and spherical pseudovirus particles can be produced by expressing murine leukemia virus gag and Ebolavirus GP[263]. Receptor binding and fusion kinetics could be compared among different Ebolavirus strains. For example, during the 2014 outbreak the prevailing strain, Makona 2014, contained the mutation A82V in GP[264]. Viruses with this mutation had increased tropism for human cells, decreased tropism for bat cells[265], and a lower activation barrier for reaching the fusion-active conformation[266]. However, the kinetics of fusion of this strain have not been measured or compared to the prototypical research strain, Mayinga 1976. Such analysis could provide valuable insight into the adaptations that make particular strains prone to causing outbreaks.

4.8 Acknowledgements

The authors of this work are Lakshmi Nathan, Isabella Yang, Chih-yun Hsia, Judith White, Gary Whittaker and Susan Daniel. L.N. wrote the text, performed experiments, and analyzed data. I.Y. performed bulk fusion experiments, C.Y.H. assisted with NPC1 antibody binding experiments, J.W. provided reagents and guidance on experiments, S.D and G.W. conceived the project and provided guidance

and oversight. L.N. was supported by the NSF Graduate Fellowship Program (Grant No. DGE-1650441) and the Samuel C. Fleming Family Graduate Fellowship, I.Y. was supported by an Engineering Learning Initiative Grant from Cornell. This work was also supported by National Science Foundation Grant 1504846 (to S.D.).

CHAPTER 5

MAMMALIAN CELL BLEB-BASED VACCINES

5.1 Introduction

Blebs form naturally during apoptosis[267]. Their formation can also be induced chemically via the addition of formaldehyde and DTT[268,269]. Blebs have been used for investigating the formation of lipid raft domains[270], membrane permeability[271] and protein mobility[146]. Virus-like blebs have been used to investigate fusion of enveloped viruses with host membranes[155] but have not been investigated for potential as vaccines. Blebs from apoptotic leukemia cells have been tested as potential vaccines for acute myeloid leukemia[272], indicating that cell membrane blebs are capable of producing an immune response. Our work is the first to report the use of blebs as vaccines to prevent viral infection.

The largest outbreak of Ebola virus disease occurred in 2014. The virus infected more than 28,000 people and killed more than 11,000[273]. In the current ongoing outbreak in the Democratic Republic of the Congo nearly 2,000 individuals have been infected[49]. The development of an Ebola vaccine is critical to stopping future outbreaks. Vaccines candidates that have advanced the furthest through clinical trials are based on pseudoviruses or virus-like particles[274,275]. Here, we present virus-like plasma membrane blebs as an alternative vaccine platform.

Ebola virus is decorated with the spike glycoprotein, GP, which is responsible for cell entry, binding, and fusion, and is the primary antigenic target for vaccines. We have created plasma membrane blebs coated with Ebola GP. We compared this GP to the GP found on viral particles and added exogenous furin to supplement GP

maturation as needed. Mouse studies to measure the immunogenicity of blebs in general and the ability of GP blebs to induce a specific immune response are ongoing.

5.2 Methods and Materials

5.2.1 Cell lines and plasmids

HEK 293T cells from ATCC were grown in DMEM (CellGro) supplemented with 10% fetal bovine serum (Gibco), 100 U/mL penicillin and 10 μg/mL streptomycin (CellGro), and 1 % HEPES (CellGro). Cells were maintained at 37°C, 5% CO_2.

5.2.2 Preparation of blebs

Buffer A (150 mM NaCl, 10 mM HEPES, and 2mM $CaCl_2$ at pH 7.4) was the buffer primarily used for bleb dilution and storage. Blebbing buffer (Buffer A supplemented with 2mM ditiothreitol (Sigma) and 25 mM formaldehyde (Sigma) was used to induce blebbing. The pCDNA plasmid encoding EBOV GP Zaire was obtained from BEI Resources (NR-19814). For transfection, HEK 293T cells were seeded at a density of 50×10^4 cells/mL in 10 cm culture dishes (Corning) and incubated for 24h. Thirty-six μL of TurboFect (ThermoScientific) was used to transfect the cells with 6 μg of DNA per dish. Twenty-four hours post-transfection, cells were incubated with 6 mL of Buffer A and 4 mL blebbing buffer at room temperature with rocking for 1 h and at 37°C for 1 h. The supernatant was harvested and placed in a 15 mL tube on ice for 15 min to allow cell debris to settle out. The top 9 mL were collected, pelleted at 20,000 rpm in a SW-41 rotor (Beckman-Coulter) for 1 h at 4°C. Blebs not treated with proteases were resuspended in 200 μL of Buffer A. Protease-treated GP blebs were resuspended in 30 μL of furin buffer (100 mM Hepes,

0.5% TritonX, 1mM $CaCl_2$, 1 mM 2 mercaptoethanol) with 200 U/mL furin and incubated overnight at 37°C if used in Western Blot analysis or for 30 minutes at 37°C if used in immunization. GP blebs treated with both furin and thermolysin were simultaneously treated with 0.167 mg/mL thermolysin overnight. Blebs used for immunization were resuspended in 10 mL Buffer A after protease cleavage.

5.2.3 Preparation of pseudotyped virus

Pseudotyped viruses were produced following published protocols [94,95]. Briefly, particles were produced by transfecting HEK 293T cells with plasmids encoding for luciferase, Murine Leukemia Virus gag and polymerase, and the viral spike protein of interest using Lipofectamine 2000 following the manufacturer's instructions. Supernatant was harvested 48 h post-transfection, filtered through a 0.45 μm membrane, and stored at -80 °C. To remove the glycan cap, pseudovirus particles were pelleted by ultracentrifugation at 42000 rpm, 4°C for 2h in a TLA 55 rotor (Beckman Coulter), the resuspended in a buffer (50 mM Tris, 10 mM $CaCl_2$, 150 mM NaCl, 0.05% Brij -35) containing 0.167 mg/mL thermolysin. The particles were then placed at 37°C overnight.

5.3 Results

5.3.1 Production and characterization of virus-like blebs

Blebs were produced from HEK 293T cells according to the protocol described in Methods and Materials. In summary, cells were transfected with 6 μg GP from the Mayinga 1976 strain of Ebolavirus. Twenty four hours after transfection, cells were incubated with 4 mL blebbing buffer. Cells were incubated at room temperature with

rocking for 1 h then placed at 37°C for 1 h. The supernatant was harvested and allowed to settle on ice for 15 minutes. The top 9 mL of the solution was collected and ultracentrifuged at 20,000 rpm in a SW-41 rotor (Beckman-Coulter) for 1 h at 4°C to pellet the blebs. Blebs were resuspended in Buffer A.

Size characterization of the blebs as determined by Nanosight indicates that the blebs are 173 nm in diameter (Figure 5.1A). They are similar in size but more polydisperse than viral particles pseudotyped with GP (Figure 5.1B).

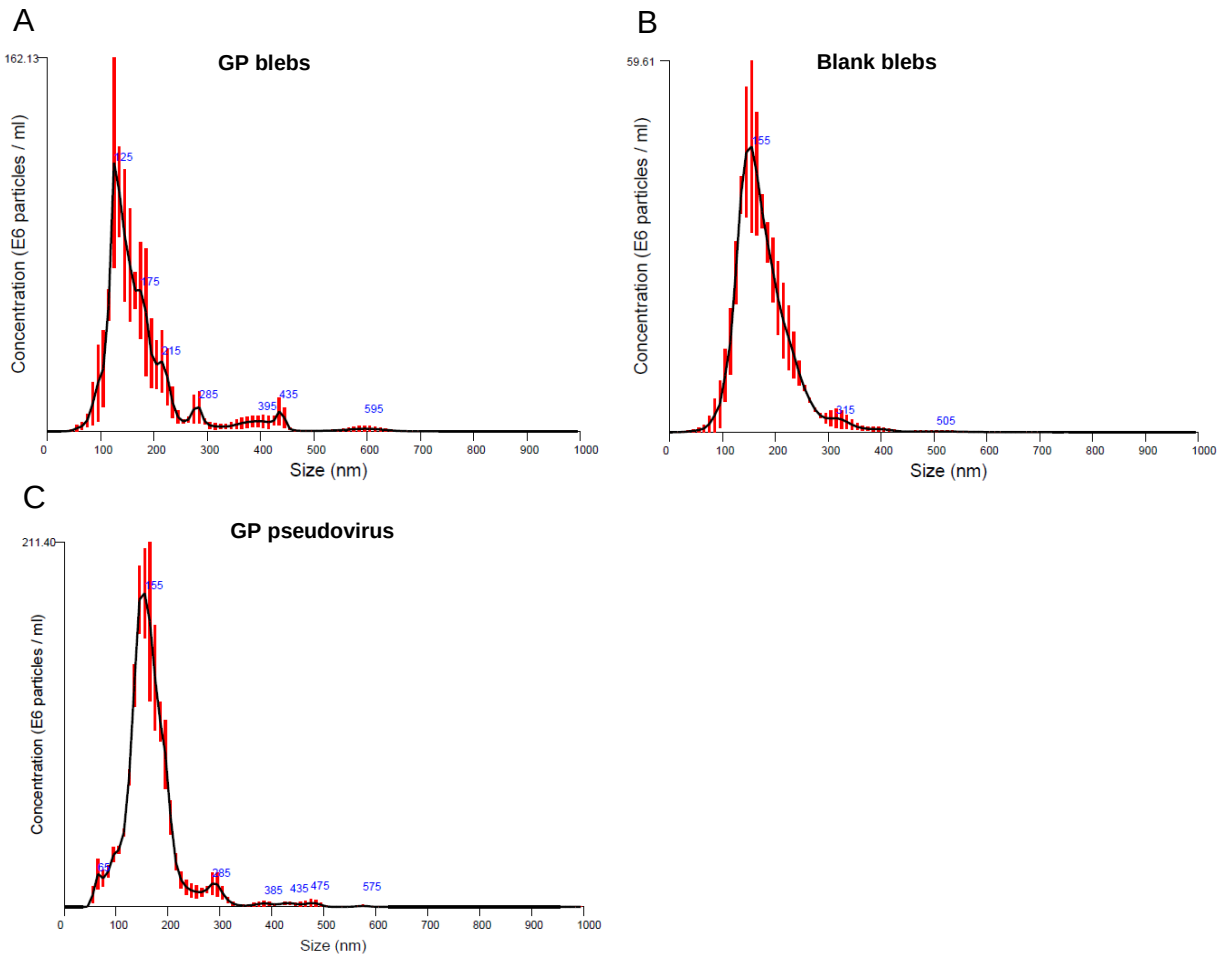

Figure 5.1 Size distribution of blebs and pseudovirus particles. A) Blebs containing GP b) Blebs from untransfected HEK 293T cells C) Pseudovirus particles containing GP. Red error bars indicate +/- 1 standard error of the mean.

To confirm that the GP in blebs is the same form as GP found in the virus and therefore physically relevant for immunization, blebs and pseudovirus were analyzed by Western Blot. Western Blots on the blebs show that the blebs contain a form of GP that is slightly heavier than the GP found in pseudovirus (Figure 5.2). To test whether

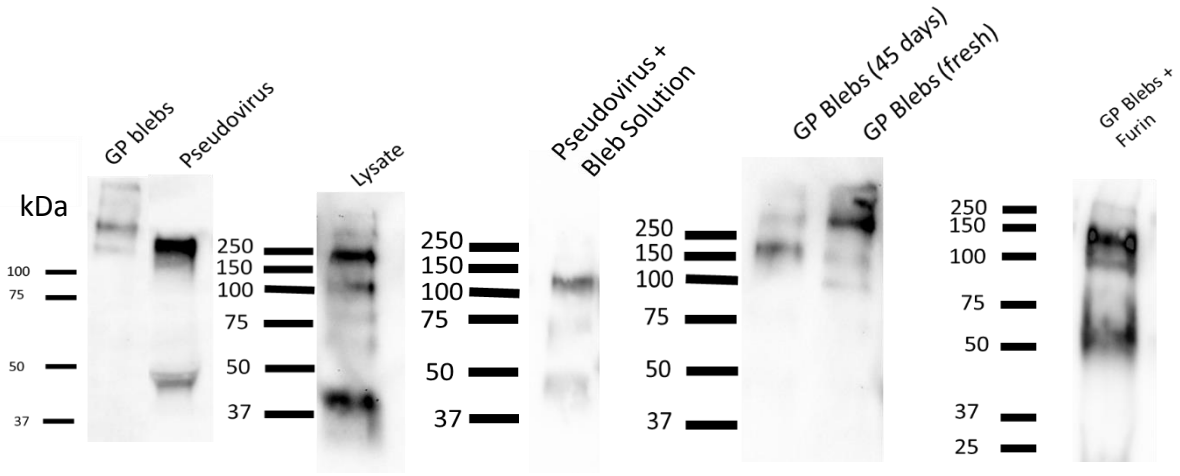

Figure 5.2. Western Blot detection of GP. Samples were prepared under reducing conditions and probed with an anti-GP1 antibody.

this was an artifact of the blebbing buffer crosslinking the protein, we compared blebs left in blebbing solution for 45 days, blebs with the blebbing solution removed immediately after harvesting, pseudovirus stored in blebbing solution for 45 days, and lysate from transfected cells. The blebs that were stored for 45 days in blebbing solution did not contain the heavier species of GP, whereas the freshly harvested blebs did, indicating that the heavier species were not caused by blebbing solution crosslinking GP. Mixing pseudovirus with blebbing solution also does not produce the heavier form. Lysate from cells transfected with GP showed the presence of forms of GP heavier than 130 kDa. This agrees with observations reported in literature[256]; we hypothesized that the virus preferentially incorporates GP that has been cleaved by furin while the blebs and lysate contain the uncleaved form of GP. When GP blebs were treated overnight with 0.2 U/μL furin at 37°C, they primarily contained the 130

kDa form of GP, confirming that by treating the blebs with furin we can obtain the form of GP found in the virus. It is possible that the bond that gets cleaved by furin is somewhat unstable and can degrade over time, or that a low amount of furin is present in the bleb supernatant, which is why the blebs incubated for 45 days lacked the heavier species.

5.3.2 Methodology for mouse immunization

Animal studies will conducted through a collaboration with the University of New Mexico Medical School. Mice will be immunized with 10 μg of blebs/mouse with either GP blebs or blank blebs supplemented with incomplete Freud's adjuvant. Five mice will be used for each condition. A prime/boost scheme will be utilized with the first boost occurring 3 weeks after priming and a second boost 3 weeks after the first. Sera will be collected throughout the experiment and checked for the presence of neutralizing antibodies specific to GP. Should these initial immunization experiments be successful, the likely next step would be to conduct a challenge study where mice are vaccine and subsequently exposed to Ebola virus to assess the ability of the vaccine to provide protection.

5.5 Discussion and future work

Chemical induction of blebs is a robust technique. Our lab has produced blebs from a variety of cell types including baby hamster kidney cells, human embryonic kidney cells, and African green monkey kidney cells. Furthermore in addition to the virus-like blebs produced with Ebola virus GP as presented here, influenza hemagglutinin has also successfully been incorporated into blebs[155], demonstrating the potential for virus-like blebs to be used for a variety of vaccines.

If antibody tiers are low, loading of GP onto blebs could be further optimized since antigen mulitvalency enables a more effective immune response. Estimation of the number of GP trimers per bleb could be obtained through flow cytometry in which fluorescent anti-GP antibodies would be bound to blebs; GP concentration could then be estimated from the fluorescence intensity. Transfection could be adjusted to maximize GP expression and incorporation into blebs.

Bleb samples contain roughly 1.07 EU/mL of endotoxin, the source of which appears to be the water used in Buffer A. If this endotoxin level has undesirable effects on the mice, Buffer A could be adjusted to minimize endotoxin. Alternatively, an endotoxin removal step could be added after the blebs have been produced. A number of endotoxin removal options are available; Triton X-114, which has successfully been used by our collaborators to remove endotoxin from virus-like particles without removing the particles themselves from solution, could serve as a starting point.

In the long-term, identification and resolution of bottlenecks in the scale-up of blebbing need to be resolved. One such challenge is the use of transient transfection to express GP. Stably expressing cells lines could be produced using lentiviral transfection. Another challenge is the production of blebs batch-wise, when continuous production is preferred industrially. It has not been determined how long a batch of cells can produce blebs before they become lysed or if the same batch of blebs can be blebbed multiple times; these are both avenues for future investigation. Similarly, overexpression of furin in the cells may eliminate the requirement for exogenous batch-wise furin treatment.

Virus-like plasma membrane blebs have the advantage of being a “plug and play” system that can easily be modified for other enveloped viruses. This is particularly of value in the development of vaccines against filoviruses because neither

natural infection nor vaccination against a particular species is cross-protective against other members of the family. Blebs only require optimization of a single transfection, rather than the multiple simultaneous or sequential transfections required to produce pseudoviruses or virus-like particles. In principle, virus-like plasma membrane blebs are similar to bacterial outer membrane vesicles, but because blebs are made from mammalian cells, proteins in the blebs are naturally glycosylated.

5.6 Acknowledgements

The authors of this work are Lakshmi Nathan, Brooke Cohen, Steven Bradfute, Bryce C. Chackerian, and Susan Daniel. LN prepared and characterized the blebs, designed experiments, and wrote the text. B. C. assisted with bleb characterization, S.B. will perform neutralization studies, B.C.C will conduct immunization studies, and B. C. C. and S.D. conceived the project and provided guidance. L.N. would like to thank Tyler Moeller for helpful discussions related to this work. This work is supported by National Science Foundation 1504846 (to S.D.).

CHAPTER 6
CONCLUSIONS AND OUTLOOK

This work was motivated by the 2014 outbreak of Ebola virus, which was the largest outbreak ever recorded. The virus infected nearly 30,000 people and killed more than 11,000[273]. On average Ebola virus outbreaks have a lethality of 50%, though it has ranged from 39% to 66% over the past five years; the highest lethality ever recorded is 90%[276]. There are currently no therapeutics or vaccines licensed in the United States. The World Health Organization has identified Ebola virus and the closely related Marburg virus as priority diseases which urgently need accelerated research and development to prevent future public health emergencies[277,278]. This thesis addresses that need in three key areas: providing fundamental insight into host factors critical for virus entry, establishing tools to enable further characterization of the Ebola virus entry process, and finally developing a new vaccine platform.

My work adds a key piece of information about the cellular factors involved in entry of enveloped viruses, namely the importance of calcium in enabling fusion of Ebola virus and potentially all filoviruses. This research contributes to a growing body of evidence that certain families of enveloped viruses rely on calcium for fusion, namely coronaviruses and retroviruses. However, compared to other host factors, such as proteases and endosome acidification, the role of cations in viral fusion remains relatively understudied. Further study of the relationship between cations and viral fusion could enable the development of broad-spectrum antivirals that are effective against multiple virus families. Given the potential of certain filoviruses and

coronaviruses to cause outbreaks, such therapeutics would be a useful tool in combating epidemics.

This work also outlines the development of tools that enable the tracking of individual virions as they undergo entry, binding, and fusion. Tracking virions in live cells is particularly well-suited to investigating movement of virions from one cell to another, interaction of virions and viral components with the cell cytoskeleton, endosomal escape, and movement near the nucleus. Tracking of virions with biomimetic membranes provides detailed information on the effects of host membrane composition, viral movement on the surface of the membrane, dynamics of receptor binding, timing and sequence of fusion triggers, and kinetics of hemifusion and pore formation. These methods provide complementary data, which can be combined with traditional virology techniques and structural information to provide the full picture of viral entry. Further developments in microscopy will increase the special and temporal resolution of data obtained through single virion techniques.

Single virion tracking of Ebola virus with a biomimetic membrane has not previously been reported. I have adapted the single-particle tracking platform of the Daniel lab for use in such experiments. The well-defined nature of this platform makes it optimally suited for identifying the Ebola virus fusion trigger, which has remained elusive. The complex interplay of glycan cap removal, pH dependence of the protease necessary for glycan cap cleavage, and receptor binding had made determination of the fusion trigger challenging. Each of these factors has successfully been incorporated into the single-virion tracking platform, and along with the insight that calcium is critical, the platform is poised to finally determine the fusion trigger.

Addressing the need for vaccines that are easily and quickly adaptable to future outbreaks, we present virus-like plasma membrane blebs as vaccine candidates. Similar to the "plug-and-play" promise of bacterial outer membrane vesicle-based vaccines, blebs can be made to mimic any enveloped virus as long as the viral spike protein has been identified, and a plasmid encoding that protein can be transfected into a mammalian cell. Viral proteins are often heavily glycosylated, so production of vaccines in mammalian cells that naturally contain the appropriate glycosylation machinery is advantageous. This technology requires only a single transfection, in contrast to the production of virus like particles or pseudoviruses, which require multiple simultaneous transfections. At the time of this writing, mouse studies are underway to determine the ability of Ebola virus-like blebs to produce a specific immune response. Should these pilot studies be successful, substantial further research is needed; this includes investigating the optimal dosing regimen, identification of any off-target effects, optimizing the immunogenicity of the particles, and confirmation of protection through challenge studies. However, this work has the potential to launch a new category of vaccines that could be valuable tools against outbreaks of Ebola virus and beyond.

APPENDIX A

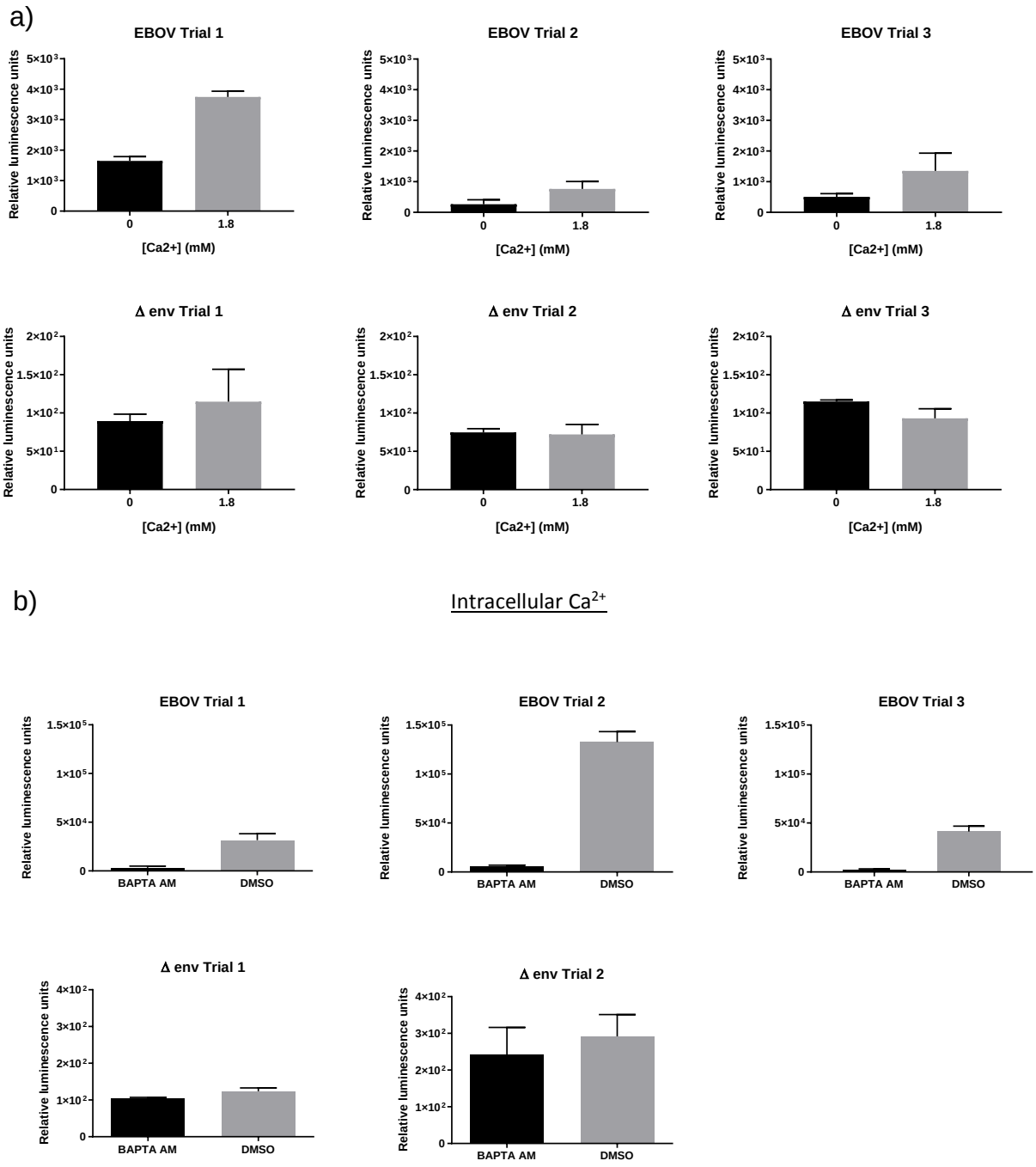

Figure A1. Raw data of a) extracellular and b) intracellular calcium experiments. Δ env is a pseudotyped virus that lacks a spike protein and thus serves as a non-infectious negative control. It is produced by omitting the spike protein plasmid during transfection of HEK 293T cells for pseudotyped virus production. Error bars represent s.d. among 3 technical replicates. Note the difference in scale between graphs.

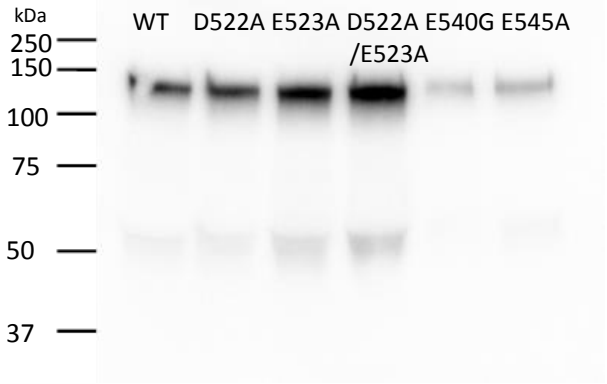

Figure A2. Western Blot confirming incorporation of WT and mutant GP into pseudotyped virus particles. Supernatant from transfected cells was harvested 48 h post-transfection, filtered through a 0.45 μm membrane, and stored at -80°C. After thawing from -80 °C, particles were pelleted at 42000 rpm and resuspended in 30 μL PBS to concentrate the sample prior to blotting.

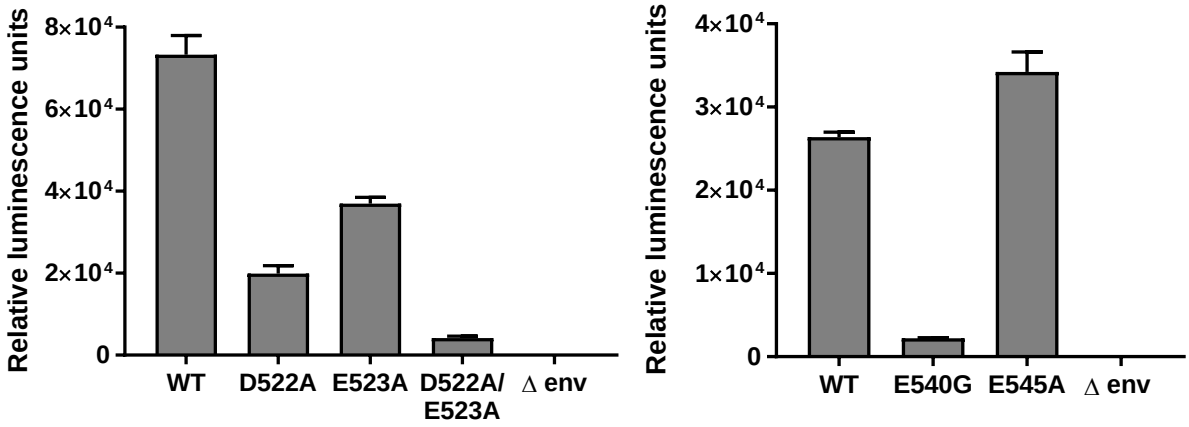

Figure A3. Infectivity of mutant GP pseudotyped virus and non-infectious control (Δ env). Error bars indicate s.d among 3 technical replicates from testing the same batch of virus.

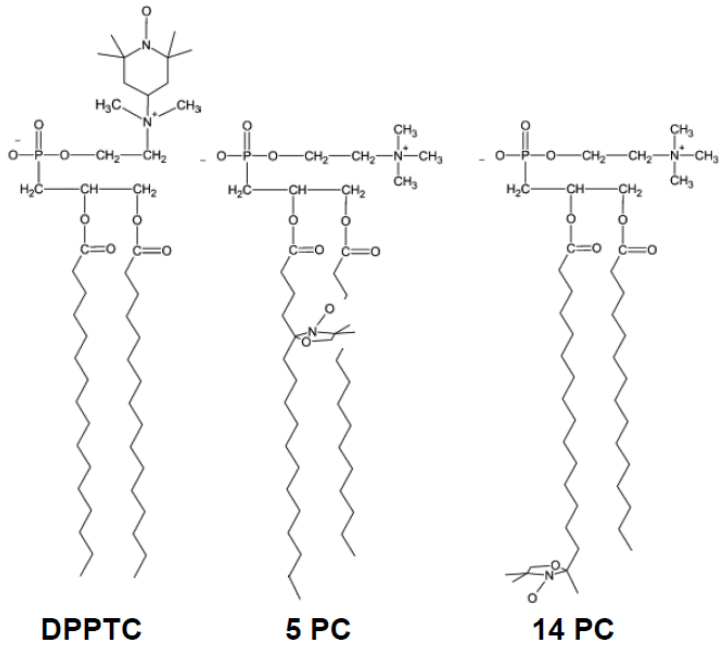

Figure A4. Structure of spin labeled lipids.

a)

Long FP 501-560

G S I E G R A Q P K C N P N L H Y W T T Q D E **G A A I G L A**
W I P Y F G P A A E G I Y I E G L M H N Q D G L I C G L R Q

Short FP 524-539

G A A I G L A W I P Y F G P A A

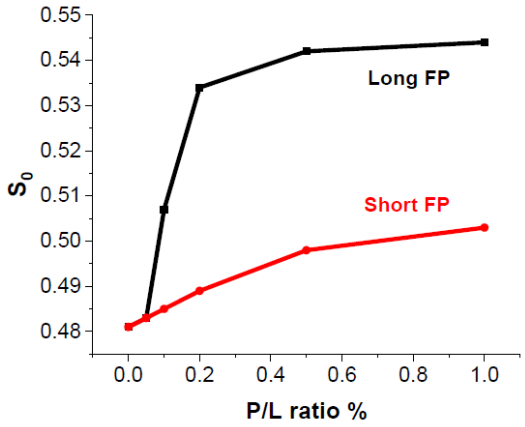

Figure A5. The long FP has a stronger ordering effect than the short FP. a) Amino acid sequences of the long and short FP. b) Plot of order parameter (S_0) of DPPTC versus peptide:lipid ratio (P/L ratio) of FP.

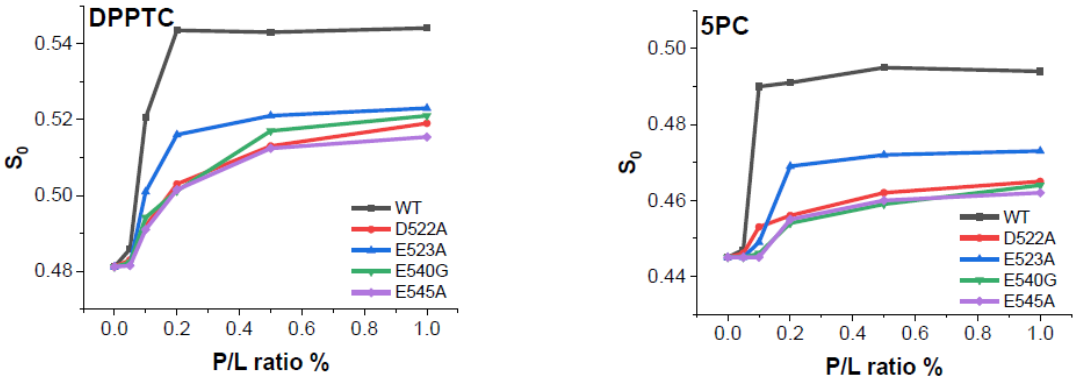

Figure A6. Comparing the membrane ordering effects of the WT and mutant EBOV FPs on DPPTC (left) and 5PC (right) as a function of peptide:lipid ratio (P/L ratio). Black, WT FP; red, D522A; blue, E523A; green,E540G ; purple, E545A.

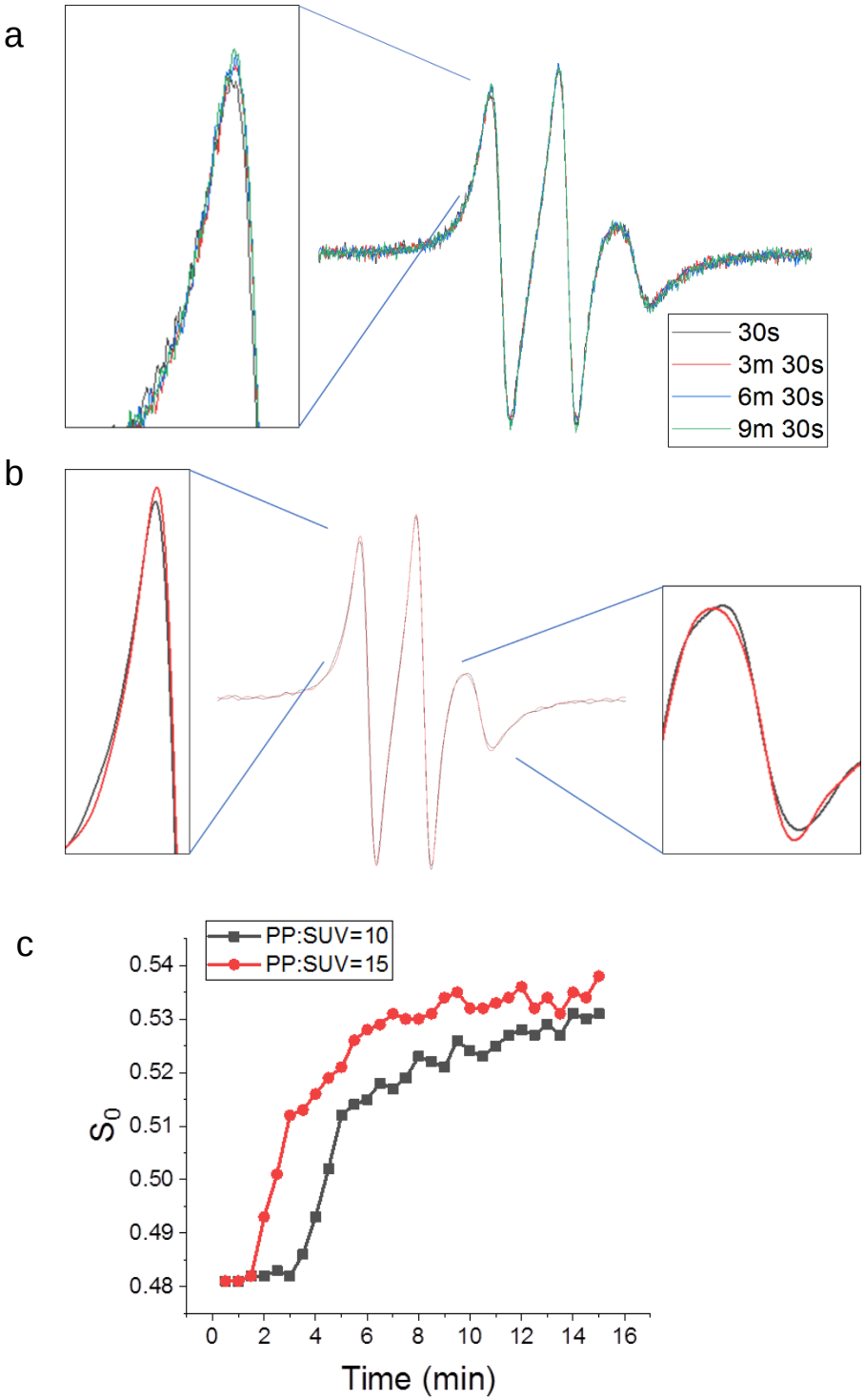

Fig. S7. A) The shape of ESR curves of DPPTC on SUV change after the activation by acidification in the SUV:PP mixture. Black, collected at 0.5 min, red, at 3.5 min, blue, at 6.5 min, and green at 9.5 min. B) after Wavelet Denoising, the change is more obvious, black, collected at 0.5 min, red, at 3.5 min. C) the plot of S0-time, showing the "jump" time is related to the PP:SUV ratio. Black, PP:SUV=10, red, PP:SUV=15.

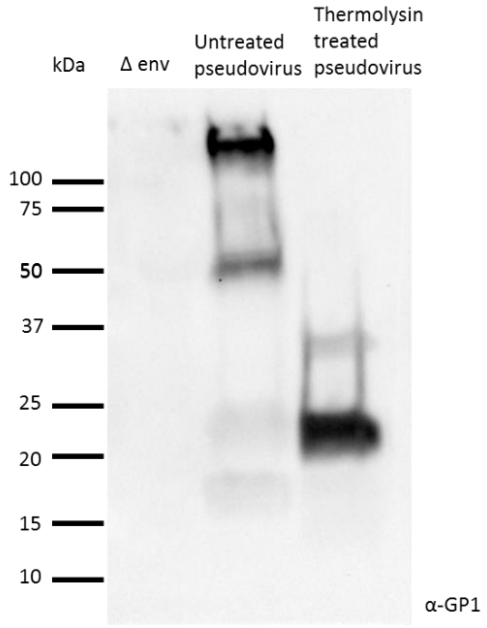

Figure A8. Treatment with thermolysin removes the glycan cap.

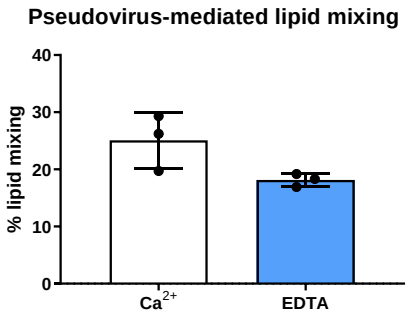

Figure A9. Lipid mixing mediated by pseudovirus

REFERENCES

1. Jahn, R. Principles of exocytosis and membrane fusion. *Annals of the New York Academy of Sciences* **1014**, 170–178 (2004).
2. Chapman, E. R. Synaptotagmin: A Ca2+ sensor that triggers exocytosis? *Nat. Rev. Mol. Cell Biol.* **3**, 498–508 (2002).
3. Gomperts, B. D., Tatham, P. E. R. (Life scientist) & Kramer, I. M. Intracellular Calcium. in *Signal transduction* (ed. Kramer, I. M.) 381–439 (Elsevier/Academic Press, 2009).
4. Helenius, A. Virus Entry and Uncoating. in *Fields Virology* (eds. Knipe, D.M & Howley, P. M.) 87–114 (Wolters Kluwer Lippincott Willams & Wilkins, 2013).
5. White, J. M., Delos, S. E., Brecher, M. & Schornberg, K. Structures and mechanisms of viral membrane fusion proteins: multiple variations on a common theme. *Crit. Rev. Biochem. Mol. Biol.* **43**, 189–219 (2008).
6. White, J. M. & Whittaker, G. R. Fusion of Enveloped Viruses in Endosomes. *Traffic* **17**, 593–614 (2016).
7. Dubé, M., Rey, F. A. & Kielian, M. Rubella virus: first calcium-requiring viral fusion protein. *PLoS Pathog.* **10**, e1004530 (2014).
8. Lai, A. L., Millet, J. K., Daniel, S., Freed, J. H. & Whittaker, G. R. The SARS-CoV Fusion Peptide Forms an Extended Bipartite Fusion Platform that Perturbs Membrane Order in a Calcium-Dependent Manner. *J. Mol. Biol.* **429**, 3875–3892 (2017).
9. Nathan, L. *et al. Calcium Ions Enhance Entry of Ebola Virus by Directly Targeting the Fusion Peptide*. (2019).
10. Ferro-Novick, S. & Jahn, R. Vesicle fusion from yeast to man. *Nature* **370**, 191–193 (1994).
11. Brunger, A. T. Structure and function of SNARE and SNARE-interacting proteins. *Q. Rev. Biophys.* **38**, 1 (2006).
12. Clary, D. O. & Rothman, J. E. Purification of three related peripheral membrane proteins needed for vesicular transport. *J. Biol. Chem.* **265**, 10109–17 (1990).
13. Sakaba, T., Stein, A., Jahn, R. & Neher, E. Distinct Kinetic Changes in Neurotransmitter Release After SNARE Protein Cleavage. *Science (80-.).* **309**, 491–494 (2005).
14. Söllner, T. *et al.* SNAP receptors implicated in vesicle targeting and fusion. *Nature* **362**, 318–324 (1993).
15. Burgoyne, R. D. Neuronal calcium sensor proteins: generating diversity in neuronal Ca2+ signalling. *Nat. Rev. Neurosci.* **8**, 182–193 (2007).
16. Chapman, E. R. & Jahn, R. Calcium-dependent interaction of the cytoplasmic region of synaptotagmin with membranes. Autonomous function of a single C2-homologous domain. *J. Biol. Chem.* **269**, 5735–41 (1994).
17. Nalefski, E. A. & Falke, J. J. The C2 domain calcium-binding motif: Structural and functional diversity. *Protein Sci.* **5**, 2375–2390 (1996).
18. Ubach, J., Zhang, X., Shao, X., Südhof, T. C. & Rizo, J. Ca2+ binding to synaptotagmin: how many Ca2+ ions bind to the tip of a C2-domain? *EMBO J.* **17**, 3921–30 (1998).

19. Allgrove, J. Physiology of Calcium, Phosphate and Magnesium. in *Calcium and Bone Disorders in Children and Adolescents* **16**, 8–31 (KARGER, 2009).
20. Zhou, Y., Frey, T. K. & Yang, J. J. Viral calciomics: Interplays between Ca2+ and virus. *Cell Calcium* **46**, 1–17 (2009).
21. Kinoshita, S. *et al.* The T Cell Activation Factor NF-ATc Positively Regulates HIV-1 Replication and Gene Expression in T Cells. *Immunity* **6**, 235–244 (1997).
22. Ding, W. *et al.* Human T-cell lymphotropic virus type 1 p12(I) expression increases cytoplasmic calcium to enhance the activation of nuclear factor of activated T cells. *J. Virol.* **76**, 10374–82 (2002).
23. Gearhart, T. L. & Bouchard, M. J. Replication of the hepatitis B virus requires a calcium-dependent HBx-induced G1 phase arrest of hepatocytes. *Virology* **407**, 14–25 (2010).
24. Bergqvist, A., Sundström, S., Dimberg, L. Y., Gylfe, E. & Masucci, M. G. The hepatitis C virus core protein modulates T cell responses by inducing spontaneous and altering T-cell receptor-triggered Ca2+ oscillations. *J. Biol. Chem.* **278**, 18877–83 (2003).
25. Li, Y., Boehning, D. F., Qian, T., Popov, V. L. & Weinman, S. A. Hepatitis C virus core protein increases mitochondrial ROS production by stimulation of Ca 2+ uniporter activity. *FASEB J.* **21**, 2474–2485 (2007).
26. Zoeteweij, J. P. *et al.* Targeted inhibition of calcineurin signaling blocks calcium-dependent reactivation of Kaposi sarcoma-associated herpesvirus. *Blood* **97**, 2374–80 (2001).
27. Sharon-Friling, R., Goodhouse, J., Colberg-Poley, A. M. & Shenk, T. Human cytomegalovirus pUL37x1 induces the release of endoplasmic reticulum calcium stores. *Proc. Natl. Acad. Sci. U. S. A.* **103**, 19117–22 (2006).
28. Ebenbichler, C. F., Stoiber, H., Schneider, R., Patsch, J. R. & Dierich, M. P. The human immunodeficiency virus type 1 transmembrane gp41 protein is a calcium-binding protein and interacts with the putative second-receptor molecules in a calcium-dependent manner. *J. Virol.* **70**, 1723–8 (1996).
29. Dimitrov, D. S., Broder, C. C., Berger, E. A. & Blumenthal, R. Calcium ions are required for cell fusion mediated by the CD4-human immunodeficiency virus type 1 envelope glycoprotein interaction. *J. Virol.* **67**, 1647–52 (1993).
30. Burmeister, W. P., Ruigrok, R. W. & Cusack, S. The 2.2 A resolution crystal structure of influenza B neuraminidase and its complex with sialic acid. *EMBO J.* **11**, 49–56 (1992).
31. DuBois, R. M. *et al.* Functional and evolutionary insight from the crystal structure of rubella virus protein E1. *Nature* **493**, 552–556 (2013).
32. Jaimes, J. A. *No Title*. (2019).
33. Wallin, M., Ekström, M. & Garoff, H. Isomerization of the intersubunit disulphide-bond in Env controls retrovirus fusion. *EMBO J.* **23**, 54–65 (2004).
34. Yu, H., Alfsen, A., Tudor, D. & Bomsel, M. The binding of HIV-1 gp41 membrane proximal domain to its mucosal receptor, galactosyl ceramide, is structure-dependent. *Cell Calcium* **43**, 73–82 (2008).
35. Larsen, C. E. *et al.* Human immunodeficiency virus type 1 (HIV-1) fusion with

model membranes: kinetic analysis and the role of lipid composition, pH and divalent cations. *Biochim. Biophys. Acta - Biomembr.* **1147**, 223–236 (1993).
36. Sáez-Cirión, A. & Nieva, J. L. Conformational transitions of membrane-bound HIV-1 fusion peptide. *Biochim. Biophys. Acta - Biomembr.* **1564**, 57–65 (2002).
37. Davletov, B. A. & Sudhof, T. C. A Single C2 Domain & om Synaptotagmin I Is Sufficient for High. *J. Biol. Chem.* **268**, 26386–26390 (1993).
38. Dubé, M., Etienne, L., Fels, M. & Kielian, M. Calcium-Dependent Rubella Virus Fusion Occurs in Early Endosomes. *J. Virol.* **90**, 6303–13 (2016).
39. Ruiz-Argüello, M. B., Goñi, F. M., Pereira, F. B. & Nieva, J. L. Phosphatidylinositol-dependent membrane fusion induced by a putative fusogenic sequence of Ebola virus. *J. Virol.* **72**, 1775–81 (1998).
40. Suárez, T. *et al.* Calcium-dependent conformational changes of membrane-bound Ebola fusion peptide drive vesicle fusion. *FEBS Lett.* **535**, 23–28 (2003).
41. Jaimes, J. A. & Whittaker, G. R. Feline coronavirus: Insights into viral pathogenesis based on the spike protein structure and function. *Virology* **517**, 108–121 (2018).
42. Shao, X., Fernandez, I., Südhof, T. C. & Rizo, J. Solution Structures of the Ca2+-free and Ca2+-bound C2A Domain of Synaptotagmin I: Does Ca2+ Induce a Conformational Change?†. (1998). doi:10.1021/BI981789H
43. Haywood, A. M. & Boyer, B. P. Sendai virus membrane fusion: time course and effect of temperature, pH, calcium, and receptor concentration. *Biochemistry* **21**, 6041–6046 (1982).
44. Sakurai, Y. *et al.* Two-pore channels control Ebola virus host cell entry and are drug targets for disease treatment. *Science (80-.).* **347**, 995–998 (2015).
45. Gunaratne, G. S., Yang, Y., Li, F., Walseth, T. F. & Marchant, J. S. NAADP-dependent Ca2+ signaling regulates Middle East respiratory syndrome-coronavirus pseudovirus translocation through the endolysosomal system. *Cell Calcium* **75**, 30–41 (2018).
46. Godfraind, T. Discovery and Development of Calcium Channel Blockers. *Front. Pharmacol.* **8**, (2017).
47. Feldmann, H. & Geisbert, T. W. Ebola haemorrhagic fever. *Lancet* **377**, 849–62 (2011).
48. Centers for Disease Control and Prevention. Years of Ebola Virus Disease Outbreaks. Available at: https://www.cdc.gov/vhf/ebola/history/chronology.html. (Accessed: 24th May 2018)
49. WHO | Ebola virus disease – Democratic Republic of the Congo. *WHO* (2019).
50. Regules, J. A. *et al.* A Recombinant Vesicular Stomatitis Virus Ebola Vaccine. *N. Engl. J. Med.* **376**, 330–341 (2017).
51. Ledgerwood, J. E. *et al.* Chimpanzee Adenovirus Vector Ebola Vaccine. *N. Engl. J. Med.* **376**, 928–938 (2017).
52. Milligan, I. D. *et al.* Safety and Immunogenicity of Novel Adenovirus Type 26– and Modified Vaccinia Ankara–Vectored Ebola Vaccines. *JAMA* **315**, 1610 (2016).
53. Cross, R. W., Mire, C. E., Feldmann, H. & Geisbert, T. W. Post-exposure

treatments for Ebola and Marburg virus infections. *Nat. Rev. Drug Discov.* **17**, 413–434 (2018).
54. Sweiti, H., Ekwunife, O., Jaschinski, T. & Lhachimi, S. K. Repurposed Therapeutic Agents Targeting the Ebola Virus: A Systematic Review. *Curr. Ther. Res.* **84**, 10–21 (2017).
55. Hayden, F. G., Friede, M. & Bausch, D. G. Experimental Therapies for Ebola Virus Disease: What Have We Learned? *J. Infect. Dis.* **215**, jiw496 (2017).
56. Johansen, L. M. *et al.* FDA-approved selective estrogen receptor modulators inhibit Ebola virus infection. *Sci. Transl. Med.* **5**, 190ra79 (2013).
57. Johansen, L. M. *et al.* A screen of approved drugs and molecular probes identifies therapeutics with anti-Ebola virus activity. *Sci. Transl. Med.* **7**, 290ra89 (2015).
58. Madrid, P. B. *et al.* Evaluation of Ebola Virus Inhibitors for Drug Repurposing. *ACS Infect. Dis.* **1**, 317–326 (2015).
59. Aleksandrowicz, P. *et al.* Ebola virus enters host cells by macropinocytosis and clathrin-mediated endocytosis. *J. Infect. Dis.* **204 Suppl**, S957-67 (2011).
60. Kaletsky, R. L., Simmons, G. & Bates, P. Proteolysis of the Ebola virus glycoproteins enhances virus binding and infectivity. *J. Virol.* **81**, 13378–84 (2007).
61. Schornberg, K. *et al.* Role of endosomal cathepsins in entry mediated by the Ebola virus glycoprotein. *J. Virol.* **80**, 4174–8 (2006).
62. Simmons, J. A. *et al.* Ebolavirus Glycoprotein Directs Fusion through NPC1+ Endolysosomes. *J. Virol.* **90**, 605–10 (2016).
63. Carette, J. E. *et al.* Ebola virus entry requires the cholesterol transporter Niemann-Pick C1. *Nature* **477**, 340–3 (2011).
64. Miller, E. H. *et al.* Ebola virus entry requires the host-programmed recognition of an intracellular receptor. *EMBO J.* **31**, 1947–60 (2012).
65. Côté, M. *et al.* Small molecule inhibitors reveal Niemann-Pick C1 is essential for Ebola virus infection. *Nature* **477**, 344–8 (2011).
66. Spence, J. S., Krause, T. B., Mittler, E., Jangra, R. K. & Chandran, K. Direct Visualization of Ebola Virus Fusion Triggering in the Endocytic Pathway. *MBio* **7**, e01857-15- (2016).
67. Lee, J. E. *et al.* Structure of the Ebola virus glycoprotein bound to an antibody from a human survivor. *Nature* **454**, 177–182 (2008).
68. Gregory, S. M. *et al.* Structure and function of the complete internal fusion loop from Ebolavirus glycoprotein 2. *Proc. Natl. Acad. Sci.* **108**, 11211–11216 (2011).
69. Scott, C. C. & Gruenberg, J. Ion flux and the function of endosomes and lysosomes: pH is just the start. *BioEssays* **33**, 103–110 (2011).
70. Huotari, J. & Helenius, A. Endosome maturation. *EMBO J.* **30**, 3481–500 (2011).
71. Gerasimenko, J. V., Tepikin, A. V., Petersen, O. H. & Gerasimenko, O. V. Calcium uptake via endocytosis with rapid release from acidifying endosomes. *Curr. Biol.* **8**, 1335–1338 (1998).
72. Albrecht, T., Zhao, Y., Nguyen, T. H., Campbell, R. E. & Johnson, J. D.

Fluorescent biosensors illuminate calcium levels within defined beta-cell endosome subpopulations. *Cell Calcium* **57**, 263–274 (2015).
73. Christensen, K. a, Myers, J. T. & Swanson, J. A. pH-dependent regulation of lysosomal calcium in macrophages. *J. Cell Sci.* **115**, 599–607 (2002).
74. Tymianski, M. *et al.* Mechanism of Action and Persistence of Neuroprotection by Cell-Permeant Ca $^{2+}$ Chelators. *J. Cereb. Blood Flow Metab.* **14**, 911–923 (1994).
75. Sakurai, Y. *et al.* Ebola virus. Two-pore channels control Ebola virus host cell entry and are drug targets for disease treatment. *Science* **347**, 995–8 (2015).
76. Fan, H. *et al.* Selective inhibition of Ebola entry with selective estrogen receptor modulators by disrupting the endolysosomal calcium. *Sci. Rep.* **7**, 41226 (2017).
77. Tang, N. & Skibsted, L. H. Calcium Binding to Amino Acids and Small Glycine Peptides in Aqueous Solution: Toward Peptide Design for Better Calcium Bioavailability. *J. Agric. Food Chem.* **64**, 4376–4389 (2016).
78. Budil, D. E., Lee, S., Saxena, S. & Freed, J. H. Nonlinear-least-squares analysis of slow-motion EPR spectra in one and two dimensions using a modified Levenberg-Marquardt algorithm. *J. Magn. Reson. Ser. A* **120**, 155–189 (1996).
79. Lou, Y., Ge, M. & Freed, J. A Multifrequency ESR Study of the Complex Dynamics of Membranes. *J Phys Chem B* **105**, 11053–11056 (2001).
80. Lai, A. L. & Freed, J. H. Interaction between the influenza HA fusion peptide and transmembrane domain affects membrane structure. *Biophys J.* **109**, 1–14 (2015).
81. Lai, A. L., Moorthy, A. E., Li, Y. & Tamm, L. K. Fusion Activity of HIV gp41 Fusion Domain Is Related to Its Secondary Structure and Depth of Membrane Insertion in a Cholesterol-Dependent Fashion. *J. Mol. Biol.* **418**, 3–15 (2012).
82. Pinello, J. F. *et al.* Structure-Function Studies Link Class II Viral Fusogens with the Ancestral Gamete Fusion Protein HAP2. *Curr. Biol.* **27**, 651–660 (2017).
83. Srivastava, M., Anderson, C. L. & Freed, J. H. A New Wavelet Denoising Method for Selecting Decomposition Levels and Noise Thresholds. *IEEE Access* **4**, 3862–3877 (2016).
84. Gehring, G. *et al.* The clinically approved drugs amiodarone, dronedarone and verapamil inhibit filovirus cell entry. *J. Antimicrob. Chemother.* **69**, 2123–2131 (2014).
85. Lloyd-Evans, E. *et al.* Niemann-Pick disease type C1 is a sphingosine storage disease that causes deregulation of lysosomal calcium. *Nat. Med.* **14**, 1247–1255 (2008).
86. Ruiz-Argüello, M. B., Goñi, F. M., Pereira, F. B. & Nieva, J. L. Phosphatidylinositol-Dependent Membrane Fusion Induced by a Putative Fusogenic Sequence of Ebola Virus. *J. Virol.* **72**, 1775–1781 (1998).
87. Lee, J. *et al.* Structure of the Ebola virus envelope protein MPER/TM domain and its interaction with the fusion loop explains their fusion activity. *Proc. Natl. Acad. Sci. U. S. A.* **114**, E7987–E7996 (2017).
88. Kobayashi, T. *et al.* Separation and Characterization of Late Endosomal Membrane Domains. *J. Biol. Chem.* **277**, 32157–32164 (2002).

89. Lai, A. L. & Freed, J. H. HIV gp41 fusion peptide increases membrane ordering in a cholesterol-dependent fashion. *Biophys. J.* **106**, 172–181 (2014).
90. Calcraft, P. J. *et al.* NAADP mobilizes calcium from acidic organelles through two-pore channels. *Nature* **459**, 596–600 (2009).
91. Gerasimenko, J. V., Tepikin, A. V., Petersen, O. H. & Gerasimenko, O. V. Calcium uptake via endocytosis with rapid release from acidifying endosomes. *Curr. Biol.* **8**, 1335–1338 (1998).
92. Christensen, K. A., Myers, J. T. & Swanson, J. A. pH-dependent regulation of lysosomal calcium in macrophages. *J. Cell Sci.* **115**, 599–607 (2002).
93. Maxfield, F. R. & Yamashiro, D. J. Endosome Acidification and the Pathways of Receptor-Mediated Endocytosis. in 189–198 (Springer, Boston, MA, 1987). doi:10.1007/978-1-4684-5442-0_16
94. Bartosch, B., Dubuisson, J. & Cosset, F.-L. Infectious hepatitis C virus pseudo-particles containing functional E1-E2 envelope protein complexes. *J. Exp. Med.* **197**, 633–42 (2003).
95. Millet, J. K. & Whittaker, G. R. Murine Leukemia Virus (MLV)-based Coronavirus Spike-pseudotyped Particle Production and Infection. *Bio-protocol* **6**, (2016).
96. Ge, M. & Freed, J. H. Hydration, structure, and molecular interactions in the headgroup region of dioleoylphosphatidylcholine bilayers: an electron spin resonance study. *Biophys J* **85**, 4023–4040 (2003).
97. Louis-Jeune, C., Andrade-Navarro, M. A. & Perez-Iratxeta, C. Prediction of protein secondary structure from circular dichroism using theoretically derived spectra. *Proteins Struct. Funct. Bioinforma.* **80**, 374–381 (2012).
98. Marsh, M. & Helenius, A. Virus entry: Open sesame. *Cell* **124**, 729–740 (2006).
99. Suomalainen, M. & Greber, U. F. Uncoating of non-enveloped viruses. *Curr. Opin. Virol.* **3**, 27–33 (2013).
100. Flint, S. J., Enquist, L. W., Racaniello, V. R. & Skalka, A. M. *Principles of Virology, Volume I: Molecular Biology*. (ASM Press, 2009).
101. Matsuyama, S., Ujike, M., Morikawa, S., Tashiro, M. & Taguchi, F. Protease-mediated enhancement of severe acute respiratory syndrome coronavirus infection. *Proc. Natl. Acad. Sci. U. S. A.* **102**, 12543–7 (2005).
102. Yamauchi, Y. & Greber, U. F. Principles of Virus Uncoating: Cues and the Snooker Ball. *Traffic* **17**, 569–592 (2016).
103. Harrison, S. C. Viral membrane fusion. *Virology* **479**–**480**, 498–507 (2015).
104. Ma, Y. *et al.* Real-Time Imaging of Single HIV-1 Disassembly with Multicolor Viral Particles. *ACS Nano* **10**, 6273–6282 (2016).
105. Lakadamyali, M., Rust, M. J., Babcock, H. P. & Zhuang, X. Visualizing infection of individual influenza viruses. *Proc. Natl. Acad. Sci. U. S. A.* **100**, 9280–5 (2003).
106. Floyd, D. L., Harrison, S. C. & Van Oijen, A. M. Analysis of kinetic intermediates in single-particle dwell-Time distributions. *Biophys. J.* **99**, 360–366 (2010).
107. Costello, D. A. *et al.* Influenza Virus-Membrane Fusion Triggered by Proton

Uncaging for Single Particle Studies of Fusion Kinetics. *Anal. Chem.* **84**, 8480–8489 (2012).
108. Suomalainen, M. *et al.* Microtubule-dependent plus- and minus end-directed motilities are competing processes for nuclear targeting of adenovirus. *J. Cell Biol.* **144**, 657–72 (1999).
109. Ewers, H. & Schelhaas, M. Analysis of Virus Entry and Cellular Membrane Dynamics by Single Particle Tracking. *Methods Enzymol.* **506**, 63–80 (2012).
110. Helenius, A., Kartenbeck, J., Simons, K. & Fries, E. On the entry of Semliki forest virus into BHK-21 cells. *J. Cell Biol.* **84**, 404–20 (1980).
111. Seisenberger, G. *et al.* Real-time single-molecule imaging of the infection pathway of an adeno-associated virus. *Science* **294**, 1929–32 (2001).
112. Costello, D. A., Millet, J. K., Hsia, C. Y., Whittaker, G. R. & Daniel, S. Single particle assay of coronavirus membrane fusion with proteinaceous receptor-embedded supported bilayers. *Biomaterials* **34**, 7895–7904 (2013).
113. Michalet, X. *et al.* Detectors for single-molecule fluorescence imaging and spectroscopy. *J. Mod. Opt.* **54**, 239 (2007).
114. Shen, H. *et al.* Single Particle Tracking: From Theory to Biophysical Applications. *Chemical Reviews* **117**, 7331–7376 (2017).
115. Otterstrom, J. & Van Oijen, A. M. Visualization of membrane fusion, one particle at a time. *Biochemistry* **52**, 1654–1668 (2013).
116. Wang, I.-H., Burckhardt, C., Yakimovich, A. & Greber, U. Imaging, Tracking and Computational Analyses of Virus Entry and Egress with the Cytoskeleton. *Viruses* **10**, 166 (2018).
117. Brandenburg, B. & Zhuang, X. Virus trafficking - learning from single-virus tracking. *Nat. Rev. Microbiol.* **5**, 197–208 (2007).
118. Axelrod, D. Total internal reflection fluorescence microscopy in cell biology. *Methods Enzymol.* **361**, 1–33 (2003).
119. Mattheyses, A. L., Simon, S. M. & Rappoport, J. Z. Imaging with total internal reflection fluorescence microscopy for the cell biologist. *J. Cell Sci.* **123**, 3621–8 (2010).
120. Icha, J., Weber, M., Waters, J. C. & Norden, C. Phototoxicity in live fluorescence microscopy, and how to avoid it. *BioEssays* **39**, 1700003 (2017).
121. Sun, E., He, J. & Zhuang, X. Live cell imaging of viral entry. *Curr. Opin. Virol.* **3**, 34–43 (2013).
122. Huang, L.-L. & Xie, H.-Y. Progress on the labeling and single-particle tracking technologies of viruses. *Analyst* **139**, 3336–3346 (2014).
123. Liu, S.-L., Wang, Z.-G., Zhang, Z.-L. & Pang, D.-W. Tracking single viruses infecting their host cells using quantum dots. *Chem. Soc. Rev.* **45**, 1211–1224 (2016).
124. McDonald, D. *et al.* Visualization of the intracellular behavior of HIV in living cells. *J. Cell Biol.* **159**, 441–52 (2002).
125. Charpilienne, A. *et al.* Individual rotavirus-like particles containing 120 molecules of fluorescent protein are visible in living cells. *J. Biol. Chem.* **276**, 29361–7 (2001).
126. Desai, P. & Person, S. Incorporation of the green fluorescent protein into the

herpes simplex virus type 1 capsid. *J. Virol.* **72**, 7563–8 (1998).
127. Floyd, D. L., Ragains, J. R., Skehel, J. J., Harrison, S. C. & van Oijen, A. M. Single-particle kinetics of influenza virus membrane fusion. *Proc. Natl. Acad. Sci. U. S. A.* **105**, 15382–7 (2008).
128. Wessels, L., Elting, M. W., Scimeca, D. & Weninger, K. Rapid Membrane Fusion of Individual Virus Particles with Supported Lipid Bilayers. *Biophys. J.* **93**, 526–538 (2007).
129. Padilla-Parra, S. *et al.* Quantitative imaging of endosome acidification and single retrovirus fusion with distinct pools of early endosomes. *Proc. Natl. Acad. Sci. U. S. A.* **109**, 17627–32 (2012).
130. Lee, D. W., Hsu, H.-L., Bacon, K. B. & Daniel, S. Image Restoration and Analysis of Influenza Virions Binding to Membrane Receptors Reveal Adhesion-Strengthening Kinetics. *PLoS One* **11**, e0163437 (2016).
131. Kukura, P. *et al.* High-speed nanoscopic tracking of the position and orientation of a single virus. *Nat. Methods* **6**, 923–927 (2009).
132. Meijering, E., Dzyubachyk, O., Smal, I. & van Cappellen, W. A. Tracking in cell and developmental biology. *Seminars in Cell and Developmental Biology* **20**, 894–902 (2009).
133. Carter, B. C., Shubeita, G. T. & Gross, S. P. Tracking single particles: a user-friendly quantitative evaluation. *Phys. Biol.* **2**, 60–72 (2005).
134. Sbalzarini, I. F. & Koumoutsakos, P. Feature point tracking and trajectory analysis for video imaging in cell biology. *J. Struct. Biol.* **151**, 182–195 (2005).
135. Ruthardt, N., Lamb, D. C. & Bräuchle, C. Single-particle tracking as a quantitative microscopy-based approach to unravel cell entry mechanisms of viruses and pharmaceutical nanoparticles. *Mol. Ther.* **19**, 1199–211 (2011).
136. Lowy, R. J., Sarkar, D. P., Chen, Y. & Blumenthal, R. Observation of single influenza virus-cell fusion and measurement by fluorescence video microscopy. *Proc. Natl. Acad. Sci.* **87**, 1850–1854 (1990).
137. Georgiou, G. N., Morrison, I. E. G. & Cherry, R. J. Digital fluorescence imaging of fusion of influenza virus with erythrocytes. *FEBS Lett.* **250**, 487–492 (1989).
138. Niles, W. D. & Cohen, F. S. Fusion of influenza virions with a planar lipid membrane detected by video fluorescence microscopy. *J. Gen. Physiol.* **97**, 1101–19 (1991).
139. Niles, W. D. & Cohen, F. S. The role of N-acetylneuraminic (sialic) acid in the pH dependence of influenza virion fusion with planar phospholipid membranes. *J. Gen. Physiol.* **97**, 1121–40 (1991).
140. Castellana, E. T. & Cremer, P. S. Solid supported lipid bilayers: From biophysical studies to sensor design. *Surf. Sci. Rep.* **61**, 429–444 (2006).
141. Tanaka, M. & Sackmann, E. Polymer-supported membranes as models of the cell surface. *Nature* **437**, 656–663 (2005).
142. Sackmann, E. Supported membranes: scientific and practical applications. *Science* **271**, 43–8 (1996).
143. Bally, M. *et al.* Norovirus GII.4 Virus-like Particles Recognize Galactosylceramides in Domains of Planar Supported Lipid Bilayers. *Angew.*

Chemie Int. Ed. **51**, 12020–12024 (2012).
144. van der Borg, G., Braddock, S., Blijleven, J. S., van Oijen, A. M. & Roos, W. H. Single-particle fusion of influenza viruses reveals complex interactions with target membranes. *J. Phys. Condens. Matter* **30**, 204005 (2018).
145. Pace, H. *et al.* Preserved Transmembrane Protein Mobility in Polymer-Supported Lipid Bilayers Derived from Cell Membranes. *Anal. Chem.* **87**, 9194–9203 (2015).
146. Richards, M. J. *et al.* Membrane Protein Mobility and Orientation Preserved in Supported Bilayers Created Directly from Cell Plasma Membrane Blebs. *Langmuir* **32**, 2963–2974 (2016).
147. Costello, D. A. & Daniel, S. Single particle tracking assay to study coronavirus membrane fusion. *Methods Mol. Biol.* **1282**, 183–94 (2015).
148. Liu, H.-Y., Chen, W.-L., Ober, C. K. & Daniel, S. Biologically Complex Planar Cell Plasma Membranes Supported on Polyelectrolyte Cushions Enhance Transmembrane Protein Mobility and Retain Native Orientation. *Langmuir* acs.langmuir.7b02945 (2017). doi:10.1021/acs.langmuir.7b02945
149. Johnson, S. J. *et al.* Structure of an adsorbed dimyristoylphosphatidylcholine bilayer measured with specular reflection of neutrons. *Biophys. J.* **59**, 289–294 (1991).
150. Bayerl, T. M. & Bloom, M. Physical properties of single phospholipid bilayers adsorbed to micro glass beads. A new vesicular model system studied by 2H-nuclear magnetic resonance. *Biophys. J.* **58**, 357–362 (1990).
151. Matos, P. M. *et al.* Anionic lipids are required for vesicular stomatitis virus G protein-mediated single particle fusion with supported lipid bilayers. *J. Biol. Chem.* **288**, 12416–25 (2013).
152. Hsia, C.-Y., Richards, M. J. & Daniel, S. A review of traditional and emerging methods to characterize lipid–protein interactions in biological membranes. *Anal. Methods* **7**, 7076–7094 (2015).
153. Tatulian, S. A., Hinterdorfer ', P., Baber, G. & Tamm2, L. K. Influenza hemagglutinin assumes a tilted conformation during membrane fusion as determined by attenuated total reflection FTIR spectroscopy. *EMBO J.* **14**, 5514–5523 (1995).
154. Hinterdorfer, P., Baber, G. & Tamm, L. K. Reconstitution of Membrane Fusion Sites. *J. Biol. Chem.* **269**, 20360–20368 (1994).
155. Costello, D. A., Hsia, C. Y., Millet, J. K., Porri, T. & Daniel, S. Membrane fusion-competent virus-like proteoliposomes and proteinaceous supported bilayers made directly from cell plasma membranes. *Langmuir* **29**, 6409–6419 (2013).
156. Szklarczyk, O. M. *et al.* Receptor Concentration and Diffusivity Control Multivalent Binding of Sv40 to Membrane Bilayers. *PLoS Comput. Biol.* **9**, e1003310 (2013).
157. Hubner, W. *et al.* Quantitative 3D Video Microscopy of HIV Transfer Across T Cell Virological Synapses. *Science (80-.).* **323**, 1743–1747 (2009).
158. Felts, R. L. *et al.* 3D visualization of HIV transfer at the virological synapse between dendritic cells and T cells. *Proc. Natl. Acad. Sci. U. S. A.* **107**, 13336–

41 (2010).
159. Dale, B. M. *et al.* Cell-to-Cell Transfer of HIV-1 via Virological Synapses Leads to Endosomal Virion Maturation that Activates Viral Membrane Fusion. *Cell Host Microbe* **10**, 551–562 (2011).
160. Cudmore, S., Cossart, P., Griffiths, G. & Way, M. Actin-based motility of vaccinia virus. *Nature* **378**, 636–638 (1995).
161. Granstedt, A. E., Brunton, B. W. & Enquist, L. W. Imaging the transport dynamics of single alphaherpesvirus particles in intact peripheral nervous system explants from infected mice. *MBio* **4**, e00358-13 (2013).
162. Yang, X. *et al.* Immobilization of Pseudorabies Virus in Porcine Tracheal Respiratory Mucus Revealed by Single Particle Tracking. *PLoS One* **7**, e51054 (2012).
163. Lehmann, M. J., Sherer, N. M., Marks, C. B., Pypaert, M. & Mothes, W. Actin- and myosin-driven movement of viruses along filopodia precedes their entry into cells. *J. Cell Biol.* **170**, 317–25 (2005).
164. van der Schaar, H. M. *et al.* Dissecting the Cell Entry Pathway of Dengue Virus by Single-Particle Tracking in Living Cells. *PLoS Pathog.* **4**, e1000244 (2008).
165. Pelkmans, L., Püntener, D. & Helenius, A. Local actin polymerization and dynamin recruitment in SV40-induced internalization of caveolae. *Science* **296**, 535–9 (2002).
166. Ewers, H. *et al.* Single-particle tracking of murine polyoma virus-like particles on live cells and artificial membranes. *Proc. Natl. Acad. Sci.* **102**, 15110–15115 (2005).
167. Mercer, J. & Helenius, A. Vaccinia Virus Uses Macropinocytosis and Apoptotic Mimicry to Enter Host Cells. *Science (80-.).* **320**, 531–535 (2008).
168. Xu, H. *et al.* Real-time Imaging of Rabies Virus Entry into Living Vero cells. *Sci. Rep.* **5**, 11753 (2015).
169. Burckhardt, C. J. *et al.* Drifting Motions of the Adenovirus Receptor CAR and Immobile Integrins Initiate Virus Uncoating and Membrane Lytic Protein Exposure. *Cell Host Microbe* **10**, 105–117 (2011).
170. Helmuth, J. A., Burckhardt, C. J., Koumoutsakos, P., Greber, U. F. & Sbalzarini, I. F. A novel supervised trajectory segmentation algorithm identifies distinct types of human adenovirus motion in host cells. *J. Struct. Biol.* **159**, 347–358 (2007).
171. Coyne, C. B. & Bergelson, J. M. Virus-induced Abl and Fyn kinase signals permit coxsackievirus entry through epithelial tight junctions. *Cell* **124**, 119–131 (2006).
172. Rust, M. J., Lakadamyali, M., Zhang, F. & Zhuang, X. Assembly of endocytic machinery around individual influenza viruses during viral entry. *Nat. Struct. Mol. Biol.* **11**, 567–573 (2004).
173. Peerboom, N. *et al.* Binding Kinetics and Lateral Mobility of HSV-1 on End-Grafted Sulfated Glycosaminoglycans. *Biophys. J.* **113**, 1223–1234 (2017).
174. Kunze, A., Bally, M., Höök, F. & Larson, G. Equilibrium-fluctuation-analysis of single liposome binding events reveals how cholesterol and Ca2+ modulate glycosphingolipid trans-interactions. *Sci. Rep.* **3**, 1452 (2013).

175. Bally, M. *et al.* Interaction of Single Viruslike Particles with Vesicles Containing Glycosphingolipids. *Phys. Rev. Lett.* **107**, 188103 (2011).
176. Bally, M., Graule, M., Parra, F., Larson, G. & Höök, F. A virus biosensor with single virus-particle sensitivity based on fluorescent vesicle labels and equilibrium fluctuation analysis. *Biointerphases* **8**, 4 (2013).
177. Nasir, W., Bally, M., Zhdanov, V. P., Larson, G. & Höök, F. Interaction of Virus-Like Particles with Vesicles Containing Glycolipids: Kinetics of Detachment. *J. Phys. Chem. B* **119**, 11466–11472 (2015).
178. Block, S., Zhdanov, V. P. & Höök, F. Quantification of Multivalent Interactions by Tracking Single Biological Nanoparticle Mobility on a Lipid Membrane. *Nano Lett.* **16**, 4382–4390 (2016).
179. Lee, D., Allison, A., Bacon, K., Parrish, C. & Daniel, S. Single-Particle Tracking Shows that a Point Mutation in the Carnivore Parvovirus Capsid Switches Binding between Host-Specific Transferrin Receptors. *J. Virol.* **90**, 4849–4853 (2016).
180. Yang, S.-T., Kiessling, V., Simmons, J. A., White, J. M. & Tamm, L. K. HIV gp41–mediated membrane fusion occurs at edges of cholesterol-rich lipid domains. *Nat. Chem. Biol.* **11**, 424–431 (2015).
181. Yang, S.-T. *et al.* HIV virions sense plasma membrane heterogeneity for cell entry. *Sci. Adv.* **3**, e1700338 (2017).
182. Conboy, J. C., McReynolds, K. D., Gervay-Hague, J. & Saavedra, S. S. Gp120 Binds Cooperatively to Several Biologically Relevant Glycosphingolipids: Quantitative Measurements at Equilibrium by Total Internal Reflection Fluorescence Microscopy. *Angew. Chemie* **39**, 2882–2884 (2000).
183. Conboy, J. C., McReynolds, K. D., Gervay-Hague, J. & Saavedra, S. S. Quantitative measurements of recombinant HIV surface glycoprotein 120 binding to several glycosphingolipids expressed in planar supported lipid bilayers. *J. Am. Chem. Soc.* **124**, 968–977 (2002).
184. Myszka, D. G. *et al.* Energetics of the HIV gp120-CD4 binding reaction. *Proc. Natl. Acad. Sci. U. S. A.* **97**, 9026–31 (2000).
185. Wahlberg, J. M., Bron, R., Wilschut, J. & Garoff, H. Membrane fusion of Semliki Forest virus involves homotrimers of the fusion protein. *J. Virol.* **66**, 7309–7318 (1992).
186. Kielian, M. C. & Helenius, A. Role of cholesterol in fusion of Semliki Forest virus with membranes. *J. Virol.* **52**, 281–3 (1984).
187. Stevens, J. *et al.* Structure and receptor specificity of the hemagglutinin from an H5N1 influenza virus. *Science* **312**, 404–10 (2006).
188. Hidari, K. I. P. J., Shimada, S., Suzuki, Y. & Suzuki, T. Binding kinetics of influenza viruses to sialic acid-containing carbohydrates. *Glycoconj. J.* **24**, 583–590 (2007).
189. Rydell, G. E., Dahlin, A. B., Hook, F. & Larson, G. QCM-D studies of human norovirus VLPs binding to glycosphingolipids in supported lipid bilayers reveal strain-specific characteristics. *Glycobiology* **19**, 1176–1184 (2009).
190. Banerjee, S., Maurya, S. & Roy, R. Single-molecule fluorescence imaging: Generating insights into molecular interactions in virology. *J. Biosci.* 1–22

(2018). doi:10.1007/s12038-018-9769-y
191. Ehrlich, M. *et al.* Endocytosis by random initiation and stabilization of clathrin-coated pits. *Cell* **118**, 591–605 (2004).
192. Pietiäinen, V. *et al.* Echovirus 1 endocytosis into caveosomes requires lipid rafts, dynamin II, and signaling events. *Mol. Biol. Cell* **15**, 4911–25 (2004).
193. Weir, D. L., Laing, E. D., Smith, I. L., Wang, L.-F. & Broder, C. C. Host cell virus entry mediated by Australian bat lyssavirus G envelope glycoprotein occurs through a clathrin-mediated endocytic pathway that requires actin and Rab5. *Virol. J.* **11**, 40 (2014).
194. Li, Q. *et al.* Single-Particle Tracking of Human Immunodeficiency Virus Type 1 Productive Entry into Human Primary Macrophages. *ACS Nano* **11**, 3890–3903 (2017).
195. Liu, H., Liu, Y., Liu, S., Pang, D.-W. & Xiao, G. Clathrin-mediated endocytosis in living host cells visualized through quantum dot labeling of infectious hematopoietic necrosis virus. *J. Virol.* **85**, 6252–62 (2011).
196. Liebl, D. *et al.* Mouse polyomavirus enters early endosomes, requires their acidic pH for productive infection, and meets transferrin cargo in Rab11-positive endosomes. *J. Virol.* **80**, 4610–22 (2006).
197. Meier, O. *et al.* Adenovirus triggers macropinocytosis and endosomal leakage together with its clathrin-mediated uptake. *J. Cell Biol.* **158**, 1119–31 (2002).
198. Nakano, M. Y., Boucke, K., Suomalainen, M., Stidwill, R. P. & Greber, U. F. The first step of adenovirus type 2 disassembly occurs at the cell surface, independently of endocytosis and escape to the cytosol. *J. Virol.* **74**, 7085–95 (2000).
199. Luisoni, S. *et al.* Co-option of Membrane Wounding Enables Virus Penetration into Cells. *Cell Host Microbe* **18**, 75–85 (2015).
200. Burckhardt, C. J. *et al.* Drifting Motions of the Adenovirus Receptor CAR and Immobile Integrins Initiate Virus Uncoating and Membrane Lytic Protein Exposure. *Cell Host Microbe* **10**, 105–117 (2011).
201. Damm, E.-M. *et al.* Clathrin- and caveolin-1–independent endocytosis. *J. Cell Biol.* **168**, 477–488 (2005).
202. Lakadamyali, M., Rust, M. J. & Zhuang, X. Ligands for clathrin-mediated endocytosis are differentially sorted into distinct populations of early endosomes. *Cell* **124**, 997–1009 (2006).
203. Iyengar, S., Hildreth, J. E. & Schwartz, D. H. Actin-dependent receptor colocalization required for human immunodeficiency virus entry into host cells. *J. Virol.* **72**, 5251–5 (1998).
204. Sieczkarski, S. B., Brown, H. A. & Whittaker, G. R. Role of protein kinase C betaII in influenza virus entry via late endosomes. *J. Virol.* **77**, 460–9 (2003).
205. Elphick, G. F. *et al.* The human polyomavirus, JCV, uses serotonin receptors to infect cells. *Science* **306**, 1380–3 (2004).
206. Vonderheit, A. & Helenius, A. Rab7 Associates with Early Endosomes to Mediate Sorting and Transport of Semliki Forest Virus to Late Endosomes. *PLoS Biol.* **3**, e233 (2005).
207. Nicola, A. V & Straus, S. E. Cellular and viral requirements for rapid endocytic

entry of herpes simplex virus. *J. Virol.* **78**, 7508–17 (2004).
208. Georgi, A. *et al.* Detection of individual fluorescently labeled reovirions in living cells. *Microbiology* **87**, 6579–6583 (1990).
209. Xiao, P.-J. & Samulski, R. J. Cytoplasmic trafficking, endosomal escape, and perinuclear accumulation of adeno-associated virus type 2 particles are facilitated by microtubule network. *J. Virol.* **86**, 10462–73 (2012).
210. Arhel, N. *et al.* Quantitative four-dimensional tracking of cytoplasmic and nuclear HIV-1 complexes. *Nat. Methods* **3**, 817–824 (2006).
211. Vaughan, J. C., Brandenburg, B., Hogle, J. M. & Zhuang, X. Rapid actin-dependent viral motility in live cells. *Biophys. J.* **97**, 1647–1656 (2009).
212. Bremner, K. H. *et al.* Adenovirus Transport via Direct Interaction of Cytoplasmic Dynein with the Viral Capsid Hexon Subunit. *Cell Host Microbe* **6**, 523–535 (2009).
213. Wang, I.-H., Burckhardt, C. J., Yakimovich, A., Morf, M. K. & Greber, U. F. The nuclear export factor CRM1 controls juxta-nuclear microtubule-dependent virus transport. *J. Cell Sci.* **130**, 2185–2195 (2017).
214. Jun, S. *et al.* Direct Visualization of HIV-1 with Correlative Live-Cell Microscopy and Cryo-Electron Tomography. *Structure* **19**, 1573–1581 (2011).
215. Chen, J. *et al.* Cytoplasmic HIV-1 RNA is mainly transported by diffusion in the presence or absence of Gag protein. *Proc. Natl. Acad. Sci. U. S. A.* **111**, E5205-13 (2014).
216. Albanese, A., Arosio, D., Terreni, M. & Cereseto, A. HIV-1 Pre-Integration Complexes Selectively Target Decondensed Chromatin in the Nuclear Periphery. *PLoS One* **3**, e2413 (2008).
217. Babcock, H. P., Chen, C. & Zhuang, X. Using single-particle tracking to study nuclear trafficking of viral genes. *Biophys. J.* **87**, 2749–58 (2004).
218. Wolfstein, A. *et al.* The Inner Tegument Promotes Herpes Simplex Virus Capsid Motility Along Microtubules in vitro. *Traffic* **7**, 227–237 (2006).
219. Luxton, G. W. G. *et al.* Targeting of herpesvirus capsid transport in axons is coupled to association with specific sets of tegument proteins. *Proc. Natl. Acad. Sci. U. S. A.* **102**, 5832–7 (2005).
220. Antinone, S. E. *et al.* The Herpesvirus capsid surface protein, VP26, and the majority of the tegument proteins are dispensable for capsid transport toward the nucleus. *J. Virol.* **80**, 5494–8 (2006).
221. Döhner, K., Radtke, K., Schmidt, S. & Sodeik, B. Eclipse phase of herpes simplex virus type 1 infection: Efficient dynein-mediated capsid transport without the small capsid protein VP26. *J. Virol.* **80**, 8211–24 (2006).
222. Strunze, S., Trotman, L. C., Boucke, K. & Greber, U. F. Nuclear targeting of adenovirus type 2 requires CRM1-mediated nuclear export. *Mol. Biol. Cell* **16**, 2999–3009 (2005).
223. Miyauchi, K., Kim, Y., Latinovic, O., Morozov, V. & Melikyan, G. B. HIV Enters Cells via Endocytosis and Dynamin-Dependent Fusion with Endosomes. *Cell* **137**, 433–444 (2009).
224. Markosyan, R. M., Cohen, F. S. & Melikyan, G. B. Time-resolved Imaging of HIV-1 Env-mediated Lipid and Content Mixing between a Single Virion and

Cell Membrane. *Mol. Biol. Cell* **16**, 5502–5513 (2005).
225. Melikyan, G. B., Barnard, R. J. O., Abrahamyan, L. G., Mothes, W. & Young, J. A. T. Imaging individual retroviral fusion events: from hemifusion to pore formation and growth. *Proc. Natl. Acad. Sci. U. S. A.* **102**, 8728–33 (2005).
226. Jha, N. K. *et al.* Imaging Single Retrovirus Entry through Alternative Receptor Isoforms and Intermediates of Virus-Endosome Fusion. *PLoS Pathog.* **7**, e1001260 (2011).
227. Padilla-Parra, S., Marin, M., Kondo, N. & Melikyan, G. B. Synchronized Retrovirus Fusion in Cells Expressing Alternative Receptor Isoforms Releases the Viral Core into Distinct Sub-cellular Compartments. *PLoS Pathog.* **8**, e1002694 (2012).
228. Le Blanc, I. *et al.* Endosome-to-cytosol transport of viral nucleocapsids. *Nat. Cell Biol.* **7**, 653–664 (2005).
229. Blijleven, J. S., Boonstra, S., Onck, P. R., van der Giessen, E. & van Oijen, A. M. Mechanisms of influenza viral membrane fusion. *Seminars in Cell and Developmental Biology* **60**, 78–88 (2016).
230. Zhang, Y. & Dudko, O. K. Statistical Mechanics of Viral Entry. *Phys. Rev. Lett.* **114**, 018104 (2015).
231. Van Duijl-Richter, M. K. S., Blijleven, J. S., van Oijen, A. M. & Smit, J. M. Chikungunya virus fusion properties elucidated by single-particle and bulk approaches. *J. Gen. Virol.* **96**, 2122–2132 (2015).
232. Chao, L. H., Klein, D. E., Schmidt, A. G., Peña, J. M. & Harrison, S. C. Sequential conformational rearrangements in flavivirus membrane fusion. *Elife* **3**, e04389 (2014).
233. Kim, I. S. *et al.* Mechanism of membrane fusion induced by vesicular stomatitis virus G protein. *Proc. Natl. Acad. Sci. U. S. A.* **114**, E28–E36 (2017).
234. Costello, D. A., Whittaker, G. R. & Daniel, S. Variations in pH sensitivity, acid stability, and fusogenicity of three influenza virus H3 subtypes. *J. Virol.* **89**, 350–60 (2015).
235. Ivanovic, T., Choi, J. L., Whelan, S. P., van Oijen, A. M. & Harrison, S. C. Influenza-virus membrane fusion by cooperative fold-back of stochastically induced hemagglutinin intermediates. *Elife* **2013**, e00333 (2013).
236. Lee, D. W., Thapar, V., Clancy, P. & Daniel, S. Stochastic Fusion Simulations and Experiments Suggest Passive and Active Roles of Hemagglutinin during Membrane Fusion. *Biophys. J.* **106**, 843–854 (2014).
237. Ivanovic, T. & Harrison, S. C. Distinct functional determinants of influenza hemagglutinin-mediated membrane fusion. *Elife* **4**, e11009 (2015).
238. Hsu, H.-L., Millet, J. K., Costello, D. A., Whittaker, G. R. & Daniel, S. Viral fusion efficacy of specific H3N2 influenza virus reassortant combinations at single-particle level. *Sci. Rep.* **6**, 35537 (2016).
239. Otterstrom, J. J. *et al.* Relating influenza virus membrane fusion kinetics to stoichiometry of neutralizing antibodies at the single-particle level. *Proc. Natl. Acad. Sci.* **111**, E5143–E5148 (2014).
240. White, J., Matlin, K. & Helenius, A. Cell fusion by Semliki Forest, influenza, and vesicular stomatitis viruses. *J. Cell Biol.* **89**, 674–9 (1981).

241. Markosyan, R. M., Bates, P., Cohen, F. S. & Melikyan, G. B. A study of low pH-induced refolding of Env of avian sarcoma and leukosis virus into a six-helix bundle. *Biophys. J.* **87**, 3291–3298 (2004).
242. Melikyan, G. B., Barnard, R. J. O., Markosyan, R. M., Young, J. A. T. & Cohen, F. S. Low pH is required for avian sarcoma and leukosis virus Env-induced hemifusion and fusion pore formation but not for pore growth. *J. Virol.* **78**, 3753–62 (2004).
243. Blumenthal, R., Sarkar, D. P., Durell, S., Howard, D. E. & Morris, S. J. Dilation of the influenza hemagglutinin fusion pore revealed by the kinetics of individual cell-cell fusion events. *J. Cell Biol.* **135**, 63–71 (1996).
244. Spruce, A. E., Iwata, A., White, J. M. & Almers, W. Patch clamp studies of single cell-fusion events mediated by a viral fusion protein. *Nature* **342**, 555–558 (1989).
245. Spruce, A. E., Iwata, A. & Almers, W. The first milliseconds of the pore formed by a fusogenic viral envelope protein during membrane fusion. *Proc. Natl. Acad. Sci. U. S. A.* **88**, 3623–3627 (1991).
246. Cohen, F. S. & Melikyan, G. B. Methodologies in the study of cell-cell fusion. *Methods* **16**, 215–26 (1998).
247. Struck, D. K., Hoekstra, D. & Pagano, R. E. Use of resonance energy transfer to monitor membrane fusion. *Biochemistry* **20**, 4093–4099 (1981).
248. Hoekstra, D., De Boer, T., Klappe, K. & Wilschut, J. Fluorescence method for measuring the kinetics of fusion between biological membranes. *Biochemistry* **23**, 5675–5681 (1984).
249. Cavrois, M., de Noronha, C. & Greene, W. C. A sensitive and specific enzyme-based assay detecting HIV-1 virion fusion in primary T lymphocytes. *Nat. Biotechnol.* **20**, 1151–1154 (2002).
250. de la Vega, M. *et al.* Inhibition of HIV-1 endocytosis allows lipid mixing at the plasma membrane, but not complete fusion. *Retrovirology* **8**, 99 (2011).
251. Clague, M. J., Schoch, C. & Blumenthal, R. Delay Time for Influenza Virus Hemagglutinin-Induced Membrane Fusion Depends on Hemagglutinin Surface Density. *J. Virol.* **65**, 2402–2407 (1991).
252. Nieva, J. L., Bron, R., Corver, J. & Wilschut, J. Membrane fusion of Semliki Forest virus requires sphingolipids in the target membrane. *EMBO J.* **13**, 2797–804 (1994).
253. 2014 Ebola Outbreak in West Africa - Case Counts | Ebola Hemorrhagic Fever | CDC. Available at: http://www.cdc.gov/vhf/ebola/outbreaks/2014-west-africa/case-counts.html. (Accessed: 29th July 2015)
254. Mahanty, S. & Bray, M. Pathogenesis of filoviral haemorrhagic fevers. *Lancet. Infect. Dis.* **4**, 487–98 (2004).
255. Elshabrawy, H. A., Erickson, T. B. & Prabhakar, B. S. Ebola virus outbreak, updates on current therapeutic strategies. *Rev. Med. Virol.* (2015). doi:10.1002/rmv.1841
256. Volchkov V, Feldmann H, Volchkova V & Klenk H. Processing of the Ebola virus glycoprotein by the proprotein convertase furin. *Proc. Natl. Acad. Sci.* **95**, 5762–5767 (1998).

257. Miller, E. H. *et al.* Ebola virus entry requires the host-programmed recognition of an intracellular receptor. *EMBO J.* **31**, 1947–60 (2012).
258. Côté, M. *et al.* Small molecule inhibitors reveal Niemann–Pick C1 is essential for Ebola virus infection. *Nature* **477**, 344–348 (2011).
259. Carette, J. E. *et al.* Ebola virus entry requires the cholesterol transporter Niemann-Pick C1. *Nature* **477**, 340–3 (2011).
260. Markosyan, R. M. *et al.* Induction of Cell-Cell Fusion by Ebola Virus Glycoprotein: Low pH Is Not a Trigger. *PLoS Pathog.* **12**, e1005373 (2016).
261. Chandran, K., Sullivan, N. J., Felbor, U., Whelan, S. P. & Cunningham, J. Endosomal Proteolysis of the Ebola Virus Glycoprotein Is Necessary for Infection. *Science (80-.).* **308**, 1643–1645 (2005).
262. Noda, T. *et al.* Ebola virus VP40 drives the formation of virus-like filamentous particles along with GP. *J. Virol.* **76**, 4855–65 (2002).
263. Li, Q., Liu, Q., Huang, W., Li, X. & Wang, Y. Current status on the development of pseudoviruses for enveloped viruses. *Rev. Med. Virol.* **28**, e1963 (2018).
264. Diehl, W. E. *et al.* Ebola Virus Glycoprotein with Increased Infectivity Dominated the 2013–2016 Epidemic. *Cell* **167**, 1088-1098.e6 (2016).
265. Urbanowicz, R. A. *et al.* Human Adaptation of Ebola Virus during the West African Outbreak. *Cell* **167**, 1079-1087.e5 (2016).
266. Wang, M. K., Lim, S.-Y., Lee, S. M. & Cunningham, J. M. Biochemical Basis for Increased Activity of Ebola Glycoprotein in the 2013–16 Epidemic. *Cell Host Microbe* **21**, 367–375 (2017).
267. Coleman, M. L. *et al.* Membrane blebbing during apoptosis results from caspase-mediated activation of ROCK I. *Nat. Cell Biol.* **3**, 339–345 (2001).
268. Scott, R. E. Plasma membrane vesiculation: a new technique for isolation of plasma membranes. *Science* **194**, 743–5 (1976).
269. Holowka, D. & Baird, B. Structural studies on the membrane-bound immunoglobulin E-receptor complex. 1. Characterization of large plasma membrane vesicles from rat basophilic leukemia cells and insertion of amphipathic fluorescent probes. *Biochemistry* **22**, 3466–74 (1983).
270. Baumgart, T. *et al.* Large-scale fluid/fluid phase separation of proteins and lipids in giant plasma membrane vesicles. *Proc. Natl. Acad. Sci.* **104**, 3165–3170 (2007).
271. Säälik, P. *et al.* Penetration without cells: Membrane translocation of cell-penetrating peptides in the model giant plasma membrane vesicles. *J. Control. Release* **153**, 117–125 (2011).
272. Ruben, J. M. *et al.* Apoptotic blebs from leukemic cells as a preferred source of tumor-associated antigen for dendritic cell-based vaccines. *Cancer Immunol. Immunother.* **63**, 335–345 (2014).
273. Ebola Situation Reports | Ebola. Available at: http://apps.who.int/ebola/ebola-situation-reports. (Accessed: 3rd February 2016)
274. Feldmann, H., Feldmann, F. & Marzi, A. Ebola: Lessons on Vaccine Development. *Annu. Rev. Microbiol.* **72**, 423–446 (2018).
275. Malvy, D., McElroy, A. K., de Clerck, H., Günther, S. & van Griensven, J.

Ebola virus disease. *Lancet* **393**, 936–948 (2019).
276. World Health Organization. Ebola virus disease. (2019). Available at: https://www.who.int/news-room/fact-sheets/detail/ebola-virus-disease. (Accessed: 24th May 2019)
277. World Health Organization. *2018 Annual review of diseases prioritized under the Research and Development Blueprint*. *WHO Research and Development Blueprint* (World Health Organization, 2018).
278. WHO. *An R&D Blueprint for Action to Prevent Epidemics: Plan of Action, May 2016*. (2016).